FUNDACIÓN PÚBLICA ANDALUZA PARA LA INVESTIGACIÓN BIOSANITARIA DE ANDALUCÍA ORIENTAL ALEJANDRO OTERO

Proyecto FP7 HEALTH-2007-2.3.4-1 “NANOTRYP”.

Departamento de Bioquímica y Biología Molecular 3 e Inmunología
Facultad de Medicina
Universidad de Granada

New therapeutic approaches for Human African trypanosomiasis

Tesis Doctoral

Juan Diego Unciti Broceta

Editor: Editorial de la Universidad de Granada
Autor: Juan Diego Unciti Broceta
D.L.: GR 1062-2014
ISBN: 978-84-9028-968-6

New therapeutic approaches for Human African trypanosomiasis

Memoria presentada por el licenciado en Farmacia,
Juan Diego Unciti Broceta,
para optar al Título de Doctor.

Fdo.: Juan Diego Unciti Broceta

Vº Bº del Director

Fdo.: Jose Antonio García Salcedo
Doctor en Parasitología

Universidad de Granada
Septiembre 2012

El Doctorando D. Juan Diego Unciti Broceta y el Director de la tesis Dr. Jose Antonio García Salcedo, garantizamos, al firmar esta tesis doctoral, que el trabajo ha sido realizado por el doctorando bajo la dirección del director de la tesis y hasta donde nuestro conocimiento alcanza, en la realización del trabajo, se han respetado los derechos de otros autores a ser citados, cuando se han utilizado sus resultados o publicaciones.

Granada, Julio de 2012

Director de la Tesis	Doctorando
Fdo.: Dr. Jose Antonio García Salcedo	Fdo.: Juan Diego Unciti Broceta

Esta tesis doctoral ha sido realizada en el
Instituto de Parasitología y Biomedicina “López-Neyra” (C.S.I.C.)
Granada

“Al carro de la cultura española,
le falta la rueda de la ciencia”

Santiago Ramón y Cajal

“La libertad no la tienen
los que no tienen su sed”

Rafael Alberti

A Luis

A Mª Carmen

A Asier

Agradecimientos

Quiero agradecer y dedicar mi Tesis a mis padres, Luis y Mari Carmen, por ser los pilares de mi vida, por ser como sois, por apoyarme, por guiarme, por abrazarme, por enseñarme a superar y a digerir los buenos y los malos momentos, por quererme tal como soy y porque os quiero con locura, GRACIAS.

A mi hermano, Asier, por esa maravillosa infancia, por esos increíbles años de Universidad, por estar siempre a mi lado, por confiar en mí y por todo lo que nos queda por recorrer juntos, te quiero gordo.

A mí cuñada Belén por querer a Asi y por enseñarme la valentía de dejarlo todo por amor.

A mis abuelos, en especial a Sabino porque quiero ser como tú, todos deberíamos ser como tú, te echamos de menos.

A mis tíos; Pepe y Estrella; Javi y Ana; y, Carlos y Marieta, vosotros me habéis enseñado lo que es una familia unida y feliz. Tita Estrella, hoy te siento conmigo.

A mis primos Carlos-Mª Carmen, y mi sobrina María; Pablo-Isa-Pablito; Gonzalo-Yesi; Ramón-Andrea; Tere-Eddi; Ainoa-Cata y a Javi, dicen que la familia no se elige pues que afortunado soy; os quiero por darme tanto sin pediros nada, por ser mis amigos, gracias.

No voy a olvidarme de todos los que han estado al lado de mi familia durante tantos años, a los incondicionales de los Unciti-Broceta, porque a vosotros también os quiero: Marcos-Nani-Isabel; África-Cristi-Javi-Tomás, Santi-África, Antonio-Paqui, Manolo-Isabel, etc,...

Es imposible no nombrar en mi vida a mi Pollo, soy tu Padre y siempre lo seré.

A Jose, te quiero crack ¡¡¡¡Gracias por todo!!!

A Ana Juárez, a Nieves Luengo y a Alfonso Vera por ser unos maravillosos profesores para mí.

A Jose Luis Arias y a su grupo de Galénica por su gran trabajo con las nanopartículas.

A Paco Martín, por animarme siempre a seguir por aquí.

A Estela, Sonia y Paco del LEC, por ayudarnos en todos, y repito, todos nuestros problemas proteicos.

Al equipazo del Animalario del López: Paco, Clara, Bea, Begoña, Fernando,…que a gusto me he sentido a vuestro lado, muchísimas gracias por todo.

A Santiago Castanys y a Paco Gamarro

A Jose María Pérez-Victoria por ayudarnos con la Nicotinamida.

A Jose Manuel, Jana y Javier Oliver por ayudarme siempre con la apoptosis.

A Jean Mathieu por ayudarme con las microscopías y con mil y un protocolos.

A Mario Delgado, Elena González y Jenny, por tantas cosas que me habéis aconsejado, gracias.

A Antonio Estévez porque siempre estás ahí, eres un grande.

A Asun y a mis tocayos.

A Salva, Jose Luis, Antonio Mérida y Antonio Larios.

A Vivi, porque siempre me alegras el día.

A Ignacio Molina, por enseñarme a ser científico.

A mis compañeros de Inmunología: Ester, Raquel, María José, Irene, Zule, Jorge, Pablo, Alex, Domi, Karina, Manu, Marta y Lucía.

A mi tita Api, que decirte Apita…que te siento siempre conmigo.

A mi Sarita, la amistad llega en cualquier momento y tú eres mi prueba; eres genial, increíble, maravillosa y mejor amiga aún, has sido mi salvación, me tienes y me tendrás, te quiero.

A Packman, Juanan, Magda, Pepe, Edu, Caro, Jon, Martin, David, Pili, Antoñito, Araceli, Jose Antonio y Juanjo.

A Gise, Rober, Ali, Elena, Roge, Ezequiel, Lara y Eva.

A Mary, Nacho, Sebas, Raquel, David y Luis, muchas gracias 203-204.

A Javi Oliver y Ceci; a Antonio Caler y a Peni!!! Porque aunque lejos os siento cerca.

A Manu Picón y a Toni, porque sois únicos, especiales, no cambiéis figuras.

A Potito, por ayudarme tanto con mis correcciones, mis paranoias,… ¡te quiero!

A Kiko, eres el más grande en todos los sentidos ¡nos merecemos unas vacaciones ya!
A Tali por ayudarme con mi inglés gaditano, muchas gracias princesa del Pacífico.

A Morel porque siempre me ayudas, incluso cuando me das caña.

A Beíta, porque no hay nadie con tanta mala leche y tanto amor a la vez. Gracias por esa maravillosa portada.

A mi Sara, porque nunca te sentí en Edimburgo, siempre te tuve aquí conmigo.

A Paco, porque eres el gruñón más buena gente que me he echado a la cara.

A Darío, dicen que nunca es tarde para conocer verdaderos amigos, púes Yo he conocido a uno y de mi pueblo encima, fíjate tu… su shoshio. Te quiero shurman!!!

A mi pequeña Fany; que suerte he tenido al conocerte, te mereces lo mejor de esta vida, no sabes cuánto tengo que agradecerte, te quiero muchísimo.

A Adela y Mónica, porque esto es sólo el principio.

A Jose y a Mari, mis titols, os quiero poderosos, que suerte tengo de teneros como amigos. Gracias por estar siempre conmigo.

A Carlitos, Chico, Rocío y Mari.

A les meves princeses, a la meva cosina la Bazaco, a la Silvia i a la Zaidita us estimo molt.

A mi clan granaíno: Sale, Maca, María y Felipe os quiero muchísimo. Que sepáis que nos quedan muchos años más por disfrutar.

A mis amigos de la facultad: Iván, Raquelilla, Antonio, Carlos, Vane, Juan, Mª Ángeles, Mari Pepa, Ana, etc.,…por esos maravillosos 5 años que pasamos y porque aún estamos unidos como una gran familia.

Al clan putrefacto: Ana Bombón, Ricardo y Sol, y el pequeño Mateo, gracias amigos.

A mis compañeros de piso de Madrid y de Granada, por ser mi familia: Pedro, Germán, Simone, Norberto, Pez, Cari, Dani, Fabri, la Pantelaro, Pedrito (Australia), Runa, Venla, David, Piia, la perra Lola, etc.,… y en especial a Alberto, Vicu, Ventu, Elenilla, Manolillo y mi Susa, os quiero.

A Armando, Abi y Maria, porque sigo con vosotros

A Flor, porque hiciste que Bruselas fuese mi casa.

A mi Beíta chica, mi belga-sevillana, te echo de menos.

To Stefan Magez, thank you for the opportunity to be in Brussels during those amazing months.

To Raluka, Yan, Steven and Liese, my team in Brussels, thank you so much.

To Cécile, thank you from my heart.

To Harry De Koning, thank you for help me to understand the resistances.

A mi laboratorio el 214:

A Miguel, por su gran trabajo corrigiendo y sus charletas, ¡¡¡muchas gracias!!!

Al Sensei Carlichi por sus grandes consejos, ¡¡¡gracias!!!

A Tesi por tu gran ayuda, tus correcciones, tus consejos y tus ánimos constantes, ¡¡¡gracias!!!

A Betty, por darme siempre tu apoyo, por animarme las mañanas y por siempre recibirme con una sonrisa, ¡¡¡gracias pequeña!!!

A mi hada madrina, mi Sonia. Agradecido por todo lo que siempre haces por mí, ¡¡¡Te quiero muchísimo pupi!!!

Es de ley pero de ley darle las gracias a mi amigo Pepe. Pepiño esta tesis es nuestra, tuya y mía. Eres el mejor trabajador de la historia y mejor tío aún ¡¡¡¡¡¡Inmensamente agradecido!!!!!!

A Jose Antonio (Salcedo, para todos), no te puedes hacer una idea de lo importante que son las segundas oportunidades; y a mí me la diste tú y siempre te lo agradeceré. Me diste tu confianza y eso me ha hecho crecer como persona y como científico. Me lo he pasado genial trabajando, y lo sabes. Gracias también por ofrecerme Kenia, Mozambique,… y sobre todo por Bruselas, ya que, espero que sea mi futuro. Muchas gracias de todo corazón.

CONTENT

ABBREVIATIONS

Ag	Antigen
AMC	7-amido-4-methylcoumarin hydrochloride
AnTat	Antwerpen trypanozoon antigenic type
AP	Alkaline phosphatase
ApoL1	Apolipoprotein L1
AQP	*Aquaglyceroporin* gene
Arg or R	Arginine
ATP	Adenosine-5'-triphosphate
BBB	Blood brain barrier
bp	base pair
BSA	Bovine serum albumin
CCV-I	Class I clathrin vesicles coated
CCV-II	Class II clathrin vesicles coated
CDR	Complementarity determining regions
CH1, 2 and 3	Constant domain 1, 2 and 3 of heavy chains immunoglobulins.
ChNP	Chitosan nanoparticle
CNS	Central nervous system
C-terminal	Carboxi terminal
DAPI	4',6-diamidino-2-phenylindole
DDW	Double distilled water
DMFO	Diethylfluoromethylornitihine
EC	Enzyme commission
ELISA	Enzyme link immunosorbent assay
ER	Endoplasmic reticulum
ESAG	Expression site associated gene
ETat	Edinburgh trypanozoon antigenic type
Fab	Fragment antigen binding
FACS	Fluorescence activated cell sorting
FAZ	Flagellar attachment zone
Fc	Fragment cristallizable region
FP	Flagellar pocket
G_0 (Gap0)	Resting phase
G_1 (Gap1)	Postmitotic phase
G_2 (Gap2)	Pre-mitotic phase
Gly	Glycine
GPI	Glycosylphosphathidylinositol
HA	Hemagglutinin
HAPT1	High affinity pentamidine transporter
HAT	Human African trypanosomiasis
HcAbs	Heavy chain antibodies
H-chain	Heavy chain
HDL	High density lipoproteins

HRP	horseradish peroxidase
i.p.	Intraperitoneal
IC50	Half-inhibitory concentration
IPTG	Isopropyl β-D-1-thiogalactopyranoside
ISG	Invariant surface glycoprotein
K	Kinetoplast
LAPT1	Low affinity pentamidine transporter
L-chain	Light chain
Leu	Leucine
M	Mitosis phase
mAb	Monoclonal antibody
MW	Molecular weight
N	Nucleus
NADH	Nicotinamide adenine dinucleotide
NAM	Nicotinamide
Nb	Nanobody
Nbs	Nanobodies
NHS	Normal human serum
NP	Nanoparticle
N-terminal	Amine terminal
O.D.	Optic density
P	Pearson symbol
PBMC	Peripheral blood mononuclear cells
PBS	Phosphate buffered saline
PCR	Polymerase chain reaction
PE	Periplasmic space
PEG	Polyethylene glycol
PFA	Paraformaldehyde
Phe	Phenylalanine
PI	Propidium iodide
r.p.m.	Revolutions per minute
RNAi	Ribonucleic acid interference
S	Synthesis phase
SD	Standard deviation
SEM	Standard error of mean
SRA	Serum resistant associated protein
SRA	Serum resistant associated protein gene
Tb*AT1/P2*	*Trypanosoma brucei* adenosine transporter P2 gene
TbCatB	*T. brucei* cathepsin B-like gene
TbCatB	*T. brucei* cathepsin B-like protein
TbOPD	*T. brucei* Oligopeptidase B protein
TDB	Trypanosome dilution buffer

TfR	Transferrin receptor
TLF1	Trypanosome lytic factor 1
TLF2	Trypanosome lytic factor 2
Trp	Tryptophan
Tyr	Tyrosine
u_e	Electrophoretic mobility
Uv-Vis	Ultraviolet-visible spectrophotometry
Val	Valine
VH	Variable domain of heavy chain of conventional antibody
VHH	Variable domain of heavy chain of heavy chain antibody
VHH-DJ	VHH diverse and joining gene segment
VSG	Variable surface glycoprotein
***VSG*-ES**	VSG expression site
WHO	World health organization
WT	Wild type
ζ	zeta potential value

RESUMEN

La tripanosomiasis es una enfermedad parasitaria con un devastador impacto socio-económico en el África subsahariana a través de la infección directa del hombre y el ganado. La tripanosomiasis Africana Humana es causada por el parásito protozoario *Trypanosoma brucei gambiense* y *Trypanosoma brucei rhodesiense*, siendo una enfermedad mortal si no se trata. Actualmente, la quimioterapia usada para su tratamiento se basa en el uso de cinco medicamentos que presentan limitaciones que abarcan desde problemas con la absorción oral y toxicidad, hasta la aparición de resistencias, que es la mayor causa de preocupación unida a la ausencia de una vacuna o alternativas terapéuticas. Todos los mecanismos de resistencia conocidos a los fármacos tripanocidas se asocian con la pérdida de funcionalidad de transportadores de superficie, excepto en el caso del nifurtimox.

En este trabajo se presenta la actividad tripanocida de la nicotinamida (NAM), un compuesto soluble de la vitamina B3. El tratamiento con nicotinamida produce en *T. brucei,* la inhibición del crecimiento celular y el dimorfismo de la bolsa flagelar, lugar donde se producen los procesos endocitosis y exocitosis. La medida de la actividad proteasa muestra que la nicotinamida inhibe de forma directa a la proteasa lisosomal catepsina B y posteriormente bloquea la endocitosis causando muerte celular programada. Por último, un estudio *in vivo* demuestra que la nicotinamida tiene un efecto aliviador de la enfermedad en ratones infecciosos. Todos estos resultados presentados en esta memoria apoyan el posible uso de la nicotinamida en la terapia de la tripanosomiasis Africana Humana.

Nuevos enfoques en las quimioterapias actuales se centran en el uso de sistemas de administración de fármacos o herramientas inmunológicas. Los nanobodies (Nbs) son pequeños fragmentos de anticuerpos, con propiedades únicas de reconocimiento de antígenos, derivados de anticuerpos de cadena pesada de camélidos a través de tecnología genética recombinante. Los nanobodies pueden ser utilizados para dirigirlos contra componentes biológicos activos. En este contexto, hemos elaborado nanopartículas (NP) del polímero chitosan funcionalizadas con polietilenglicol (PEG) cargadas de pentamidina y recubiertas por un nanobody dirigido contra la superficie de *T. brucei*. Las nanopartículas cargadas de pentamidina y recubiertas de nanobodies se unen a la superficie del tripanosoma y entran por endocitosis, introduciendo al fármaco por este mecanismo en lugar de por los clásicos transportadores de membrana. El uso de la nueva formulación presentada fue significativamente más eficaz que la pentamidina sola, matando a los tripanosomas a dosis inferiores. Estudios *in vitro* revelaron que la concentración media inhibitoria (IC50) de nanopartículas de chitosan funcionalizadas con polietilenglicol (PEG)

cargadas de pentamidina y recubiertas de nanobodies fue 14 veces menor que la IC50 de la pentamidina sola. Experimentos *in vivo* en modelo murino de la fase aguda de la tripanosomiasis africana determinó que la dosis curativa de la nueva formulación es 100 veces menor que la dosis de pentamidina sola. Por otra parte, en el laboratorio se estableció una línea celular resistente a pentamidina, la cual se obtuvo mediante el cultivo de los parásitos en concentraciones crecientes de pentamidina. Estudios genéticos y funcionales revelaron que el mecanismo de resistencia a la pentamidina de esta línea celular era debido a una mutación en el gen de la *aquagliceroporina 2*, un transportador de superficie celular localizado en la bolsa flagelar. Un estudio *in vitro* demostró que esta línea celular no presentaba resistencia a las nanopartículas de chitosan funcionalizadas con polietilenglicol (PEG) cargadas de pentamidina y recubiertas de nanobodies.

El desarrollo de nanopartículas de chitosan cargadas con los actuales fármacos tripanocidas y recubiertas por nanobodies específicos contra antígenos invariantes de la superficie del tripanosoma podría reducir la dosis mínima curativa mínima de éstos, minimizando la toxicidad y evitando las resistencias. Por otra parte, las posibilidades que ofrece este sistema basado en nanopartículas recubiertas de nanobodies son enormes y podría adaptarse para transportar cualquier sustancia con una acción tripanocida testada, como por ejemplo, la nicotinamida. Por último, los prometedores resultados obtenidos con esta nueva formulación abren un abanico de nuevas terapias potenciales para su aplicación a otras enfermedades.

SUMMARY

Trypanosomiasis is a parasitic disease with a devastating socio-economic impact in Sub-Saharan Africa through the direct infection of humans and livestock. Human African trypanosomiasis is caused by the protozoan parasite *Trypanosoma brucei gambiense* and *Trypanosoma brucei rhodesiense*. The disease is fatal if left untreated. Current chemotherapy relies only on five drugs that have many limitations, ranging from problems with oral absorption, acute toxicities and the emergence of trypanosomal resistance, which is a major concern owing to the absence of a vaccine or therapeutic alternatives. All the resistance mechanisms known are associated with loss of surface transporters except nifurtimox.

Here we report the trypanocidal activity of nicotinamide (NAM), a soluble analogue of vitamin B3. Nicotinamide treatment results in *T. brucei* cell growth inhibition and dimorphism of the flagellar pocket, the site for both endocytosis and exocitosis and the subjacent endocytic compartment. Protease assays shows that nicotinamide inhibits directly the lysosomal protease cathepsin B and subsequently blocks endocytosis causing programmed cell death. Finally, an *in vivo* study shows that nicotinamide has an alleviating effect on *Trypanosoma brucei*-infected mice. The results presented here support the possible use of NAM in HAT therapy.

New approaches in currents chemotherapies are focused on the use of drug delivery systems or immune tools. Nanobodies (Nbs) are small antibody fragments, with unique antigen recognition properties, derived from heavy chain camelids antibodies through recombinant gene technology. These can be used to target biologically active components. In this context, we have prepared pentamidine-loaded nanoparticles of chitosan polymer coated by a specific nanobody that target the surface of *Trypanosoma brucei*. The nanobody-coated pentamidine-loaded chitosan nanoparticles bind to the trypanosome surface and the drug is taken up by endocytosis instead of its classical membrane transporters. The new formulation was significantly more efficient than pentamidine alone in killing trypanosomes. *In vitro* studies revealed that the half-inhibitory concentration (IC50) of pentamidine-loaded in nanobody-coated PEGlycated chitosan nanoparticles was 14 fold lower than pentamidine alone. An *in vivo* experiment in murine model of the acute phase of African trypanosomiasis determined that the curative dose of pentamidine-loaded in nanobody-chitosan nanoparticles was 100 fold lower than pentamidine alone. Moreover, a pentamidine resistant cell line was obtained by growing the parasites in increasing concentration. Genetic and functional assays revealed that the resistance mechanism to pentamidine of this cell line was due to mutation in *aquaglyceroporin 2*, a cell surface transporter.

An *in vitro* study showed that this cell line was not resistant to pentamidine-loaded nanobody-coated chitosan nanoparticles.

The development of trypanocidal drugs loaded in chitosan nanoparticles coated by specific nanobodies against trypanosome invariant surface antigens may reduce the minimal curative dose of all these drugs, minimize drug toxicity and circumvent drug resistance. Furthermore, the possibilities offered by this nanobody-based system are enormous and could be adapted to load any substance with a reported trypanocidal action, for instance nicotinamide. Finally, the promising results obtained with this new formulation open a range of new potential therapies with application to other diseases

INTRODUCTION

1. Sleeping sickness.

African trypanosomiasis is a disease with a devastating socio-economic impact in Sub-Saharan Africa through the direct infection of humans and livestock. Human African Trypanosomiasis (HAT), also known as sleeping sickness, and nagana in cattle, is a vector-borne disease caused by *Trypanosoma brucei spp.* which is transmitted by tsetse flies bites of the genus *Glossina* between humans or domestic-wild animals [1,2,3]. In humans, the disease is caused by two sub-species of *T. brucei*, *T. brucei gambiense* and *T. brucei rhodesiense*. *T. b. gambiense* is responsible for around 95% of all cases of the disease.

1.1. Clinical features.

The disease presents two stages, the early stage or haemolymphatic phase and the late stage or neurological phase which is characterized by the invasion of the central nervous system (CNS). After tsetse fly bite, where usually appears a painful sore known as chancre, trypanosomes multiply in bloodstream and lymphatic nodes producing fever, swollen lymph glands, aching muscles and joints, weight loss, weakness, headaches and irritability, typical symptoms of early stage. After a time, trypanosomes cross the blood-brain barrier (BBB) invading CNS producing the neurological stage, characterized by changes of behavior, confusion, sensory disturbances, poor coordination and disorder of the sleep cycle, which gives the disease its name.

The disease can be chronic or acute depending on the subspecie responsible for the infection. *T. b. gambiense* infection leads to a disease that follows a chronic course which can take months or even years without appearance of major signs or symptoms. However, *T. b. rhodesiense* causes an acute infection, which develops rapidly producing the appearance of signs and symptoms a few weeks after infection, and death occurring within weeks to months [4,5,6] .

1.2. Epidemiology.

Sleeping sickness is a neglected tropical disease that prospers in impoverished rural parts of sub-Saharian Africa. The disease is endemic in 36 countries (tsetse flies area) where millions of people are at risk of infection [7]. However, the presence of tsetse flies does not necessarily means that the disease is present. The control of sleeping sickness is based on reducing of the reservoirs of infection, access to

diagnosis, access to treatment and control of tsetse flies, but these strategies have been inadequate [8,9]. The prevalence has been variable during the twentieth century, coinciding the re-emergence of the number of cases with famine and war times [10,11]. In 2000, World Health Organization (WHO) began a HAT control program in 24 endemic countries supporting them in technical assistance, access to diagnosis and treatment [12]. As consequence, in 2009 the WHO reported, for first time in 50 years, a drop of cases below 10,000 and this tendency was maintained in 2010 (registering 7139 new cases; 155 cases of infection by *T. b. rhodesiense* and 6984 cases of *T. b. Gambiense*; http://apps.who.int/ghodata/?vid=720) [12]. However, the impact of the disease is still enormous with an estimated burden of 1.3 million Disability Adjusted Life Years (DALYs) and economic losses in excess of $1 billion due to human and animal trypanosomiasis [13,14] .

However, the demonstrated capacity of HAT to recur after periods of time, where the disease has been kept under control, shows the need for more research and development in diagnosis and treatment.

1.3. Treatment.

Trypanosomes have developed an antigenic variation strategy consisted in a continuous change of the variant surface glycoproteins (VSGs), allowing the parasites to evade the host immune response hampering the generation of conventional vaccines [15]. Therefore, this neglected tropical disease has to be combated with chemotherapy (http://www.who.int/trypanosomiasis_african/diagnosis/en/index.html). Current treatment of HAT is based on the use of 5 chemotherapeutic agents: pentamidine, suramine, melarsoprol, eflornithine and nifurtimox (included in "essential medicine list" in 2009). All drugs are donated to WHO by producers (Bayer and Sanofi). However, these drugs have many limitations, ranging from problems with oral absorption, poor efficacy, acute toxicity and increase drug resistances that together with absence of vaccines or other therapeutic alternatives, is the main clinical problem.

The use of either chemotherapics agents varies depending on the causative agent and on the stage of the disease. The structures of the following drugs have been extracted from “Chemotherapy of human African trypanosomiasis: current and future prospects” **Alan H. Fairlamb. TRENDS in Parasitology Vol.19 No.11 November 2003**.

- Pentamidine (pentamidine isethionate):

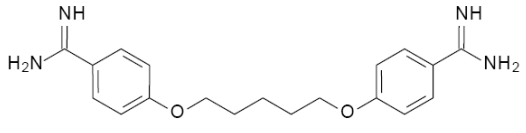

Pentamidine isethionate is the drug of choice since the 30's for the treatment of early stage of infection caused by *T. b. gambiense*. Pentamidine is a water-soluble aromatic diamidine with antiprotozoal effect which is not yet fully understood. Pentamidine activity is speculated to be multi-factorial due to the rapid accumulation in millimolar levels inside the parasites [16]. It is ineffective in the late stage of *T. b. gambiense* because does not enter to the spinal fluid and in any stage of *T. b. rhodesiense* infections [17,18]. The routes of administration are parenteral or intramuscular, due to poor absorption when is administered orally. Many side effects have been described, but the most important is the pancreas injury which results in hypoglycaemia due to the massive release of insulin. In areas where pentamidine resistance occurs, suramin may be used as an alternative drug. Pentamidine is also used against leishmaniasis and *Pneumocystis carinii* infections (www.kompendium.ch; Pentacarinat, 2008).

Although the mode of action is unclear, the uptake is well understood. Pentamidine uptake is mediated by the trypanosome adenosine P2 transporter (TbAT1/P2) in combination with two other transport activities: a high-capacity low affinity pentamidine transporter (LAPT1) and a low-capacity high affinity pentamidine transporter (HAPT1) [19,20]. Besides, two new *T. brucei* transporters (nucleoside transporters NT11.1 and NT11.2) have implicated in pentamidine transport and were expressed in a heterologous system [21].

Pentamidine resistance mechanisms are classically associated with the loss of function of classical surface transporters (TbAT1/P2 and HAPT1) and are related with melaminophenyl arsenical (as melarsoprol) cross resistance, which is the most important resistance in the field [22,23,24,25,26,27]. However a recently study has linked pentamidine/melarsoprol cross resistance to aquaglyceroporins (AQPs), specifically to AQP2 which controls the susceptibility to both drugs [28,29]. Three AQPs have been identified in *T. brucei* [30]. AQPs are channels permeable for water, glycerol and other small uncharged solutes [31]. AQP1 is exclusively localized in the flagellar

membrane, AQP3 in the plasma membrane [32] and AQP2, is restricted to flagellar pocket [29,32].

- Suramin:

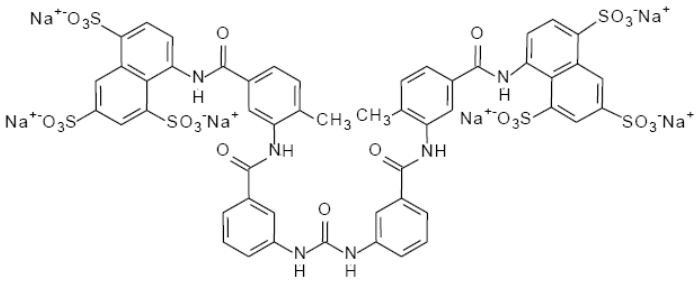

Suramin is a colourless polyanionic sulfonated naphthylamine that is chemically related with trypan red and to other dyes with *in vivo* trypanocidal activity. Suramin is, since the 20's, the drug of choice for the treatment of the early stage of infection by *T. b. rhodesiense*, and *T. b. gambiense* in cases of pentamidine resistance. Owing to its highly ionic nature, suramin does not cross the BBB and it is not utilized in the last stage of the disease. It is administered by intravenous injection as a result of its high solubility in water and its poor gastrointestinal absorption. The uptake of suramin is through fluid-phase endocytosis but the mode of action is unknown [33]. Side effects are frequent but mild and reversible such as thrombocytopenia, peripheral neuropathy, nephrotoxicity, jaundice and severe diarrhoea. Suramin is also used to treat onchocerciasis [34]. No significant clinical resistant has been described to suramine.

- Melarsoprol:

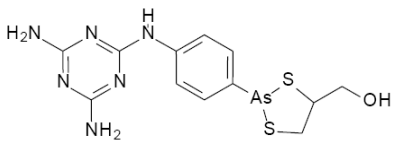

Melarsoprol is an organic arsenical compound that is used in African trypanosomiasis when the CNS is invaded. This arsenical-derived is employed since the 40's to treat the late stage of *T. b. gambiense* and *T. b. rhodesiense* African

trypanosomiasis. Melarsoprol crosses the BBB reaching high levels in the CNS, being able to kill the parasites. Due to poor gastrointestinal absorption and high toxicity that produces its solvent (propylene glycol) when is administered intramuscularly; the route of administration is intravenous. Melarsoprol is a pro-drug that in patients is rapidly converted into melarsen oxide which binds reversibly to serum proteins [35,36]. Melarsen oxide uptake is through TbAT1/P2 [37]. Once into parasites, melarsen oxide forms a toxic adduct with trypanothione, known as Mel T, which is a competitive inhibitor of trypanothione reductase, essential enzyme for maintaining the correct intracellular thiol-redox balance [38,39]. This inhibition is enough to kill parasites. One of the most important problems concerning melarsoprol chemotherapy is resistances emergence which are due to the lack of this adenosine transporter [37]. However, as mentioned before, melanophenyarsenical resistances are related to pentamidine resistances.

Melarsoprol is the most toxic drug used to treat HAT. 1-5% of patients do not overcome the treatment due to a severe encephalopathy. Other symptoms are vomiting, abdominal colic, peripheral neuropathy, arthralgia and thrombophlebitis. This high toxicity recommends its exclusive management in hospitals.

- Eflornithine (diethylfluoromethylornitihine-DMFO):

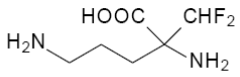

DMFO is the only new drug registered since the 40's. DMFO inhibits, irreversibly, ornithine decarboxylase, an enzyme essential for polyamine biosynthetic pathway [40,41]. DMFO readily crosses the BBB and enter in cerebrospinal fluid. It is the drug of choice to treat the late stage of *T. b. gambiense* African trypanosomiasis. However, it is not effective for the treatment of *T. b. rhodesiense* infections. The major disadvantage is the mode of administration, requiring a slow infusion every 6 hours (h) for 14 days (56 infusions in total), a regimen imposed by its short half-life of 1.5–5 h. The difficulty in administering DMFO in resource-poor settings explains why melarsoprol continues to be the first-line treatment. The most common adverse effects include: diarrhoea, anaemia, leukopenia, thrombocytopenia and convulsions. These are reversible on withdrawal of the drug. Given the increase in DMFO use, the risk of resistance is becoming a problem. Resistance mechanism of DMFO-adapted strains has been

associated with the loss of the amino acid transporter TbATT6 which control its uptake [42]. Nowadays, DMFO is used in combination with nifurtimox as alternative therapy.

- Nifurmitox:

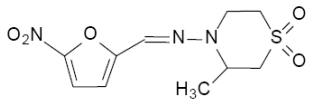

Nifutimox is a synthetic trypanocidal nitrofuran compound which is efficiently absorbed from the gastrointestinal tract. It is used in the treatment of acute American trypanosomiasis (Chagas disease). Nifurtimox alters the redox equilibrium in the parasite, forming superoxide ion which damage the DNA [43]. Adverse effects are frequent, dose-related and reversible. They include anorexia, nausea, vomiting, gastric pain, insomnia, headache, vertigo, excitability, myalgia, arthralgia and convulsions. Nifurtimox is a pro-drug activated by a NADH-dependent, mitochondrially localized, bacterial-like, type I nitroreductase. The down-regulation or loss of a single copy of the gene, which encode the enzyme, is enough to produce nifurtimox resistance [44]. The combination of DMFO+nifurtimox allows a reduction of DMFO regimen, obtaining an improved effect and a reduction of its side effects [45,46,47]. Nowadays the combination of DMFO+nifurtimox is the treatment of choice in the late stage of infection by *T. b. gambiense*.

2. *Trypanosoma brucei*.

Kinetoplastids (order Kinetoplastida) are a group of single-cell flagellated protozoans that are characterized by the presence of a DNA-containing granule, known as “kinetoplast,” in their large single mitochondrion. They divide by binary fission during which their nucleus does not undergo membrane dissolution or chromosome condensation. Trypanosomatids include several of the most serious vector-borne protist parasites of numerous vertebrates, insects, other invertebrates and plants. The major human parasites include a number of species in the genera *Leishmania* and *Trypanosoma*. In *Trypanosoma*, the two major human parasites are *T. cruzi*, the causative agent of Chagas’ disease, and *T. brucei*, the causative agent of African Trypanosomiasis (http://www.ncbi.nlm.nih.gov/genome?term=txid5691[orgn]).

T. brucei brucei is agent responsible for the nanaga, the cattle disease. This animal-pathogenic non-human infective subspecie shares many features with human infective variants being almost identical to *T. brucei rhodesiense* with the sole exception of absence of serum-resistance associated gene, which offer resistance to normal human serum (NHS) [48]. Due to this homology that shares with these variants is used as model of human infections in laboratory.

2.1. Life cycle.

T. brucei exhibit a complex life cycle which involves alternation between two very different environments, the mammalian host and the tsetse fly host. Due to the large differences between these two hosts, the trypanosome undergoes complex changes in cell morphology, gene expression and metabolism to allow the survival of the parasite during the life cycle.

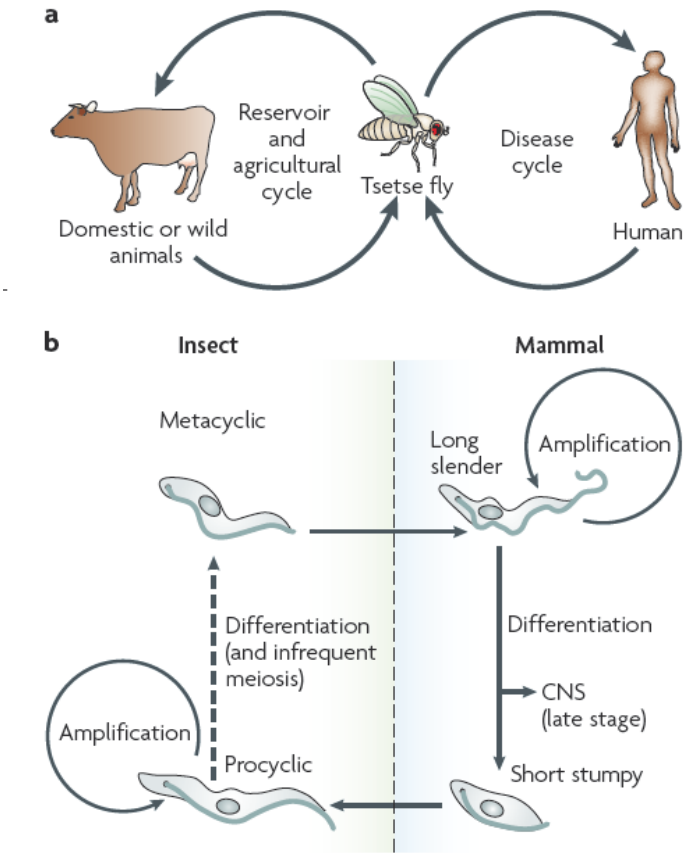

Figure 1. Life cycle diagram. "The trypanosome flagellar pocket" **Mark C. Field and Mark Carrington Nature Reviews Microbiology volume 7 November 2009 | 775**

The life cycle begins when a tsetse fly feeds on an infected mammalian host. During blood meal, tsetse flies ingest non-proliferative stumpy forms (Fig. 1). Stumpy forms are pre-adapted for their subsequent transformation, in the midgut of the fly, into

proliferative procyclic trypomastigotes. After proliferation, procyclic forms migrate from the fly's midgut to the salivary gland where they finally differentiate to the infective non-proliferative metacyclic forms, which are transmitted by injection during the next blood meal into the mammalian host. The metacyclic forms rapidly transform into proliferative long slender bloodstream forms which multiply and invade the bloodstream, lymphatic system and interstitial spaces. In mammals, the parasite survives free in the bloodstream, being able to evade host immune responses through antigenic variation strategy [15]. These forms have an inactive mitochondrion and utilize the glucose from the blood of the host, by glycolysis, as their primary energy source. Long slender bloodstream forms eventually differentiate into a non-dividing short stumpy bloodstream forms. These forms are preadapted for survival in the tsetse midgut by partial activation of the mitochondrion, which allows some metabolism of the major tsetse metabolite, proline. After a fly bite, the stumpy are ingested and the cycle is closed [3,49,50,51].

2.2. Cellular structure.

Trypanosomes have eukaryotic cell organization. Trypanosome cell shape is derived from and defined by a highly ordered microtubule cytoskeleton that forms a tightly arrayed cage directly beneath the pelicullar membrane. The single flagellum exits the cell near the posterior pole and extends towards the anterior following a defined left-handed helical path [52]. It follows the canonical eukaryotic 9+2 microtubule axonemal arrangement with an additional extra-axonemal complex known as the paraflagellar rod. For most of its length is physically attached to the cell body via the flagellum attachment zone (FAZ). The basal body is a centriole-like structure located at the base of the flagellum.

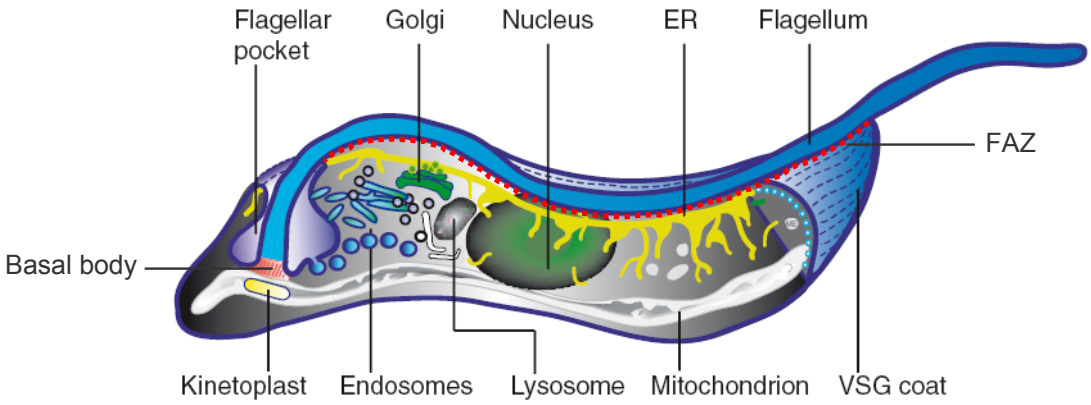

Figure 2. Schematic illustration of *T. brucei* Bloodstream forms. Extracted from "Endocytosis, membrane recycling and sorting of GPI-anchored proteins: *Trypanosoma brucei* as a model system". **Peter Overath and Markus Engstler**. **Molecular Microbiology. 2004 May; 53 (3), 735–744**

T. brucei contains a number of single copy organelles and structures: a single nucleus; a single flagellum which emerges from an invagination of the cell membrane known as the flagellar pocket; a single Golgi; a basal body associated a pro-basal body (immature); a single large and unique mitochondrion with the DNA mitochondrial referred as kinetoplast and four filamentous associated with the structures compromising the FAZ. All these structures organelles must be accurately duplicated and segregated if cell division is going to generate viable progeny [52]. As shown in figure 2, most of these organelles are concentrated between the centre and the posterior end of the cell [51].

The flagellar pocket is the only site of the cell membrane where endocytosis and exocytosis can occur. This peculiarity is due to the absence of cytoskeletal structure in this region [53,54]. Endosomes, lysosome and endoplasmic reticulum (ER), which compromised the whole cell, constitute the rest of organelles involved in vesicular trafficking [54].

The cell membrane is surrounded by a dense surface protein coat which varies in composition depending on the host where are living. In bloodstream forms is composed mostly by monolayer coat of VSGs which protect the parasites from host immune responses. This VSG coat is replaced by procyclin when the parasite differentiates to procyclic form and epimastigote form in tsetse fly (several isoforms of two different variants, one characterized for EP repeats and other for GPEET repeats; glutamic acid (E), proline (P), glycin (G), threonine (T)) [55]. Surface includes other proteins such as invariant surface glycoprotein (ISG65 and ISG75), transferrin receptor (TfR, two subunits ESAG6 and ESAG7-expression sites associated genes) [56,57,58], serum resistance-associated protein (SRA) [59], haptoglobin (Hp)–haemoglobin (Hb) receptor (HpHpR) [60], low-density lipoprotein (LDL) receptor [61], and cystein-rich acidic integral membrane (CRAM) protein [62,63].

2.3. Cell cycle.

In eukaryotic, the cell cycle consists in four phases: G_0/G_1 phase (*Gap0/Gap1)*, S phase (synthesis), G_2 phase (*Gap2 o* interphase) and M phase (mitosis). In the G_1 phase, the cell is growing, replicating cytoplasmic organelles and also preparing DNA replication by synthesizing the enzymes necessary to make the copies. DNA is replicated during S phase. In G_2 phase cells increase the biosynthesis process replicating and preparing cell division. Finally, in M the DNA is partitioned into two daughter cells. In mammalian cells, M phase is tightly coupled with cytokinesis which

starts just before chromosome segregation is completed. The activation of each phase is dependent on the proper progression and completion of the previous one. Cells that have temporarily or reversibly stopped dividing are said to have entered in a state of quiescence called G_0 phase [64].

In *T. brucei* G_1 phase, is characterized for cells having one nucleus, one kinetoplast, one flagellum and one Golgi apparatus (Figure 3) [52]. The first morphological event observed in the cell cycle progression is the elongation and maturation of the pro-basal body to a basal body and the nucleation of a new flagellum. This is followed by Golgi replication [64]. Kinetoplast S phase starts just before nuclear S phase, ending long before. During nuclear G_2 phase, kinetoplast segregation is produced. Then, the nucleus undergoes mitosis causing a cell with double genetic content which ends after cytokinesis in two identical daughter cells.

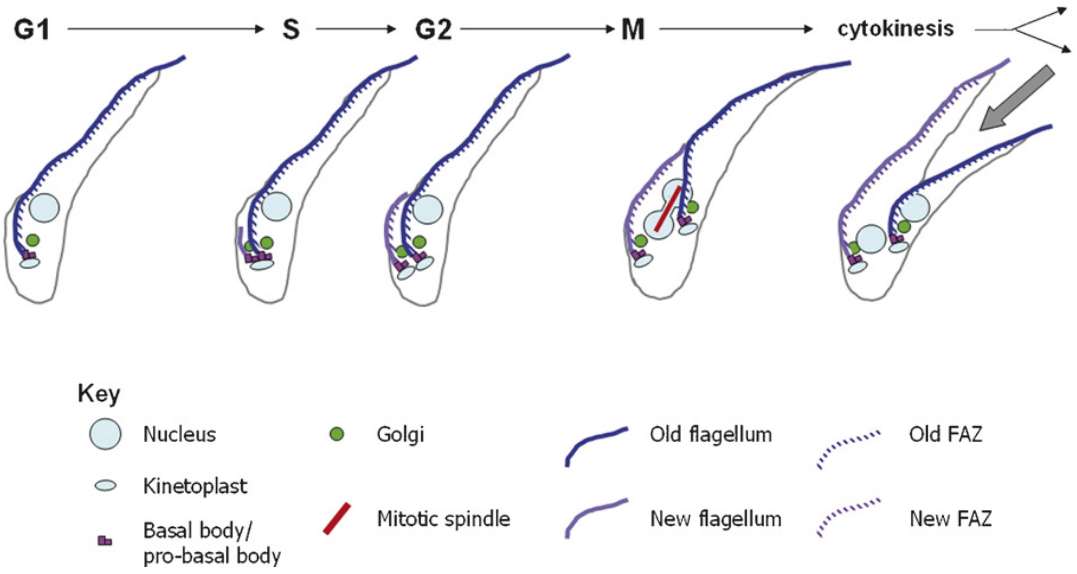

Figure 3. Schematic representation of the cell cycle phases, extracted from "Cell cycle regulation in *Trypanosoma brucei*". **Hammarton TC. Molecular Biochemical Parasitology. 2007 May; 153(1):1-8.**

2.4. Antigenic variation

T. brucei unlike to other protozoan parasites such as *T. cruzi* and *Leishmania*, lives and multiplies extracellularly in the bloodstream of the host being continuously exposed to antibody challenge. The dense surface protein coat offers to parasite a protective role against the host defense mechanisms as complement-mediated lysis. When the parasite lives in the mammalian host, presents in all its stages a monolayer coat composed of variant surface VSG [65].

A basic mechanism in the parasite ability to evade the host immune responses is called antigenic variation. Trypanosomes vary their surface coat, which consists of a single, tightly packed and highly immunogenic protein species (VSG) that covers their entire cellular surface [15]. In the mammalian-infective stage, trypanosomes express around 10^7 molecules anchored to the membrane through a glycosylphosphathidylinositol molecule (GPI) [66]. This dense coat prevents host recognition of conserved invariants proteins of the parasite membrane. The immune system has only access to the amine (N)-terminal region of the VSG, which is recognized as foreign antigen by specific B- and T-cell receptors. Generally a highly specific B-cell mediated antibody immune response is generated against to VSG epitopes. The antibody-mediated adaptive immune response eliminates most of the parasites.

However, some parasites spontaneously change the VSG coat and survive to this antibody-mediated response against the primary VSG. These parasites have undergone antigenic variation process. Due to different VSGs are distinct, this switcher parasite with a new VSG becomes a different antigenically parasite and has to be recognized as 'new' pathogen by the immune system. A new primary adaptive immune response must be generated to clear the parasites with new VSGs. The time required to generate this response, allows the parasite to proliferate and generate a new peak of parasitemia, and occasionally, change its VSG surface again. This mechanism permits the establishment of chronic cycles of infection in the mammalian hosts, thereby enhancing transmission to a new host.

Antibodies bind to VGS inducing fragment cristallizable (Fc) receptor-mediated phagocytosis by macrophages. However, the parasites remove efficiently immune surface-bound factors through capping and internalization (endocytosis) [67,68,69,70,71]. This process helps parasites to evade Fc-receptor-mediated phagocytosis but this is not enough.

The trypanosome genome contains hundreds of *VSG* genes but only one of which is expressed at a time. The *VSG* gene transcription only occurs in one of several polycistronic transcription telomeric *VSG* expression sites (*VSG*-ES). Thus, antigenic variation occurs either by gene conversion as consequence of *VSG* gene exchange from silent loci to the active expression site, or transcriptional switching between different *VSG*-ES (*in situ* activation) [15].

2.5. VSG structure.

As decribed above, the persistence of infection depends on VSG antigenic variation. VSGs have less than 25 % of amino acid sequence homology with each other. VSGs are GPI-anchored polypeptide of 400-500 amino acids which are made up for two domains. A highly variable N-terminal domain (300-400 amino acids) and a conserved carboxi (C)-terminal domain (100 amino acids) [72,73,74]. The C-terminal domain is attached to GPI anchor in the outer of the plasma membrane (Fig. 4) [66]. This conserved domain is a potential immune target, but it is masked by the N-terminal region when the maturated VSG is expressed on the surface. For this reason the conserved C-terminal domain does not compromise antigenic variation as the epitopes that can be recognized by the host antibodies are in the N-terminal domain. The VSGs have conserved cystein residues that do not affect of the antigenic variation [75]. In addition, *T. brucei*, has a N-glycosilation site, the asparagine-linked high mannose (Man_{5-9}) oligosaccharide that is common to all VSGs but it is inaccessible to conventional antibodies [76]. All these conserved structures are potential targets for the therapy of African trypanosomiasis.

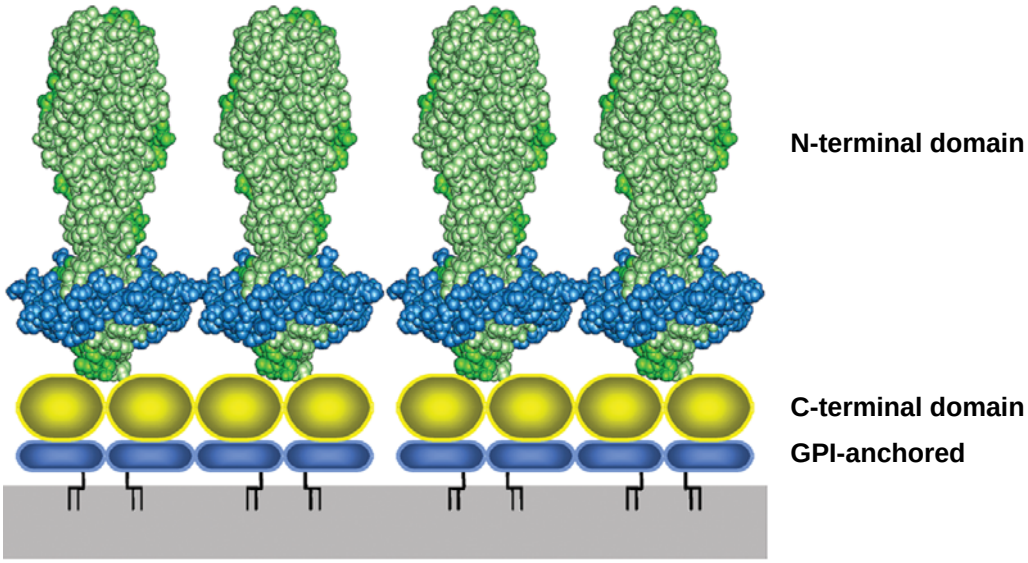

Figure 4. Schematic VSG structure, extracted from "Intracellular Membrane Transport Systems in *Trypanosoma brucei*". **Mark C. Field and Mark Carrington. Traffic. Aug 2004 ; 5: 905–913**

3. Endocytosis.

Survival of trypanosomes depends on the uptake of nutrients from their environment (tsetse fly or mammalian host) [63]. In *T. brucei*, endocytosis and

exocytosis are restricted to the flagellar pocket. Endocytosis is closely related to homeostasis of cell surface composition and with the evasion of immune response, because parasites remove host proteins and antibodies from the cell surface through capping and GIP-anchored VSG internalization-recycling process. Additional processes include: restriction of invariant receptors in the flagellar pocket, rendering them inaccessible to host immune effectors, and expression of receptors that can sequester innate immune factors [60,77,78,79]. In *T. brucei* receptor mediated endocytosis is a clathrin dependent mechanism [80,81]. RNAi directed against the *clathrin heavy chain*, causes rapid death of cells after massive enlargement of the flagellar pocket, resulting in what is known as *big eye* phenotype [80]. A similar phenotype is seen when *actin* is depleted by RNAi in bloodstream forms, implicating this protein in endocytosis and intracellular trafficking [53]. Endocytosis occurs in procyclic cells at a lower rate, and also is clathrin dependent [80,81]. Interestingly, directed RNAi is not lethal against *actin* in this life cycle stage [53].

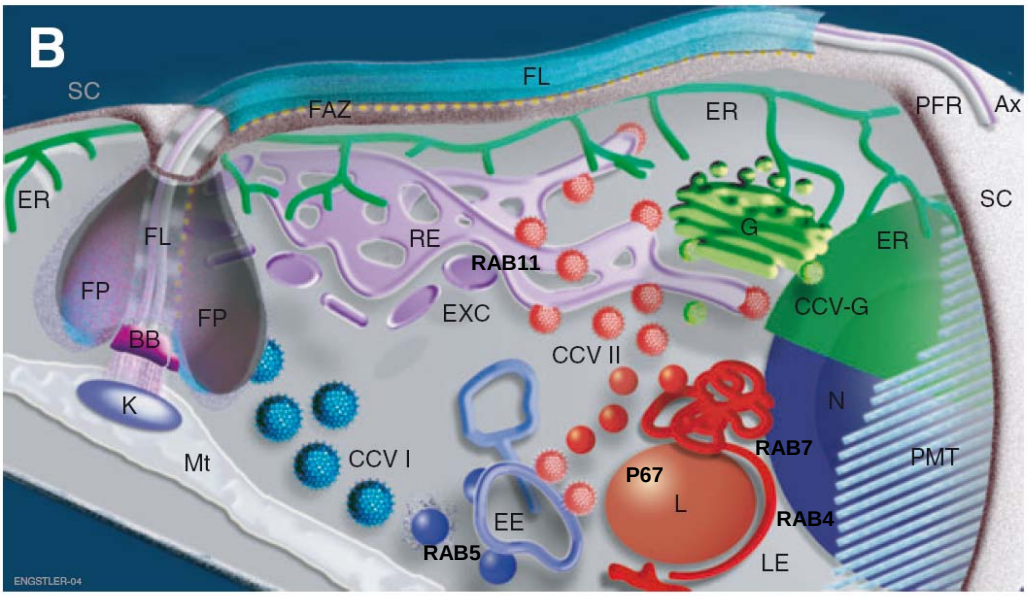

Figure 5. Schematic illustration of *T. b. brucei* Bloodstream endocytic and recycling trafficking. SC, surface coat. VSG, variant surface glycoprotein. Ax, axoneme. FL, flagellum. FP, flagellar pocket. FAZ, flagellar attachment zone. ER, endoplasmic reticulum. PFR, paraflagellar rod. PMT, pelicullar microtubule. BB, basal body. G, Golgi apparatus. K, kinetoplast. L, lysosome. Mt, mitochondrion. N, nucleus. CCV I, class I clathrin-coated vesicles EE, early endosome. LE, late endosome. CCV II, class II clathrin-coated vesicles. EXC, exocytic carrier. RE, recycling endosome. CCV-G, clathrin-coated vesicles budding from the Golgi apparatus. Extracted from "Endocytosis, membrane recycling and sorting of GPI-anchored proteins: *Trypanosoma brucei* as a model system". **Peter Overath and Markus Engstler**. **Molecular Microbiology. 2004 May. 53 (3), 735–744**

Trypanosomes have a highly polarized endocytic and recycling trafficking. Membrane proteins or flagellar pocket receptors are internalized by clathrin-coated vesicles (CCV-I, class I clathrin-coated vesicles) and delivered to a tubular endosome

network, the endomembrane system. Both, fluid phase and receptor-mediated endocytic cargo enter into an early endosomal compartment which is characterized for the presence of RAB5A/B [69,82]. Rab proteins are small GTPases (hidrolize guanosine triphosphate-GTP) that regulate vesicular transport in the eukaryotic endomembrane system [83,84,85]. After early endosome, the endocytic cargo is separated into small clathrin vesicles (CCV-II, class II clathrin-coated vesicles) for delivery into late endosomes; and in recycling endosomes, characterized for RAB11 [86], where cell surface proteins as VSG or TfR are recycled to the flagellar pocket. Late endosomes that transport soluble proteins as transferrin, IGS65 or IGS75, deliver the cargo into the lysosomal compartment to be degraded by acid hydrolase enzymes (peptidases). This trafficking until the lysosome is regulated by RAB4 and RAB7 [70,87]. The lysosome is characterized by the presence of p67 [88], a type I transmembrane glycoprotein which is essential in the function and structure of the lysosome [89].

4. Serum-resistant associated.

African trypanosomes, in addition to evade host immune responses through antibody endocytosis or antigenic variation, need to resist an efficient innate trypanolytic factor which is present in normal human serum (NHS). Humans are resistant to infection by the African trypanosome *T. brucei brucei*, but the subspecies *T. b. gambiense* and *T. b. rhodesiense* can avoid this innate immunity and cause the disease.

The innate human resistance to *T. brucei brucei* is due to two serum proteins, the specific Bcl-2 like protein apolipoprotein L-I (ApoL1) and haptoglobin-related protein (Hpr) [90]. These proteins are both associated with two serum complexes, a subfraction high densitiy lipoproteins (HDL) (specifically HLD3) and an IgM/apolipoprotein A-I (ApoA1) complex, respectively, termed trypanosome lytic factor (TLF) 1 and TLF2 [91,92]. The uptake mechanism of TLF1 is well characterized. Parasites have a trypanosome haptoglobin-hemoglobin receptor (TbHpHbR) required for parasite survival. In blood, hemoglobin (Hb) binds to the Hpr of the FL1. This formed complex binds to trypanosome HpHbR, undergoing the subsequent uptake by endocytosis. Once into parasite, produces parasite lysis [60]. Hpr acts as TLF1 ligand but the lytic activity is due to ApoL1 which form a protein pore [90]. The TLF2 uptake mechanism is not well understood but is proposed to be based on low affinity/high capacity interaction with the VSG coat explaining the trypanolitic effect by the rapid turnover of the VSG coat. Both factors can uptake by lipoprotein receptor pathway due

to TFL1 has HDL particles and TFL2 has some lipids and ApoA1. Uptake can occur through fluid-phase endocytosis [79].

T. b. gambiense and *T. b. rhodesiense* unlike to *T. b. brucei,* escape from NHS trypanolytic activity, being resistant. *T. b. gambiense* is permanently resistant to NHS. However, *T. b. rhodesiense* loses resistance when is inoculated in other animal but recover the resistance after injection of NHS [79]. The mechanism for the resistance recovery was associated with antigenic variation process. At the beginning was though that the VSG variant known as ETat 1.10 was the responsible of the resistance behavior. However, this was discarded because resistant clones expressed other VSG, including VSG expressed by NHS-sensitive clones. The selection of these trypanosomes in NHS implicated the switch of a specific *VSG*-ES, named *resistant (R)*-ES. This expression site enclosed the VSG variant ETat1.10; however the substitution of this gene kept the resistant mechanism showing that the *VSG* gene was not the responsible of the resistance. As every *VSG*-ES, *R*-ES contains several genes (*ESAG*) and one of them was identified as serum-resistance associated (*SRA*) which is selected for transcription in NHS [48,93]. This was confirmed after transfection of *SRA* into *T. b. brucei* (which is sensitive to NHS) acquiring the strain resistance to NHS [48]. *SRA* encodes a truncated VSG which has not surface-exposed loops. The product of *SRA* is a truncated VSG which accumulates in lysosomal compartment. The amino-terminal α-helix of SRA interacts with the carboxy-terminal α-helix of the apoL-I, neutralizing its activity within the lysosome [90].

T. b. rhodesiense is likely to have arisen as a clone of *T. b. brucei* that differs sole by its ability to express *SRA* on selection in human serum. *R*-ES is not active when the parasite is present in non-human sera [94]. *T. b. gambiense* does not carry *SRA* gene, despite its constitutive resistance to human serum [95]. Therefore, the resistance mechanism to lysis must be different from that of *T. b. rhodesiense*, and this mechanism is under investigation at present.

5. Peptidases.

Peptidases are a group of enzymes whose catalytic function is to hydrolyze peptide bonds of proteins. They are also named as proteolytic enzymes, proteinases, peptide hydrolases or more usually proteases. Peptidases participate in several physiological reactions ranging from simple digestion of proteins to highly regulated cascades.

The enzyme commission number (EC number), which identify peptidases, is EC 3.4. The first number defines the enzyme type, and the second, the target substrate (Nomenclature Committee of the International Union of Biochemistry and Molecular Biology). There are two sets of peptidases subclasses: the exopeptidases, enzymes that cleave peptide bonds at the amino- or carboxy-terminus, and the endopeptidases, which cleave peptide bonds internally in a polypeptide. The majority of peptidases are endopeptidases and these, in turn, are classified based on their catalytic mechanism into six groups: serin endopeptidase; cystein endopeptidase; aspartic endopeptidases; metalloendopeptidases, threonine endopeptidases and the last group enclosed those whose reaction mechanism has not been completely elucidated. By contrast, the *MEROPS* nomenclature is a structure-based classification where peptidases are grouped in families and the homologous families into clans.

5.1. Peptidases in African trypanosomes.

Peptidases in protozoan are considered virulence factors and are implicated in pathogenesis: immune evasion, absorption, penetration, infectivity, proliferation, nutrients uptake, etc…[96]. Currently are studied as candidates to be future therapeutic targets. The first evidences of peptidase activities in *T. brucei* were found during 1980's. The peptidase activities were identified in parasite extracts by their ability to cleave fluorescent peptide substrates and by the appearance on polyacrilamide gel containing protein substrate [97,98]. Nowadays, the major groups of *T. brucei* peptidases are metallopeptidases, threonine peptidase, serine peptidases and cysteine peptidases. The development of a new generation of drug to overcome trypanosomiasis is completely necessary; being peptidases suitable targets to focus the research.

- *T. brucei* has three zinc-metallopeptidases (*TbMSP*) genes: *TbMSP-A, -B* and *–C*, whose expression varies according to life cycle stage [99]. TbMSP-B is surface protein detected in procyclic trypanosomes and during differentiation of bloodstream trypanosomes to the procyclic form, but is not present in bloodstream trypanosomes. This zinc-metallopeptidase TbMSP-B and a phospholipase C, which cleave GPI-anchored proteins act in concert to remove native VSG during differentiation of short stumpy bloodstream trypanosomes to procyclic forms [100,101]

- Threonine peptidases are present in the proteasome which plays a major role in the degradation of many proteins involved in cell cycle, proliferation and apoptosis. Proteasomes also breakdown abnormal proteins that result from oxidative stress

and mutations that might otherwise disrupt normal cellular homeostasis. *T. brucei* proteasome has substrate specificity different to mammalian proteasome. Trypanosome proteasome exhibits high trypsin-like but low chymotrypsin-like activities which is the opposite that occurs in mammalian proteasome [102,103]. Proteasome inhibitors have reported trypanocidal activity by blocking cell proliferation due to the interruption of trypsin-like activity [104].

- Cysteine peptidases are characterized by the presence of a catalytic cysteine residue. All cysteine peptidase are grouped in the clan CA (*MEROPS data base*). Among them, the C1 family, that includes the lysosomal cathepsin L-like and cathepsin B-like peptidases, is the most studied in trypanosomatids The major group of lysosome cathepsins L-like are referred as evansain in *T. evansi* ; two congopain (CP1 and CP2) or trypanopain-Tc in *T. congolense* [105]*;* rhodesain in *T. brucei rhodesiense* and brucipain, also known as trypanopain–Tb, in *T. brucei brucei* [106,107]. *T. brucei* have an important cathepsin B-like enzyme, TbCatB, which is located in endosomal-lysosomal vesicles. Treatment of parasites with the cysteine protease inhibitor, benzyloxycarbonyl-phenylalanyl-alanyl diazomethane (Z-Phe-Ala-CHN_2)$_2$ was lethal *in vitro* and *in vivo* to *T. brucei* [108]. Parasites treated with this inhibitor exhibited altered cell morphology, were unable to undergo cytokinesis and were defective in host protein degradation [109] . Knockdown of *TbCatB* expression by RNAi was lethal in *T. brucei*, causing phenotypic defects similar to those seen with the inhibitor [110]. In contrast, knockdown of *rhodesain* expression produced no abnormal phenotype in cultured parasites [110]. Furthermore, RNAi of *TbCatB* was able to rescue mice from a lethal *T. brucei* infection [111]. These results indicate that among the two cystein proteases of the Clan CA family present in *T. brucei* cathepsin B is a key target of the protease inhibitor.

- Serine peptidases: *T. b. brucei* African trypanosomes also contain a serine oligopeptidase, Oligopeptidase B (TbOPB) [112]. It is a serine peptidase released into the plasma of infected animals that has been postulated to participate in the pathogenesis of the disease [113]. It has been reported trypanocidal activity of serine peptidases inhibitors and this peptidase has been identified as target of several trypanocidal drugs as pentamidine, suramine and diminazene [114,115].

6. Nicotinamide.

Nicotinamide (NAM), the amide form of vitamin B3 (niacin), serves to rapidly synthesize NAD through the salvage pathway once taken up by cells [116,117]. It has

been shown to positively affect cell survival in a variety of cell types. NAM promotes maturation of foetal cells [118] and induces proliferation and differentiation of embryonic stem cells to yield insulin-producing cells [119]. It also enhances an adaptive response to physical and chemical damage [120], protects brain cells from oxidative damage caused by reperfusion after ischemic infarction [121,122,123], and prevents injury of pancreatic islet cells during free radical exposure [124]. During disorders that include immune system dysfunction, diabetes, and aging-related diseases, nicotinamide is a robust cytoprotectant that blocks cellular inflammatory cell activation, early apoptotic phosphatidylserine exposure, and late nuclear DNA degradation. NAM is a soluble vitamin that is taken orally and cross the BBB. In fact, it is considered as a broad-spectrum neuroprotector.

NAM has also anti-microbial activity at millimolar concentrations against *Mycobacterium tuberculosis* [125], HIV [125,126], *Leishmania* [127,128], *T. cruzi* [129] and *Plasmodium* [130] but the mechanism of action has not yet been elucidated. As a general feature, nicotinamide inhibits ADP ribosylation reactions. Protein ADP ribosylation can occur in the nucleus, in the cytoplasm, and on the cell surface of lymphocytes. The activity of Poly (ADP-ribose) polymerase (PARP) is critical to the integration of foreign DNA, including proviral DNA as HIV case. The inhibition or absence of this enzyme interrupts the HIV life cycle [131], therefore NAM may be involved in this mechanism. The antimicrobial action of nicotinamide might also work through the modulation of certain sirtuins protein. Family of enzyme which catalyze with double deacetilase and ribosyl enzymatic activity that use NAD and nicotinamide is a product of reactions which catalyze. In *Plasmodium falciparum* the inhibition of the sirtuin known as PfSir2 delayed significantly *in vitro* parasite growth [130]. In the cases of *Leishmania* [127] and *T. cruzi* [129] the NAM inhibitory effect on growth is related which their specific sirtuins. This anti-microbicidal effect linked to toxicity absence, orally available, and inexpensive cost may help to use NAM as adjuvant in several infectious diseases. All of these microbicidal effects are associated to inhibition of rybosil tranferase enzymes

7. Nanobodies.

The typical functional antibodies (immunoglobulins) of all vertebrates are heteromeric molecules composed of two identical heavy (H) and two identical light (L) chains [132,133]. In 1993, in Vrije University of Brussels (Belgium), Hamers-Casterman *et al*. published [134] that *Camelidae* species (*Lama glama, Lama guanicoe; Vicugna pacos, Vicugna vicugna; Camelus bactrianus* and *Camelus dromedarius*) contained a

fraction of functional antibodies composed solely of H-chains (Fig. 6A). These immunoglobulins are referred as heavy-chain antibodies (abbreviated HcAbs). The HcAbs are not exclusive of camelids, cartilaginous fishes (sharks, skates, rays, and chimeras) have an unusual heavy chain homodimeric immunoglobulin isotype called IgNAR (Immunoglobulin new antigen receptor) [135,136].

Camelidae HcAbs are homodimers where each monomer unit (H-chain) has an antigen-binding fragment (Fab fragment) reduced to one single variable domain (VHH or nanobody® Ablynx) in contrast to conventional antibodies where the fragment Fab fragment is composed of one constant (C) and one variable (V) domain from each antibody's H and L-chain (Fig. 6A) [134,137,138]. In 1997, Vu et al [139] analyzed the sequence of the cDNA, obtained from peripheral blood mononuclear cells (PBMC) RNA isolated from dromedary and llama. They found the absence of the entire constant domain 1 (CH1) in HcAbs; reporting the direct join of the maturated VHH-DJ with the hinge region followed by the fragment crystallizable region (Fc). The sequence of CH1 domain is present in the camelids genome, however is spliced out during the messenger RNA processing due to a single mutation of the canonical splicing site at the 3' CH1/intron border [140,141].

Hence, the H-chain of HcAbs is composed, instead of four globular domains, of three globular domains: the VHH, a hinge region and two constant domains of the Fc (CH2 and CH3) (Fig. 6A). These Fc domains are highly homologous to the Fc domains of conventional antibodies although in camelids are encoded in different gene sets [140]. The organization, among VH (H-chain's variable domain of conventional antibody) and VHH is remarkably similar. Both are composed of four conserved sequences, the framework regions, surrounding for three hypervariable regions, the complementarity determining regions (CDR).

However, some differences are clear in the alignment of the VH and VHH amino acid sequences. First, CDR1 and CDR3 of the VHH are more extended than those of VH (Fig. 6B) [141]. Second, the VHH sequence carries important substitutions of highly conserved amino acids located in the framework-2 region which in conventional antibodies interact with the variable domain of the light chain [30] [142]. The hydrophobic residues Val42, Gly49, Leu50 and Trp52 in VH of conventional antibodies are substituted in the VHH of heavy-chain antibodies by the hydrophilic residues Phe/Tyr42, Glu49, Arg/Cys50 and Leu/Gly52 [137,143] (Numbering of the international ImMunoGeneTics-IMGT information system http://www.imgt.org corresponding to positions 37, 44, 45 and 47 in Kabat numbering, http://www.kabatdatabase.com). The presence of more hydrophilic amino acids in VHH explains the absence of association

with VL and the soluble behavior of VHH as a single-domain entity [137,142,143,144]. In addition, the hypervariable region loops of the VHH are substantially different in conformation, length and repertoire to those loops in human/mouse VH, being a mechanism to compensate the absence of the VH–VL combinatorial diversification in the HcAb [145,146,147].

The nanobodies (Nbs) are the smallest (2.5 nm of diameter and 4 nm of length) antigen-binding fragments (VHH) of camelids HcAbs that can be obtained. The isolation of Nbs of camelids HcAbs offers the possibility to generate fully active, stable, soluble, specific and high-affinity antibody entities without the common drawbacks of single domains fragments isolated from conventional antibodies.

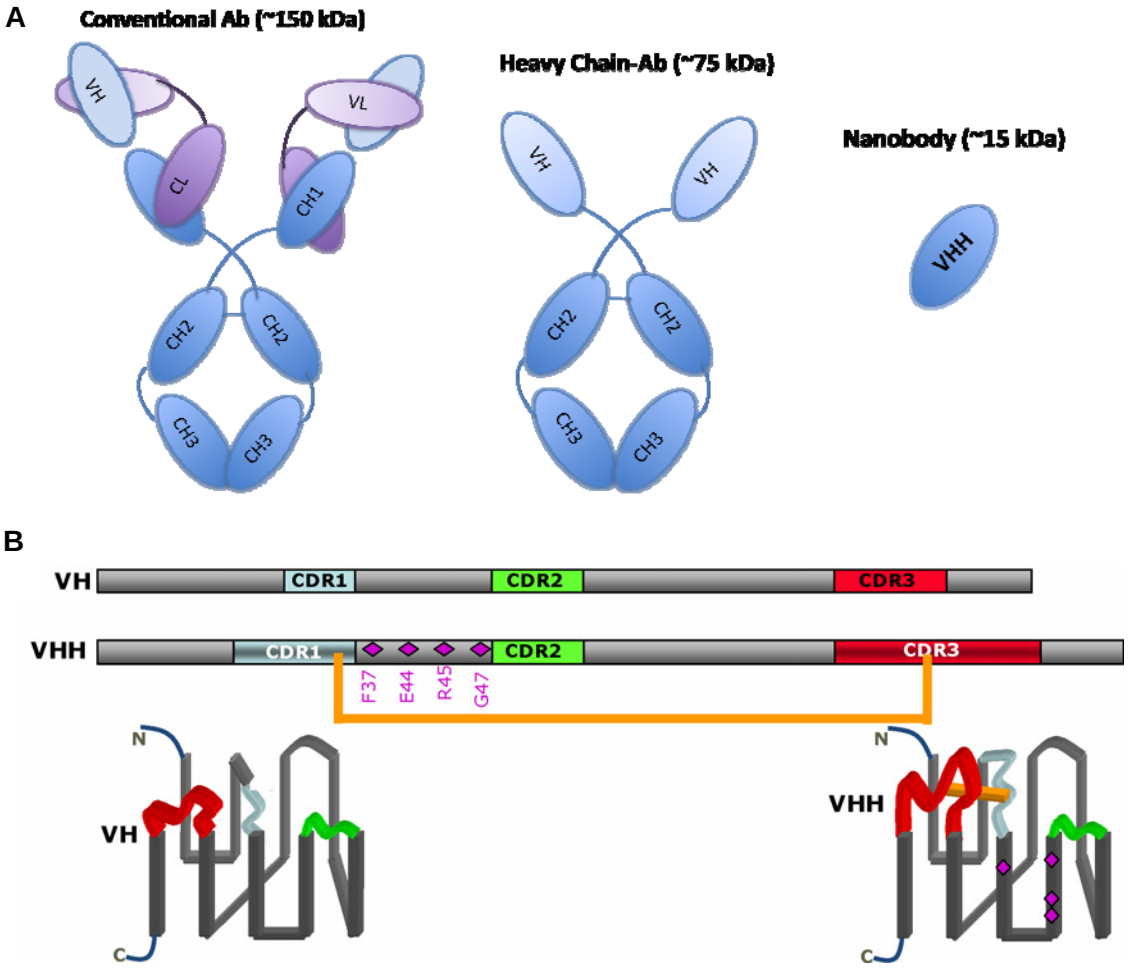

Figure 6. (A) From left to right the composition of a classical antibody (left), a heavy-chain antibody (middle) and a single-domain antigen-binding entity derived from a heavy-chain antibody, the VHH or nanobody (right). The domain structure within the H-chain and L-chains shown. **(B)** The sequence organization of the VH and VHH with framework and CDR's is schematically represented at the top of this panel. The hallmark amino acids in framework-2 within the VHH are given, as well as the inter-CDR disulfide bond occurring in the dromedary VHH. Below is the folded structure of the VH (left) and VHH domain (right with its four b-stranded sheet (back) and the five b-stranded sheet in front). The hallmark VHH residues in framework-2 are shown as squares. Extracted with some modifications from "Camelid immunoglobulins and nanobody technology" **S. Muyldermans. Veterinary Immunology and Immunopathology**. **2009. 178–183.**

Recombinant gene technology allows a high yield in the isolation of the genes encoding the antigen-specific Nb repertoire. The method consists of cloning, in phage display vectors, the Nb repertoire produced by peripheral blood lymphocytes of an immunized camelid and to select by biopanning antigen-specific Nbs [148,149]. The optimized protocol is fast and straightforward, and far superior to the selection of antigen binders from conventional antibodies avoiding the hybridoma technology. Moreover, Nbs are economically produced in bacterial, fungal or plant expression systems. Nbs are very stable and highly soluble, and bind their cognate antigen with high affinity and specificity. Nbs are expected to produce a low immunogenicity [150], however in order to reduce the possible immune response of Nbs when are injected into non-camelids host, they can be customized by altering specific amino acid sequences. In humans, Nbs can be humanized changing specific positions of the framework-2 reducing the risk of the induction of anti-nanobody antibodies in the circulatory system [151].

8. Alternatives therapies.

Resistant HAT can not be treated by increasing drug concentration due to acute side effects associated with chemotherapy. However, modifying the drug entrance route into the parasites could be a means to circumvent drug resistance mechanism associated to surface transporters. Some news alternatives could be used:

- **Nanobodies:** Nanobodies can be used to target biological active components [152,153]. For instance, the identified nanobody NbAn33, binds specifically to the conserved N-linked Man_{5-9} (oligomannose) carbohydrate of the VSG of *T. brucei,* making it an excellent candidate to target Trypanosomes [154,155]. A genetic fusion of NbAn33 to a truncated form of human apoL1 generated an immunotoxin with lytic activity against a wide range of trypanosomes [155]. Moreover, the internalisation of NbAn33 bound to its VSG specific epitope offers an alternative pathway to introduce trypanocidal agents into parasites avoiding the classical uptake mediated by cell surface transporters [71,156]. Nevertheless, direct conjugation between the nanobody and drug does not guarantee overcoming of biodistribution problems (mainly metabolization and elimination) and therapy toxicity.

- **Nanoparticles:** New therapeutic approaches for chemotherapy treatment have been focussed on the design of polymeric nanostructures as drug delivery systems. The polymers used include natural and synthetic materials and the main

characteristics required are biodegradability and biocompatibility. Nanoparticles are solid, colloidal particles consisting of macromolecular substances varying in size from 10 to 1000 nanometres. A drug can be dissolved, entrapped, adsorbed, attached or encapsulated into a nanoparticle. The advantage of using polymeric nanoparticles as colloidal carriers for advanced drug delivery is mainly their small size, which allows nanoparticles to penetrate even small capillaries and be taken up within cells, allowing efficient drug accumulation at targeted sites in the body. Also, the biodegradable polymers used for their preparation allow for sustained drug release at the targeted site over a period of days or even weeks after administration [157]. These carriers of chemotherapeutic agents enhance the effectiveness of the treatment, minimizing toxicity and preventing the biological metabolization and elimination [158]. Nanoparticles can also enhance drug transport and distribution by offering the possibility of drug targeting by modification of surface charge with inserted ligands, such as antibodies, surfactants, polymers and others [159]. Antiparasitic drug loaded nanoparticles have been used to combat parasitic infections such as leishmaniasis and animal African trypanosomiasis, even NPs are being postulated as carriers of anti-*Leishmania* vaccines [160,161,162].

OBJECTIVES

OBJECTIVE A: *NICOTINAMIDE*.

Trypanocidal effect of nicotinamide in *T. brucei*: phenotype and target identification.

OBJECTIVE B: *NANOBODY LIBRARY*.

Generation of nanobody phage display library constructed against recombinant *T. brucei* Oligopeptidase B.

OBJECTIVE C: *NANOBODY-COATED NANOPARTICLES*

Preparation and evaluation of pentamidine-loaded functionalized PEGlycated-chitosan nanoparticles coated by a nanobody that target the surface of *T. brucei*.

MATERIALS AND METHODS

Objective A: Trypanocidal effect of nicotinamide in *T. brucei*: phenotype and target identification.

A.1. Ethics statement.

Animal studies were conducted in accordance with the recommendations in the Guide for the Care and Use of Laboratory Animals of the National Institutes of Health. Experimental protocols were approved by the Ethics Committee of the Spanish Council of Scientific Research (CSIC).

A.2. Cell culture.

Wild type 427 bloodstream form trypanosomes were grown in axenic culture at 37° C and 5% CO_2 in HMI-9 media supplemented with 10% heat-inactivated foetal bovine serum (Gibco). Pleomorphic bloodstream *T. brucei* AnTat1.1 (Institute of Tropical Medicine, Belgium) was used throughout the *in vivo* experiments.

A.3. Trypanotoxicity assays.

The growth of bloodstream form trypanosomes was monitorized during three days under axenic culture conditions in medium with or without nicotinamide. Each subculture was initiated at an initial density of 1 x 10^4 parasites/ mL. Parasites were maintained at 37° C with 5% CO_2 in supplemented HMI-9 medium. Nicotinamide was added at the appropriate concentration dissolved in the same medium and the mean number of viable parasites was determined daily by counting the cells with an optical microscope with Neubauer chamber.

Nicotinamide (NAM) susceptibility was assessed using resarzurin sodium salt, modifying the procedure developed by Raz et al. [163]. Bloodstream trypanosome forms at an initial density of 1 x 10^4 parasites/mL were placed into 96-well tissue culture plates containing 100 µL supplemented HMI-9. Cells were incubated with different concentrations of NAM for 72 h at 37° C and 5% CO_2. Then, 20 µL of 0.5 mM resarzurin dye (Sigma, R7017) was added to each well and plates were incubated for a further 4 h. The reaction was stopped by adding 50 µL of sodium dodecyl sulfate (SDS) 3% and then read on a Tecan Infinite F200 reader (Tecan Austria GmbH, Austria) using an excitation wavelength of 535 nm and an emission wavelength of 590 nm [164]. Each test was set up in triplicate and repeated six times. Half-inhibitory

concentration (IC50) values were calculated using GraphPad Prism5 Software and defined as the concentration of drug required to diminish fluorescence output by 50%.

Morphological phenotype and different phases of the cell cycle were analyzed by fluorescence and optical microscopy (DIC -Differential Interference Contrast-). After different times of NAM treatment, parasites were fixed in 4% paraformaldehyde (PFA). Then, trypanosomes were washed three times and spread on poly-L-lysine-coated slides and mounted in DAPI-containing Vectashield medium (Vector Laboratories, Burlingame, CA, USA). Image acquisition was performed with an inverted Olympus IX81 microscope equipped with 3×/100× objectives and CCD camera (Orca CCD; Hamamatsu), and Cell R IX81 software. Two-hundred cells were counted per different time point. Parasites were classified according to the number of nuclei (N) and kinetoplast (K).

A.4. Cell cycle and DNA degradation by fluorescence-activated cell sorting.

DNA content was assed as described previously [165]. Treated and non treated *T. brucei* bloodstream forms ($2.5 \cdot 10^6$ cells, from each time point) were fixed in 900 µL of ice cool ethanol 70% and incubated on ice for at least 5 min, then washed with PBS and incubated with propidium iodide (PI) staining solution (PBS containing PI 40 µg/ mL and ribonuclease A -RNAse A- 100 µg/ mL) for at least 30 min. The analysis was performed with a FACScalibur flow cytometer (Becton Dickinson & Co., NJ, USA). Estimation of number of cells at G_1, S and G_2/M phases of the cell cycle was done with the BD CellQuest software. Percentage of DNA degradation was quantified base on the Sub G_1 subpopulation. Dot plots were performed using the FlowJo software. The experiment was done in triplicate and repeated at least three times.

A.5. Transmission electron microscopy.

Sample preparation for transmission electron microscopy was done as previously described [53]. Briefly, bloodstream trypanosomes (10^8) were fixed in 2.5% (vol/vol) glutaraldehyde 2% paraformaldehyde in 0.1 M sodium cacodylate buffer pH 7.2 for 24 h at 4° C and postfixed in 2% osmium tetroxide in the same buffer. Then, the samples were stained in 2% uranyl acetate for 2 h in the dark. After dehydratation in enreasing ethanol concentrations and clearing in propylene oxide, the samples were embedded in Embed 812 resin for 2 h and left to polymerize for 4 days at 60° C. Ultrathin sections (50 to 70 nm thick) were collected in Formvar-carbon-coated copper grids by using a Leica Ultracut R ultramicrotome and stained with uranyl acetate and lead citrate.

Observations were made on a TEM Libra 120 plus (Zeiss), and images were captured with a SSCCD 2K x K MegaView II camera and processed with AnalySIS and Adobe sofwares.

A.6. Acidic organelles staining.

Bloodstream-forms (10^6) treated with NAM at different time points were incubated in HMI-9 complete medium with 100 nM the acidotropic dye LysoTracker Green DND-26 (invitrogen) for 10 min at 37° C. Afterwards, the parasites were washed and resuspended in PBS. The fluorescence signal was measured by flow cytometry in a FACScalibur flow cytometer (excitation at 488 nm; emission between 515 and 545 nm) and the data analyzed with BD CellQuest software.

A.7. Fluid phase endocytosis assay.

The kinetics of fluid-phase endocytosis was measured as previously described [70]. Endocytosis was measured using fluorescein isothiocyanate-dextran average mol MW 10,000 (FD10S, Sigma). Bloodstream trypanosomes were treated with 50 mM NAM for 3 h and 6 h and untreated, used as control, were washed and resuspended in 0.5% BSA/ HMI-9 medium with FITC-dextran at 0.5 mg/ mL. Then, cells were incubated for 1 h at 37° C and fixed in 4% PFA. Fixed parasites were analyzed mounted onto poly-L-lysine slides and processed for immunofluorescence microscopy analysis.

A.8. Indirect immunofluorescence microscopy.

Immunofluorescence was performed as previously described by Landeira et al with some modifications [166]. Parasites were fixed in 4% PFA and permeabilized with 0.2% Triton X-100 in washing solution (PBS /1% Bovine serum Albumin-BSA-). Cells were then blocked with 1% BSA and incubated with the corresponding primary antibodies against p67 protein (mouse anti trypanosome) and BIP protein (rabbit anti trypanosome) both kindly provided by J. D. Bangs (University of Wisconsin-Madison, Madison, USA). Then, were washed and incubated with Alexa-488-labeled goat anti-mouse and Alexa-572-labeled goat anti-rabbit (Invitrogen). Finally, trypanosomes were washed three times and spread on poly-L-lysine-coated slides and mounted in DAPI-containing Vectashield medium (Vector Laboratories, Burlingame, CA, USA). Image acquisition was performed with an inverted Olympus IX81 microscope equipped with 3×/100× objectives and CCD camera (Orca CCD; Hamamatsu), and Cell R IX81

software. Deconvolution of 3D images was performed using Huygens Essential software (version 2.9; Scientific Volume Imaging).

A.9. Cloning, expression and purification of recombinant *T. brucei* cathepsin B-like in *Pichia pastoris*.

TbCatB construction was kindly provided by Dr. Zachary B. Mackey (University of California, USA). Methods for *TbCatB* cloning and expression of the recombinant TbCatB in *P. pastoris* have been described previously [167]. Briefly, the sequence encoding the TbCatB zymogen (pro and mature regions of the protease) was amplified from a cDNA vector that contained the entire open reading frame of *TbCatB* [110] with specific pair of primers forward (5'-GAG TAA ACG CCG CCC TCG TTG CT-3') and reverse (5'-CGC CGT GTT GGG TGC AAG AGG-3'). The amplified DNA was purified and ligated into expression vector pPICZαB (Invitrogen) and subsequent transfection and expression techniques were modified from those given by the manufacturer as previously described [107].

After 48 h of methanol induction, *P. pastoris* cultures were centrifuged at 3000 g for 10 min and the resulting supernatant containing recombinant TbCatB was lyophilized. The crude lyophilized protein was resuspended in 10% of the original volume in 50 mM sodium citrate buffer (pH 5.5) and desalted using PD-10 columns (GE Healthcare/Amersham Biosciences) by equilibrating in the same buffer. The solution was loaded onto a Mono Q 5/50 anion exchange column using an Akta Purifier-900 chromatography system (both GE Healthcare/Amersham Biosciences). A 50 mM MES (pH 6.5) buffer was used for column equilibration, sample loading, and protein elution, with a flow rate of 1 mL/min. Protein was eluted with a linear gradient of 0 to 1 M sodium chloride concentration over 20 min. Fractions of 0.5 mL were collected and subsequently checked for purity by SDS-PAGE.

A.10. Protease activity assay.

Protease activity was measured using the fluorogenic peptide substrate Z-Arginine-Arginine 7-amido-4-methylcoumarin hydrochloride (Z-Arg-Arg-AMC or Z-RR-AMC) which is cleaved by the protease to release free AMC fluorogenic leaving group. Briefly, *T. brucei* bloodstream forms (10^7 cells) were centrifuged, washed once in PBS containing 1% glucose and resuspended in a buffer containing 150 mM sodium phosphate, 200 mM NaCl, 5 mM ethylenediaminetetraacetic acid (EDTA) and 5 mM dithiothreitol (DTT), pH 6.0. Then, CHAPS at final concentration of 1% was added and incubated on ice 1 h [168]. The lysate was cleared by centrifugation at 13000 r.p.m. for

15 min at 4° C. A volume of 100 µL of supernatant containing the enzyme was preactivated in 1.8 mL of the same buffer (without CHAPS) for 10 min at 37° C and the reaction started by adding Z-RR-AMC substrate (bachem I-1135) at 10 µM final concentration. The release of AMC was measured at an excitation and emission wavelength of 350 nm and 460 nm respectively in a luminescence spectrometer (AMICO-BOWMAN). Three experiments were performed.

One-hundred nanograms of recombinant TbCatB were preincubated at 25° C for 10 min in sodium citrate buffer (50 mM, pH 5.5) containing 4 mM DTT, using different concentrations of NAM, giving a total volume of 100 µL. Following the preincubation period, 100 µL of dilute sustrate Z-RR-AMC (20 µM, prepared in the same buffer) was added to the enzyme solution to give a final concentration 10 µM and a final volume of 200 µL. Hydrolysis was measured each minute during 30 minutes at 25° C using an automated microtiter plate spectrofluorimeter (Perkin Elmer). Excitation and emission wavelengths were 350 and 460 nm, respectively. Each test was set up in repeated twelve times. IC50 values were calculated using GraphPad Prism5 Software and defined as the concentration of drug required to diminish fluorescence output by 50%.

A.11. Kinetics of transferrin uptake and degradation.

Bloodstream-forms were incubated in HMI-9 complete medium for 10 min at 37° C in presence of NAM. Non-treated parasites, as control, and parasites pre-treated with the specific inhibitor of TbCatB, Z-Phe-Ala-CHN_2 (Bachem, Heidelberg, Germany) at 10 µM, were assessed at the same conditions. Afterwards, the parasites were washed twice and resuspended in prewarmed trypanosome dilution burffer (TDB, 5 mM KCl, 80 mM NaCl, 1 mM $MgSO_4$, 20 mM Na_2HPO_4, 2 mM NaH_2PO_4, 20 mM glucose, and pH 7.4) at density of $8 \cdot 10^6$ parasites/mL. Transferrin from human serum Alexa Fluor-488 conjugated (molecular probes) was added to the suspension and the parasites were incubated at 37° C. At different times, samples of 250 µL were taken and fixed in 250 µL of ice-cool 5% PFA. The fluorescence was measured by flow cytometry in a FACScalibur flow cytometer (excitation at 495 nm; emission 519 nm). Relative fluorescence was calculated respect to the fluorescence value at time zero. Data are the means ± SD from three independent experiments.

A.12. Determination of ATP levels.

ATP was measured using a CellTiter-Glo luminescent assay (Promega), which generates a luminescent signal proportional to the amount of ATP present.

Bloodstream forms (10^5 per mL) were incubated with 50 mM NAM at the specified intervals. Aliquots of 90 µL parasites were then transferred to a white 96-well microplate, mixed with 45 µL of CellTiter-Glo reagent and incubated in the dark for 10 min at room temperature. Bioluminescence was measured using a Tecan® Infinite F200 reader (Tecan Austria GmbH, Austria).

A.13. Pyruvate flux measure (Glycolisis).

Bloodstream forms (10^8), washed twice with phosphate buffered saline (PBS), were resuspended in a buffer containing 44 mM NaCl, 57 mM K_2HPO_4, 3 mM KH_2PO_4, and 10 mM glucose. After 5 minutes at 37° C were centrifuged to remove the supernatant and resuspended in prewarmed buffer which contained 135 mM NaCl, 5 mM KCl, 5 mM, 1 mM $CaCl_2$, 1 mM $MgCl_2$ and 10 mM HEPES (4-(2-hydroxyethyl)-1-piperazineethanesulfonic acid)/Tris. Immediately, 1M glucose, 20 mM nicotinamide adenine dinucleotide (NADH) and lactate dehydrogenase (LDH) enzyme were added and the absorbance at 340 nm was started to be monitorized. The resulting pyruvate is subsequently converted to lactate by lactate dehydrogenase at the expense of oxidation of NADH and this oxidation of NADH to NAD^+ is monitorized as a decrease in absorbance at 340 nm. Five minutes after starting, NAM was added. The slope was used to check the piruvate flux.

A.14. Plasma membrane permeabilization.

Plasma membrane integrity was assessed by the entry of the vital dye SYTOX Green modifying the protocol described by Luque-Ortega and Rivas [169]. Briefly, the parasites were resuspended at a density of 4 x 10^5 parasites/mL in supplemented HMI-9 medium with 1 µM SYTOX Green at final concentration. A total of 100 µL of the cell suspension were transferred to 96-well microplate and incubated for 10 min at 37° C. The volume of each well was completed to 200 µL with prewarmed complete HMI-9 medium or with the same medium supplemented with NAM. The fluorescence, due to the binding of the dye to intracellular nucleic acids, was measured during 2.5 h at 37° C using 485-nm excitation and 520-nm emission, with an Infinite F200 microplate reader (Tecan Austria GmbH, Austria). Control for maximum fluorescence was achieved by addition of 0.1% Triton X-100.

A.15. Phosphatidylserine exposure assay.

Harvested control and NAM treated *T. brucei* bloodstream forms (2-5·10^5 cells/mL) were washed with annexin V binding buffer (10 mM HEPES, 140 mM NaCl,

3.3 mM $CaCl_2$) and resuspended in 100 µL. Five µL commercially available annexin V-FITC solution (Bender MedSystems) were added to each sample followed by incubation for 15 min in the dark at room temperature. After a final wash, the pellet was redissolved in annexin V binding buffer plus 10 µL PI (20 µg/ mL). Stained samples were immediately analyzed by flow cytometry using a FACSCalibur flow cytometer. Data were analyzed with FlowJo software.

A.16. *In vivo* therapy experiments.

Female C57BL/6J mice (8-week-old; Jackson Laboratories) were intra peritoneal injected with 5000 parasites of *T. brucei* pleomorphic strain AnTat1.1. NAM (12.2 mg/mouse) were i.p. administered every day starting 1 day after infection. Control mice received PBS. Survival was monitored every day. Parasitemia was determined daily by counting the number of trypanosomes in tail-vein blood with an optical microscope with Neubauer chamber.

Objective B: Generation of nanobody phage display library constructed against recombinant *T. brucei* Oligopeptidase B.

B.1. Camelid immunization.

An alpaca (*Vicugna pacos*) received six injections of 1 mg of recombinant *T. brucei* Oligopeptidase B (TbOPB) at weekly intervals. Serum was collected prior to each injection to follow the immune response against the immunogen. Forty-five days after the first injection, 50 mL of anti-coagulated peripheral blood was collected from the alpaca.

B.2. Isolation of peripheral blood mononuclear cells by density gradient centrifugation.

Anti-coagulated peripheral blood was diluted with sterile normal saline solution. The PMBCs were isolated by Ficoll-hystopaque density gradient centrifugation (dentisity 1,007 g/L, Sigma-Aldrich). Briefly, the diluted blood was loaded onto the gradient solution. After centrifugation at 800 g for 20 minutes without brake at room temperature, four layers were obtained. From the top: 1st plasma, 2nd PBMCs, 3rd Ficoll-hystopaque and 4th granulocytes and erythrocytes. The PBMCs layer was carefully collected and washed-twice with PBS at 200 g to remove the platelets. The PBMCs pellet was resuspended in 5 mL of PBS and counted in Neubauer camera.

B.3. Heavy chain's variable domain (VHH) of H-chain antibodies library construction.

B.3.1. RNA extraction and retrotranscription.

Total RNA from 10^7 of PBMCs was extracted using TRIZOL Reagent (Invitrogen) according manufacturing specifications. In the subsequence step, the first strand cDNA was synthesized from 40 µg total RNA using SuperScript III Reverse Transcriptase (Invitrogen) and Oligo-dT_{20} primer. Cycling parameters were: 1 cycle at 42° C for 60 min; 1 cycle at 70° C for 20 min.

B.3.2. Amplification of VHH sequences (Nbs repertoire).

Gene fragments encoding the variable regions (VH and VHH) up to the constant domain 2 of the heavy chains of all camelids immunoglobulins were amplified from

cDNA with the specific primers CALL001 (5'-GTC CTG GCT GCT CTT CTA CAA GG-3') and CALL002 (5'-GGT ACG TGC TGT TGA ACT GTT CC-3'). Polymerase chain reaction (PCR) was performed with FastStart Taq DNA polymerase (Roche) and the followings PCR parameters: 32 cycles at 94° C, 1 min; 55° C, 1 min; 72° C, 1 min. The PCR product of 700 base pair (bp) corresponding to the VHH-CH2 exon was purified and used as template in a second PCR. In order to amplify specifically the VHH sequences (Nanobodies repertoire). The nested primers were A6E (5'-GAT GTG CAG CTG CAG GAG TCT GGR GGA GG-3') and 38 (5'-GGA CTA GTG CGG CCG CTG GAG ACG GTG ACC TGG GT-3') which anneal to the framework-1 and framework-4 regions of the variable domains. These primers carried restriction sites (*Pst* I at the 5' end and *Eco91*I (*Bst* EII) at the end 3') to facilitate the next cloning step. PCR was performed with Fast Start Taq DNA polymerase (Roche) and the cycling parameters were: 20 cycles at 94° C, 1 min; 55° C, 1 min; 72° C, 1 min.

B.3.3. Cloning of Nbs repertoire into the phagemid vector pMES4.

First, 100 µg of the purified Nbs repertoire fragment and 60 µg of the phagemid vector pMES4 (GenBank: GQ907248.1) were double digested with *Pst* I (Fermentas) and *Eco91*I (*Bst* EII) (Fermentas). Ligation reaction was performed at 16° C, overnight, using T4 ligase (Roche). Ligation product was transformed by electroporation in fresh electrocompetent *Escherichia coli* TG1 cells (amber-TAG suppressor strain). Then, transformed cells were plated on big square (24 x 24 cm) LB-agar/ampicillin/glucose plates. To know the size of our library, ten-fold serial dilutions of the original transformed cells were made and 100 µL of dilutions 10^{-3}, 10^{-4} and 10^{-5} were plated on 90 mm diameter LB-agar/ ampicillin/glucose plates. After overnight incubation at 37° C, the library size was calculated multiplying the number of colonies obtained in each plate by the dilution factor and by the total of millilitres of transformed cells. All colonies from the big plates were collected and stored in LB/ampicillin with 20% glycerol at -80° C.

The percentage of colonies with the right insert size was determined by direct PCR on bacterial colonies (colony PCR). The primers used were MP57 (5'-TTA TGC TTC CGG CTC GTA TG-3') and GIII (5'-CCA CAG ACA GCC CTC ATA G-3') which anneal to Lac UV5' promoter and M13 gene III present in the flaking region of the pMES4 vector multiple cloning site. PCR was performed with Taq DNA polymerase (Roche) and cycling parameters were: 20 cycles at 94° C, 45 s; 55° C, 45 s; 72° C, 45 s.

B.4. Selection by biopanning of antigen-specific Nbs from phage display library.

B.4.1. Preparation of the phages.

The Nb library was displayed on phage particles after M13K07 helper phage infection of the transformed *E. coli* TG1 cells. This method produces virus particles with the cloned Nbs at their tips due to the M13 gene III of the phagemid pMES4 vector. Gene III encodes the M13 pIII protein, a virion surface protein located at one end of M13 tubular virion structure. It is a relative flexible and accessible molecule composed of two functional domains: an N-terminal domain that binds to the F pilus of bacteria during infection and a C-terminal domain buried within the virion that is important for morphogenesis [170,171,172]. Polypeptides can be inserted between the two domains of pIII [173] or near the N terminus [174] without destroying its functions in morphogenesis and infection.

Infected *E. coli* TG1 bacterias containing the library were growth to a mid-logarithmic in a medium supplemented with glucose which inhibits the Lac UV5 promoter and reduces the expression of the Nanobody-protein (PIII) fusion protein. This has two important effects: a reduction of toxicity due to PIII absence; and the inability possibility of infecting bacteria with phage because the inhibition of PIII expression allows the bacterial F pilus expression. Reached the logarithmic phase, bacterias were infected with an excess of M13K07 phages (helper phage:bacteria ratio 20:1). Then, glucose was removed from the medium to permit the Nanobody-PIII protein fusion expression. After overnight incubation, phages particles were isolated from the supernatant by PEG-precipitation. These phages were identified as phages from round zero. The concentration of Phage concentration was measured by optical density at 260 nm (1 O.D. = $3x10^{10}$ phage particles/ mL). Known phage particle concentration we proceed to perform the antigen selection.

B.4.2. Panning.

One well of Nunc MaxiSorp® (high protein-binding capacity polystyrene) flat-bottom 96 well enzyme link immunosorbent assay (ELISA) plate was coated with 5 µg of recombinant TbOPDB (antigen). After blocking with PBS with 2% of milk powder for 2 h at room temperature, 10^{11} phage particles from round zero, were added and incubated to allow specific binding between the antigen (Ag) and Nbs-phages. After binding, Ag-specific phages were eluted with 100 mM triethylamine (pH 11.0) and

transferred into a sterile tube and neutralized with 100 µL of 1.0 M Tris–HCl (pH 7.4). The same protocol was performed in simultaneous on uncoated well to compare the number of unspecifically bound phage particles. The eluted phages from the coated well were identified as phages from 1st round of panning. The same protocol was reproduced from each round of panning.

B.4.3. Amplification of the eluted specific phages for the next round of panning.

Specific antigen phage particles eluted from panning were used in the re-amplification step to perform new rounds of panning. The eluted phage particles from the previous round were added to exponential growing *E. coli* TG1 cells in presence of glucose. After infection, glucose was removed and the infected cells were incubated overnight at 37° C at 225 r.p.m. to multiply specific antigen phage particles. Three of rounds of panning were performed.

B.4.4. Infection of *E. coli* TG1 cells with eluted phages to calculate the antigen specific enrichment.

To know the antigen specific enrichment of the round of panning, phage particles eluted from the Ag coated and uncoated wells were ten-fold serial diluted ($0.1\text{-}10^{-7}$) and used to infect *E. coli* TG1 cells. Infected cells were streaked on a square (10 x 10 cm) LB-agar/ampicillin/glucose plate. Uninfected *E. coli* TG1 cells were streaked at the bottom of the plate (see figure 16). After overnight incubation at 37° C, phage enrichment was assessed by comparing the number of colonies growth from phages eluted from Ag coated wells versus uncoated wells [174].

B.4.5. Enrichment phage ELISA.

The antigen specific enrichment after each round of panning (explained above), was checked by ELISA. As many wells as rounds of panning plus blank were coated with 100 ng of recombinant TbOPDB in a Nunc MaxiSorp® flat-bottom 96 well ELISA plate. The same numbers of coated and uncoated wells were blocked with PBS with 2% of milk powder for 2 h at room temperature. From each round of panning, 10^{10} eluted phages particles were added to the corresponding coated and uncoated wells. The same procedure was applied to the blank but adding M13K07 helper phages without Nbs. Detection of bound phage particles was performed with horseradish peroxidase (HRP) conjugated anti-phage (M13) mouse monoclonal antibody (mAb). ELISA development was carried out with ABTS (2,2'-azino-di-(3-ethylbenzothiazoline-

6-sulphonate)) /H_2O_2 solution substrate of HRP. After 5 minutes in the dark, the plate was read at 405 nm three times each five minutes.

B.5. Identification of good binder nanobodies.

B.5.1. Periplasmic extract (PE) ELISA of the individual colonies.

In each round of panning, the infected cells with phage dilutions from 10^{-3} to 10^{-7} (section **B.4.4.**) were used to identify high affinity binders. Several colonies were induced with Isopropyl β-D-1-thiogalactopyranoside (IPTG) to express soluble Nb. The isolation of periplasmic extracts containing the expressed Nb was performed by an *osmotic shock*. The analysis of the periplasmic fraction (Periplasmic extract-PE) with the possible Ag-specific Nb was carried out by ELISA. Two controls, consisting in untransformed TG1 cells and empty pMES4 transformed TG1 cells, were analyzed at the same time. Wells of four rows of a Nunc MaxiSorp® flat-bottom 96 well ELISA plate were coated with 100 ng of recombinant TbOPDB and other four rows wells were left uncoated. After blocking with PBS with 2% of milk powder, 100 µL of PE from each colony were added to one coated and one uncoated well. The detection of soluble Ag-specific Nbs in PEs was performed using an anti-hemagglutinin (HA) tag mouse mAb primary antibody and an alkaline phosphatase (AP) conjugated anti-mouse secondary antibody. ELISA development was performed with 200 µg of AP-substrate in AP blot buffer. After 15 min in the dark, the plate was read at 405 nm three times each five min.

B.5.2. Phage ELISA in microtiter plates over positive clones to PE-ELISA.

The positive clones to PE-ELISA were seeded in a flat bottom 96-well microtiter plate. After growth in presence of glucose, $2x10^9$ M13K07 helper phages were added to each well to infect the cells. Then, the glucose was removed and the cells were incubated overnight to multiply specific antigen phage particles. The supernatant with the particles of phages containing the specific nanobodies on their tips were tested by ELISA. In this plate were seeded two controls: untransformed TG1 cells and TG1 cells transformed with empty pMES4 vector (without Nb cloned). The protocol was realized as describe in section **B.4.4.** However, the developed was performed using TMB (3,3′-5,5′-Tetramethylbenzidine) HRP substrate and the reaction was stopped with 2N H_2SO_4. After 15 min in the dark, the plate was read at 405 nm, three times each five min.

B.6. Sequencing.

The positive colonies tested as binders in the PE-ELISA were analyzed by colony PCR using the same protocol describe in section **B.3.3.** PCR products of analyzed colonies with the correct size (~700 bp) were cleaned up using ExoSAP-IT protocol. This protocol employs two hydrolytic enzymes: Exonuclease I, which removes residual single-stranded primers and any irrelevant single-stranded DNA produced in the PCR reaction; and shrimp alkaline phosphatase (SAP), which removes the remaining deoxyribonucleotide triphosphate (dNTPs) from the PCR mixture. The sequencing was perfomed using MP57 primer. The sequence analysis of the sequences was performed using two softwares: MEGA4 (Molecular Evolutionary Genetics Analysis software version 4.0.) and Serial Cloner 2.5.

Objective C: Preparation and evaluation of pentamidine-loaded functionalized PEGlycated-chitosan nanoparticles coated by a nanobody that target the surface of *T. brucei*.

C.1. Preparation of nanobody-coated pentamidine-loaded functionalized PEGlycated-chitosan nanoparticles.

Synthesis of copolymer chitosan-*g*-PEG: Chitosan hydrochloride (80 mg) was dissolved in 11.5 mL of deionized and filtered water. Methoxy polyethylen glycol carboxylic acid (MeO-PEG-CH_2CO_2H) (14.2 mg) and *N*-hydroxysuccinimide (NHS, 1.6 mg) were then added to the solution. 1-ethyl-3-(3-dimethylaminopropyl) carbodiimide (EDC, 21.7 mg) was then added gradually, and the resulting solution was stirred at room temperature for 22 h. Finally, the solution was ultrafiltered and lyophilized.

PEGlycated chitosan nanoparticles were prepared by a coacervation method avoiding the use of toxic organic solvents [175]. Briefly, the copolymer chitosan-*g*-PEG (1%, w/v) was dissolved in 10 mL of double distilled water (DDW). Then pluronic F-68 and pentamidine were added to the solution at final concentration 1% (w/v) and 0.01 M, respectively. About 2.5 mL of a solution of sodium sulphate (20%, w/v) was added dropwise (0.5 mL/ min) to the chitosan solution under mechanical stirring (2,000 rpm). The stirring was continued for 1 h to ensure the formation of pentamidine loaded functionalized PEGlycated-chitosan nanoparticles (pentamidine-chNPs). Then, the pentamidine-chNPs were cleaned by 3 consecutive cycles of centrifugation (30 min at 11,000 r.p.m. in centrifuge machine Centrikon T-124 high-speed centrifuge; Kontron, Paris, France) and re-dispersion in DDW, until the conductivity of the supernatant was ≤ 10 µS/ cm (conductimeter Crison micropH 2001, Spain). Finally, a nanobody (NbAn33) solution at 1 mg/ mL was added to the pentamidine-NPs suspension. The reaction was left 3 h at 25 ± 0.5° C under mechanical stirring (200 r.p.m.). Then, 10 mL of physiological serum pH 7.4 were added to the suspension and a unique centrifugation cycle was performed (30 min at 11,000 r.p.m. in centrifuge machine Centrikon T-124 high-speed centrifuge; Kontron, Paris, France), obtaining the NbAn33-coated pentamidine-chNPs (NbAn33-pentamidine-chNPs). Non pentamidine-loaded nanoparticles were prepared in parallel to use as a blank (NbAn33-chNPs).

C.2. Nanoparticles characterization methods.

The geometry of the obtained NPs (size and shape) was studied by high-resolution transmission electron microscopy (HRTEM, microscopy STEM PHILIPS

CM20, Netherlands) and by field emission scanning electron microscopy (FeSEM, microscopy Zeiss DSM 950, Germany). Mean particle diameter (±SD) was determined by photon correlation spectroscopy (PCS, Malvern 4700 analyzer, Malvern Instruments, England).

The superficial electrokinetic properties of the NPs were analyzed by electrophoresis using a Malvern Zetasizer 2000 electrophoresis device (Malvern Instruments Ltd.). The electrophoretic mobility (u_e) measurements can distinguish qualitatively the type of pentamidine incorporation in the NPs: adsorption into the NP matrix or adsorption on the NP surface. Briefly, the measurements were executed over 0.1 % (w/v) aqueous suspensions of Nb33-chNPs and NbAn33-pentamidine-chNPs as a function of pH and ionic strength [110]. These measurements were performed after 24 h of contact of NPs in water under mechanical stirring (50 r.p.m.) at 25 ± 0.5° C. The experimental uncertainty of the measurements was below 5%. The theory of O'Brien and White was used to convert the electrophoretic mobility (u_e) into zeta potential (ζ mV) values.

C.3. Determination of pentamidine loaded into the chitosan nanoparticles.

The ultraviolet-visible spectrophotometry (UV-Vis) technique was used to quantify of the amount of pentamidine loaded to NPs (wavelength of maximum absorbance 261 nm) (spectrophotometer 8500 UV-Vis, Dinko, Spain). After, Nb33-pentamidine-NPs synthesis the supernatant was obtained by double centrifugation (30 min at 11,000 r.p.m. in centrifuge machine Centrikon T-124 high-speed centrifuge; Kontron, Paris, France) and the amount of pentamidine was measured by the described technique. Drug incorporation to NPs was expressed in terms of pentamidine entrapment efficiency (%) (Encapsulated drug [mg]/total drug in the NP suspension [mg] × 100) and pentamidine loading (%) (Encapsulated drug [mg]/carrier [mg] × 100).

C.4. *In vitro* release studies of pentamidine from chitosan nanoparticles.

The study of pentamidine released was performed using the NbAn33-pentamidine-NPs with the maximal entrapment efficiency reached. The assay was performed at 37 ± 0.5° C , in triplicate, following the dialysis bag method (Spectrum Spectra/Por 6, EE.UU.) using NaOH-KH_2PO_4 pH 7.4 ± 0.1 buffer as the release medium. The bags were soaked in water for 12 h before use. The dialysis bag with 2,000 Da of pore size retained the NPs, but allowed the free pentamidine to diffuse through the membrane into the release medium. Samples from the released medium

were taken at different times 0.5, 1, 3, 6, 9 and 24 h, and 2, 3, 4 and 5 days, and analyzed for the pentamidine content using UV–Vis (at 261 nm). An equal volume of release medium, at the same temperature, was added after taking the samples to ensure the sink condition.

C.5. Parasites.

Bloodstream-form of *T. brucei* monomorphic AnTat1.1 strain (Institute of Tropical Medicine, Belgium) and an *in vitro* pentamidine-adapted R25 strain derived from *T. brucei* AnTat1.1 strain were grown in axenic culture at 37° C and 5% CO_2 in HMI-9 medium supplemented with 20% heat-inactivated foetal bovine serum (Gibco) [176,177]. A stable drug resistance strain was developed from *T. brucei* AnTat1.1 strain after several months of selection by increasing pentamidine concentrations.

C.6. Immunofluoresce microscopy.

NbAn33 was labelled with Alexa 488 Fluor monoclonal antibody labeling kit (Molecular Probes) according to manufacturer's instructions. *T. brucei* AnTat1.1 parasites were harvested and resuspended at 4 x 10^6 parasites/ mL in TDB and kept in ice 30 min. An unstained sample was taken and fixed in 4% PFA at final concentration, before addition of Alexa 488-labelled NbAn33. Once added the Nb, parasites were incubated at 37° C and aliquots of 50 µL were taken at 0.5, 5 and 10 min and fixed immediately in 4% PFA at final concentration. Then, the remaining cell suspension was twice washed with prewarmed TDB by spin at maximal revolutions to remove Nb excess. Finally, the parasites pellet was resuspended in 150 µL of prewarmed TDB and incubated a 37° C. Immediately, an aliquot was taken and fixed corresponding to control point 15 min. The rest of the parasites were fixed at control points 20 and 25 min. After fixing, each sample was washed three times and spread on poly-L-lysine-coated slides. Then, they were mounted in DAPI-containing Vectashield medium (Vector Laboratories, Burlingame, CA, USA). Image acquisition was performed with an inverted Olympus IX81 microscope equipped with 3×/100× objectives and CCD camera (Orca CCD; Hamamatsu), and Cell R IX81 software. Deconvolution of 3D images was performed using Huygens Essential software (version 2.9; Scientific Volume Imaging).

C.7. Trypanotoxicity assay.

As described in **Materials and methods, objective A, point A.3** with some modifications. Exponentially growing parasites were harvested and prepared at initial

density of 2 x 10^5 trypanosomes per mL to ensure that cells were in logarithmic growth phase during the entire experiment. Then, 50 µL of trypanosome culture were added to each well of flat-bottom 96 well plate containing doubling dilutions of the drugs (50 µL), excepting for two rows which received only media. Eleven dilution points were tested, ranging from 680 µM to 165 pM in final pentamidine concentration. In the case of diminazene aceturate the range was between 2 µM and 2 nM. Cultured plates were incubated at 37° C in an atmosphere of 5% CO_2 for 20 h, before the addition of 20 µL of the colorimetric viability indicator resarzurin sodium salt (Sigma, R7017) at 0.5 mM. After further 4 h incubation, the reaction was stopped by addition of 50 µL of SDS 3%. The plates were read on a Tecan Infinite F200 reader (Tecan Austria GmbH, Austria) using an excitation wavelength of 535 nm and an emission wavelength of 590 nm. The experiment was performed with six replicates per concentration and repeated at least in three occasions. The results of fluorescence were normalized to the 100% of the control. The IC50 value was determined by log (inhibitor) vs. normalized response - Variable slope using the GraphPad Software.

C.8. *In vivo* therapy experiments.

Animal experimental protocols were approved by the Ethics Committee of the Spanish Council of Scientific Research (CSIC) as **Materials and methods, Objective A: nicotinamide, point A.1.** The drug delivery system NbAn33-pentamidine-chNPs was tested *in vivo* against monomorphic AnTat1.1 strain using a modification of the approach previously described [178,179]. Briefly, five female C57BL/6J mice (8-week-old; Jackson Laboratories) per group were intraperitoneally infected with 10^4 parasites. Once detected parasites in blood, at day 3 after infection, the mice were treated daily on four consecutive days. The dosages used for each group were pentamidine 2.5 $mg \cdot kg^{-1}$; pentamidine 0.25 $mg \cdot kg^{-1}$; pentamidine 0.025 $mg \cdot kg^{-1}$; NbAn33-pentamidine-chNPs 0.25 $mg \cdot kg^{-1}$ and NbAn33-pentamidine-chNPs 0.025 $mg \cdot kg^{-1}$. Control mice were either left untreated (physiologic serum) or received pentamidine-free NbAn33-chNPs. We followed the parasitemia by counting the number of trypanosomes in tail-vein blood with an optical microscope with Neubauer chamber every day during the first week, and afterwards, a once per week until 60 days post-infection. Mice survival was monitored and recorded every day until 60 days post-infection. Mice were considered cured when there was no parasitemia relapse detected in the 60 days period.

C.9. Molecular biology.

Trypanosomes bloodstream forms were harvested from culture. RNA was extracted using TRIzol reagent (Invitrogen Life Technologies), according to the manufacturer's protocol. For first strand cDNA synthesis, SuperScript III Reverse Transcriptase (Invitrogen) was used with Oligo-dT_{20} primer. Genomic DNA was extracted using DNAzol reagent (Invitrogen), according to the manufacturer's protocol. The *TbP2/AT1* (adenosine transporter 1) complete genomic sequence (TriTrypDB Tb927.5.286b) was amplified by PCR using the specific primers AT1F (5' ATG CTC GGG TTT GAC TCA GC 3') and AT1R (5' CTA CTT GGG AAG CCC CTC AT 3') [180]. The PCR was performed with AccuTherm™ DNA polymerase (Genecraft Germany) with the followings parameters: 1 cycle of 95° C for 2 min and 35 cycles of (95° C, 50 s; 50° C, 50 s; 72° C, 2.5 min). To determine the expression of *TbAT1/P2* a RT-PCR, using the synthesized cDNA, was performed using the AT1F primer and AT1seq2 (5' CAT ACT TGT AGT ACT CGA TG 3'). Thermal cycling was carried out as follows: 1 cycle of 95° C for 10 min and 35 cycles of (95° C, 50 s; 47° C, 50 s; 72° C, 2.5 min). The PCR products were purified and sequenced. The *AQP2* (Aquaglyceroporin 2) (TriTrypDB Tb927.10.14170) and *AQP3* (Aquaglyceroporin 3) complete genomic sequences (TriTrypDB Tb927.10.14160) were amplified with AccuTherm™ DNA polymerase (Genecraft Germany) using the forward primer AQP2/3F (5' GCT CCA GAA AAT CAG AAT GC 3') and the reverse primers AQP2R (5' GCG AAG GGT ATT GAC GGT TA 3') and AQP3R (5'- GTG CCA CAC TAA TCT GCA TG -3'), respectively. The PCR conditions were: 1 cycle of 95° C for 2 min and 35 cycles of (95° C, 50 s; 47° C, 50 s; 72° C, 2.5 min). The PCR products were purified and sequenced. Two internal forward primers were designed to confirm the chimeric *AQP2/AQP3* sequence; AQP2Fi (5' GAG CGG TGG GAT GCA GAT G 3') and AQP3Fi (5' CGC CAC GGT TAT CAT TGA TGG G 3').

RESULTS AND DISCUSSION

<u>Objective A</u>: Trypanocidal effect of nicotinamide in *T. brucei*: phenotype and target identification.

A.1. Results.

A.1.1. NAM inhibits cell growth and induces morphological changes in bloodstream forms of *T. brucei*.

The trypanocidal effect of NAM on *T. brucei* bloodstream cells was evaluated by measuring parasite mediated reduction of resarzurin sodium dye.

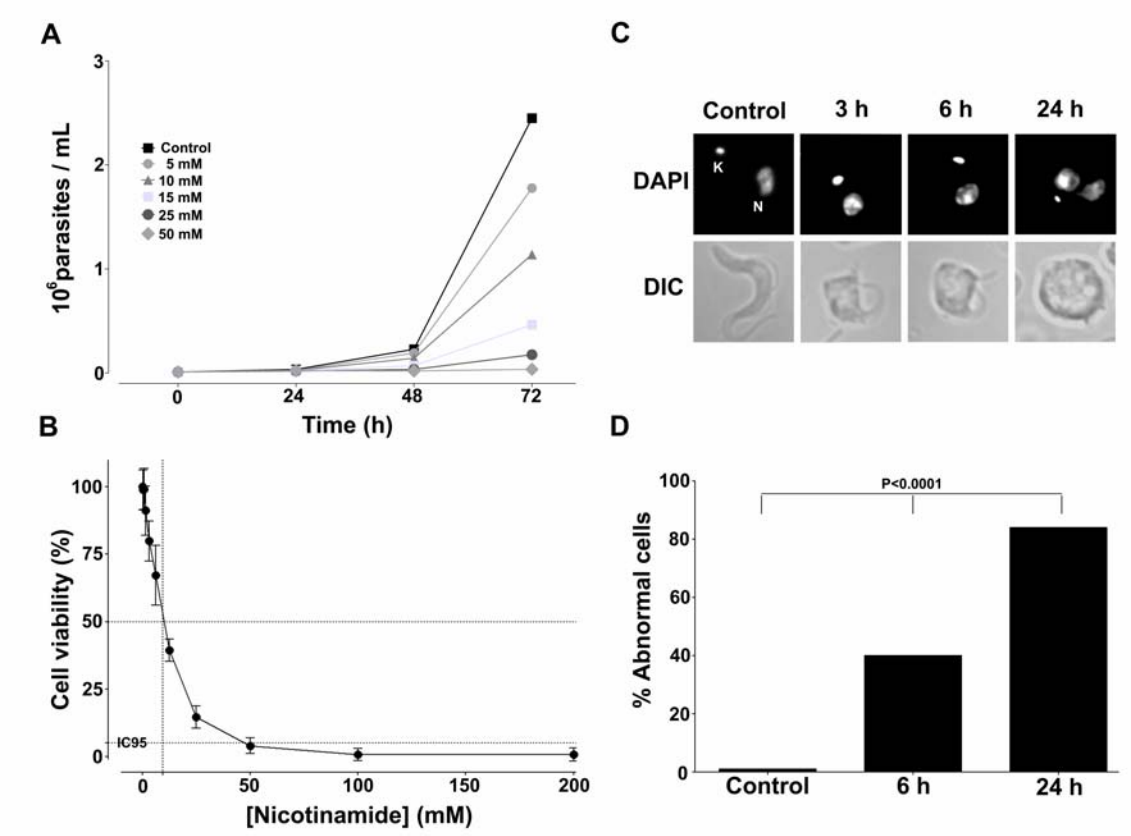

Figure 7. (A) Bloodstream forms growth curve after NAM treatment at different concentrations. Results are expressed as mean of three different experiments. **(B)** Curve dose response (cell viability percent versus NAM concentration). The IC50 value was determined by log (inhibitor) vs. normalized response - Variable slope using the GraphPad Software **(C)** Analysis of the morphological phenotype after different times of treatment. Fixed parasites DAPI-stained were observed by DIC -Differential Interference Contrast- (bottom line) and fluorescence microscopy (top line) (DAPI fluorescence is shown in white). **(D)** Quantification of abnormal cells. The percent of abnormal cells were determined by counting at least 200 cells. Statistical significance, $P < 0.0001$, was determined by a Chi-square test using the GraphPad Software.

NAM showed a dose dependent effect on cell proliferation and completely inhibited cell growth at 25-50 mM concentration range (Fig. 7A). Half-maximal inhibitory

concentration (IC50) and 95% inhibitory concentration (IC95) were 9.541 mM (Standard deviation [SD] ± 1.015) and 49.412 mM (SD ± 3.15) respectively (Fig. 7B). At these concentrations non effect on growth was observed in the 293T human renal epithelial cell line (data not shown). The IC50 in this human cell line was significantly higher (175 mM, SD ± 4.45) compare to that on *T. brucei* bloodstream forms. Moreover, similar range of concentrations (mM range) has been previously shown to exert non undesired effect on mammalian cell viability [181,182]. The IC95 (50 mM) was chosen to carry out the rest of this study.

Morphological changes in *T. brucei* treated cells were monitored by light microscopy. NAM induced an enlargement of the posterior end of the cell and this morphological abnormality was evolving with time (Fig. 7C). After six hours of incubation about 40% of the cell presented swollen flagellar pocket/endosomal compartment and by 24 hour 84% of the parasites had this morphology (Fig. 7D).

A.1.2. NAM causes cytokinesis defect, cell-cycle arrest at G2 phase and cell death.

In African trypanosomes the different phases of the cell cycle can be monitored by the configuration of the mitochondrial DNA, named kinetoplast (K), and the nucleus (N). Cell containing a single nucleus and kinetoplast (1N1K) are in G1 phase. A configuration of two kinetoplasts and one nucleus encloses cells in S phase and mitosis. Post-mitotic cells are those with two nucleus and two kinetoplasts (2K2N). Cell counts using DAPI-stained bloodstream cells (Fig. 8A) showed that the ratio of cells with one kinetoplast and one nucleus (1K1N) decreased from 83.8 % (Standard deviation [SD] ± 3.29, n = 200) in control cells to 59.9% (SD ± 8.76%, n = 200) and 46.6 % (SD ± 7.96%, n = 200) after 6 and 24 h of NAM treatment respectively. Cells with two kinetoplasts and two nuclei (2K2N) increased from 5.3% (SD ± 0.63%, n = 200) in the control cells to 9% (SD ± 3.36%, n = 200) after 24 h of incubation with NAM. Finally, aberrant cells containing several nuclei and kinetoplasts increased from 0.7% (SD ± 0.93, n = 200) to 10.2% (SD ± 0.33, n = 200) indicating that treated population of parasites was arrested in cytokinesis after completing several rounds of DNA synthesis and mitosis.

The increment in the number of aberrant cells suggested that the cell cycle was affected by NAM treatment. To further analyze this effect bloodstream forms were incubated in the presence of NAM and their DNA content was determined by measuring propidium iodide incorporation and flow cytometry analysis. Like previous

analyses of trypanosome populations [183,184], the percentage of cells at the different cell cycle phases in untreated cells presented a classical cell cycle distribution for bloodstream trypanosomes (Fig. 8B), having a major G_0/G_1 population (2C; 48.38%, SD ± 4.93), with small S phase (active DNA synthesis; 17.22%, SD ± 3.26) and G_2/M populations (4C; 34.37%, SD ± 4.75). However, the percentage of cells at G_2/M phase clearly increased to 64.42% (SD ± 6.60) and 75.42% (SD ± 9.55) after 6 and 24 h of NAM incubation respectively. Finally, this analysis also provided the proportion of dead cells represented by $SubG_1$ population (Fig. 8C). After 6 h of treatment with NAM the percentage of dead cells was 16.04% (SD ± 0.93) reaching up to 49.59% (SD ± 8.55) at 24 h of treatment and about 100% after 72 h.

The results indicate that NAM induces cell cycle arrest at G_2/M phase and interferes with cytokinesis in *T. brucei* bloodstream forms.

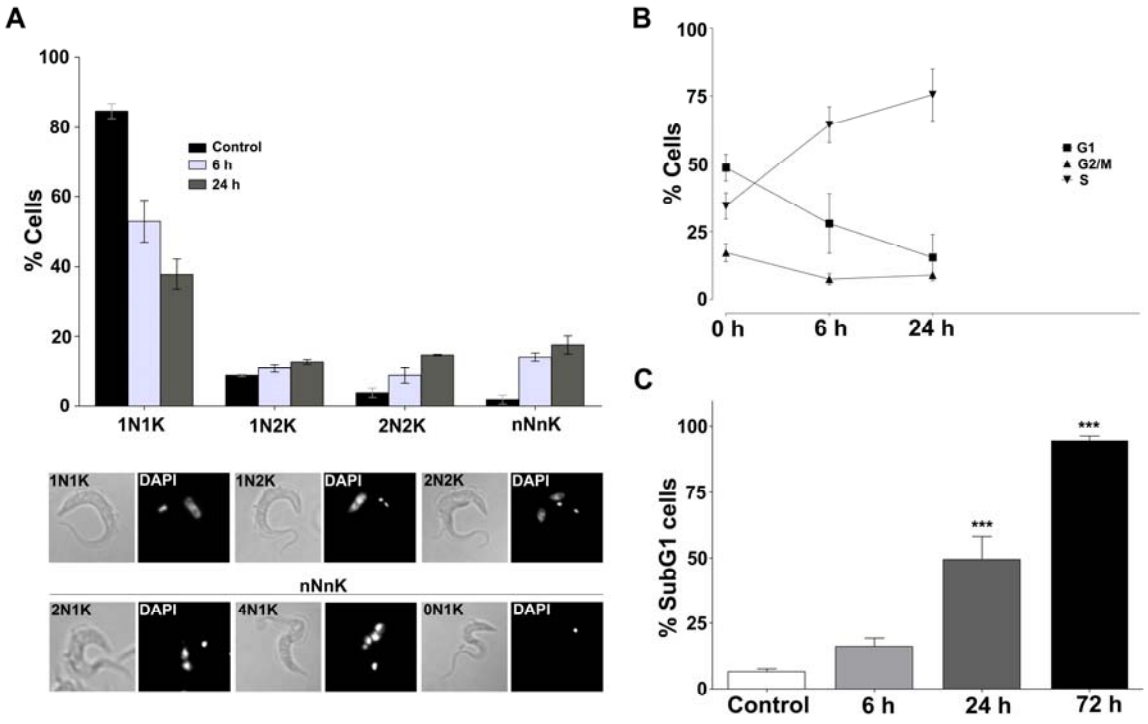

Figure 8. (A) Paraformaldehyde fixed parasites were counterstained with DAPI to determine the number of cells containing one nucleus (N) and one kinetoplast (K), 1N2K, 2N2K and nNnK (Aberrant cells). NAM treated (6 h and 24 h) and untreated parasites were analyzed. Results are expressed as mean ± SD of three experiments. Below graph are shown the three normal types: 1N1K, 1N2K and 2N2K (top panel); and three examples of aberrant cells: nNnK (bottom panel). **(B)** Percentages of cells in G_1, S, and G_2 phases at 0, 6 and 24 h. Percentages were determined using the CellQuest software (relative to the 100% of live cells, avoiding $SubG_1$) and represent the mean ± SD of three independent experiments. **(C)** FACS analysis of bloodstream forms stained with PI as describe in materials and methods to analyze the DNA degradation (SubG1 percent) after NAM treatment. Data are showed as mean ± SEM of three different experiments. The percentages were determined using the CellQuest software. Statistical significance (***, $P < 0.001$ 99.9% Confidence interval) was determined by a Tukey's multiples comparison test between treated versus control (untreated).

A.1.3. NAM inhibits endocytosis.

We have shown that NAM induces enlargement of the flagellar pocket/endosomal region. Transmission electron microscopy was used to further delineate the ultrastructural alterations induced by NAM in bloodstream *T. brucei*.

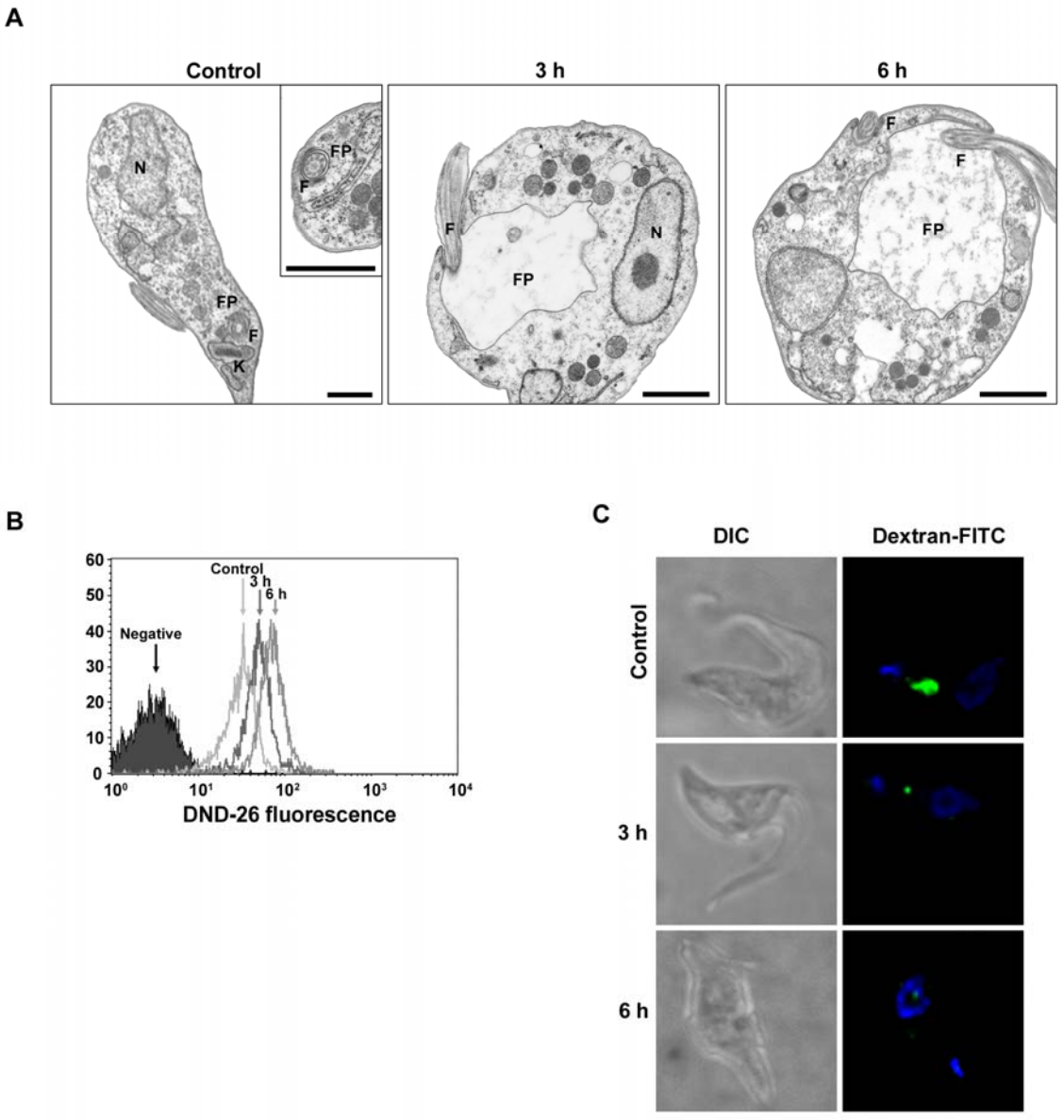

Figure 9. (A) T.E.M. (Transmission electronic microscopy) analysis of bloodstream forms after NAM treatment. N, nucleus; K, kinetoplast; F, flagellum; FP, flagellar pocket. Scale bars: 1µm. **(B)** FACS analysis to compare the increase of acid organelles after NAM treatment. Bloodstream forms after different times of NAM treatment were stained with acidotropic dye LysoTracker Green DND-26. **(C)** Dextran-FITC accumulation. Untreated trypanosomes as well as NAM pre-treated parasites were incubated for 1 hour with Dextran-FITC particles, fixed and analyzed by fluorescence microscopy.

Significantly, in many sections taken after 3-6 hours of NAM treatment the flagellar pocket was grossly enlarged, as revealed by the relative size of the flagellum

compare to the lumen of the pocket (Fig. 9A). Furthermore, multiple flagella within the flagellar pocket were also observed in some sections supporting the failure to complete the process of cell division. The enlargement of the flagellar pocket observed in electron micrographs correlated well with the presence of the enlarged vacuole observed by light microscopy in Fig. 7C. Moreover, accumulation of membranous structures, probably endosomes, to form multivesicular bodies could be detected in some cross sections after 3h and 6h of incubation with NAM (Fig. 9A). This increase in the number of intracellular acidic organelles was confirmed by FACS analysis after staining with acidotropic dye LysoTracker Green DND-26 (Fig. 9B).

In bloodstream trypanosomes enlarged flagellar pocket morphology, known as the “big eye” phenotype, is associated with the inhibition of the endocytosis process [80]. We next tested whether NAM affects endocytosis by measuring FITC-dextran (MW 10,000) uptake by bloodstream trypanosomes treated with NAM for 3 and 6 hours. A decrease of 75% and 95% in the uptake of FITC-dextran uptake respectively was observed (Fig. 9C). These data indicate that at mid-term NAM treatment interferes with the endocytosis process in bloodstream forms of *T. brucei*.

A.1.4. NAM induces lysosome disruption and cathepsin B-like (TbCatB) inhibition.

In order to identify perturbations in trafficking and pocket targeting systems we probed NAM treated cells with an antiserum to p67, a *T. brucei* lysosomal type I membrane glycoprotein [88]. In untreated bloodstream trypanosomes p67 stained a discrete organelle between the kinetoplast and the nucleus (Fig. 10A). In contrast, in treated cells p67 labeled several smaller vesicles (Fig. 10A) suggesting that NAM promoted disruption of the lysosome integrity in bloodstream trypanosomes.

We next analyzed whether NAM alters lysosomal function. For this purpose, protease activity was measure in total cellular extracts from control and treated cells using the fluorogenic peptide substrate Z-RR-AMC at pH 6.0. Surprisingly, cathepsin B activity dropped immediately after NAM addition, reaching 27.10% (SD± 4.07) with respect to control cells within the first minute of incubation (Fig. 10B). After 30 minutes of treatment protease activity was 12.93% (SD± 5) with respect to control and then remained constant (Fig. 10B). These results indicate that NAM inhibits cathepsin b protease in bloodstream trypanosomes.

Cathepsin B-like is a lysosomal protease responsible of transferrin degradation in bloodstream form of *T. brucei*. Transferrin is the unique source of iron for the parasite and is internalized from the host through receptor mediated endocytosis. The host transferrin is then rapidly degraded in the lysosome.

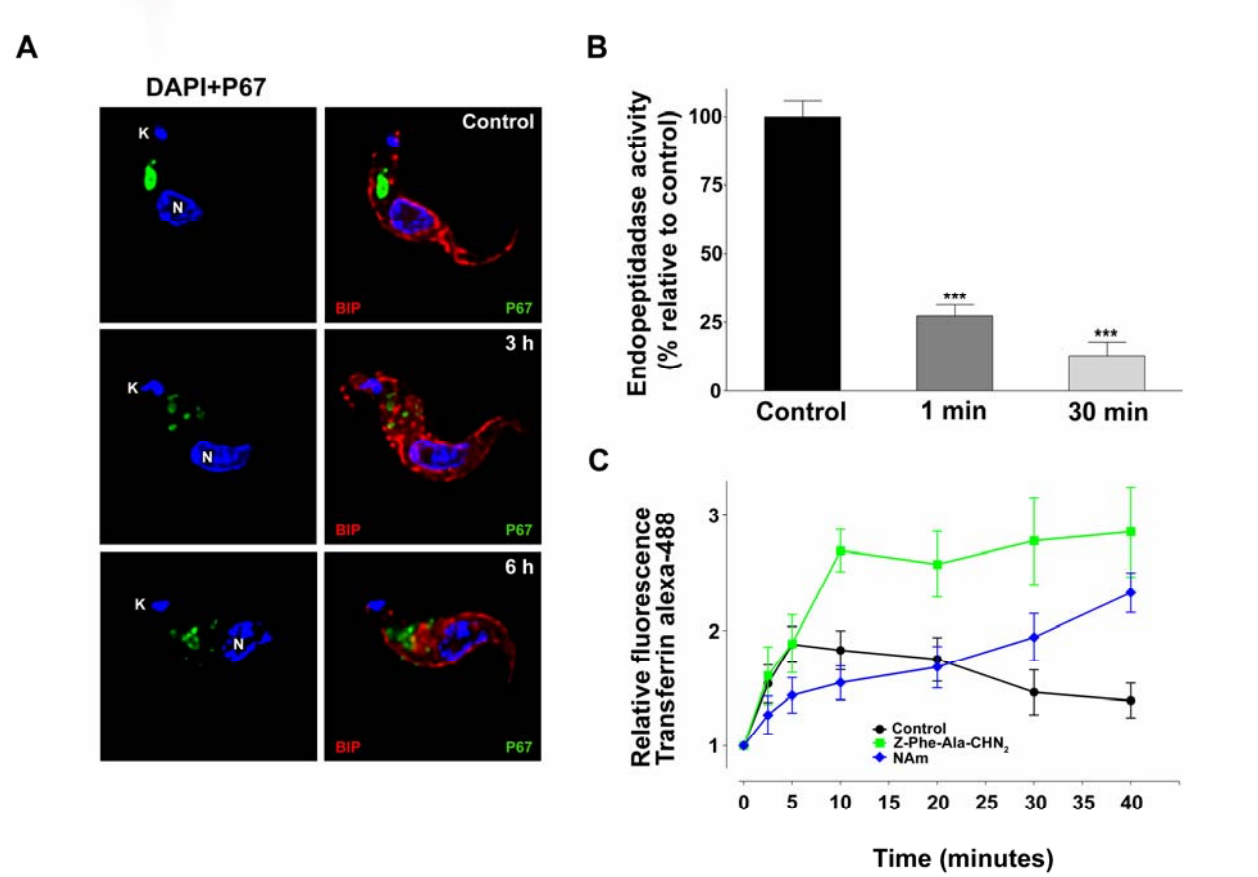

Figure 10. (A) Localization of p67. Untreated (Control) and NAM-treated (3 and 6 hours). Green, p67. Red, BIP. Blue, DAPI (N, nucleus; K, kinetoplast). **(B)** Cathepsin B activity in parasites extracts was monitorized using the fluorogenic peptide substrate Z-RR-AMC. AMC release was measured at an excitation wavelength of 350 nm and emission wavelength of 460 nm. The data were normalized to the 100% of activity of the control. Three different experiments were performed. Values are mean ± SD standard deviations of all experiments. Statistical significance (***, $P < 0.001$ 99.9% Confidence interval) was determined by a Bonferroni's multiples comparison test treated versus control. **(C)** Transferrin Alexa 488 uptake and accumulation analyzed by FACS. Results are expressed at mean ± SEM of three independent experiments.

In order to confirm the inhibitory effect of NAM on cathepsin B-like protease, bloodstream forms were incubated with Alexa 488-labeled transferrin in a time course endocytosis assay and analyzed by flow cytometry. As expected, in the presence of the cathepsin B inhibitor Z-Phe-Ala-CHN_2 the intracellular fluorescent signal rose within the first 10 minutes indicating Alexa 488-transferring uptake and then remained constant due to accumulation of undegraded transferrin. In the absence of a cathepsin B inhibitor there was an increase in the intracellular fluorescent signal within the first 5 minutes and then declined indicating an initial intracellular accumulation of Alexa 488-

transferrin followed by a rapid protein degradation (Fig. 10C). Finally, in bloodstream trypanosomes incubated with NAM a slower but continuous increase in the fluorescent signal was observed over the time course experiment suggesting an inhibitory effect on transferrin uptake and degradation (Fig. 10C). These results suggest that the inhibition of endocytosis observed in bloodstream form of *T. brucei* treated with NAM is not due to TbCatB protease inhibition.

Finally, in order to determine whether NAM exerts its inhibitory effect directly on Cathepsin B protease or this is an indirect effect we expressed and purified recombinant TbCatB. As previously reported [167], expression of the TbCatB zymogen leads to secretion of both zymogen and mature forms of TbCatB (42 and 31 kDa, respectively) from *P. pastoris* (Fig. 11A). Protease activity was monitored using the fluorogenic peptide substrate Z-RR-AMC at different NAM concentrations. IC50 value on recombinant protein was 2.14 mM (SD ± 0.09). As shown in Fig. 11B, TbCatB protease activity was completely inhibited at 25 mM.

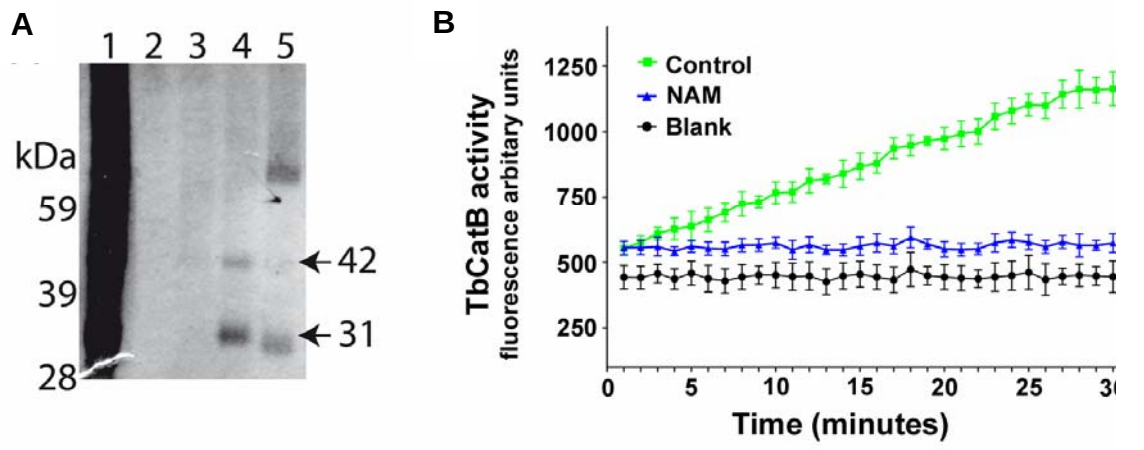

Figure 11. (A) SDS-PAGE gel of purified recombinant TbCatB. Crude protein was desalted, concentrated, and purified by anion exchange chromatography. Crude protein (lane 1), column flow-through (lane 2), and fractions (lanes 3–5) were resolved by SDS-PAGE and visualized by silver stain. Note both the zymogen at 42 kDa and more abundant mature form at 31 kDa (lane 4). **(B)** Purified recombinant TbCatB activity was monitorized using the release of AMC after hydrolysis of the specific substrate Z-RR-AMC. Data are mean ± SD of six replicates in three different experiments. Control: non-treated. NAM: 25 mM. Blank: Z-RR-AMC without protein.

A.1.5. NAM treatment and cell death markers in bloodstream trypanosomes.

In order to gain insight into the trypanocidal effect of NAM, several classical cell death markers were analyzed. We first set out an experiment to study the effect of NAM on the bioenergetic state of the cell by monitoring total ATP levels. Intracellular ATP content was measured using CellTiter-Glo luminescent assay (Promega).

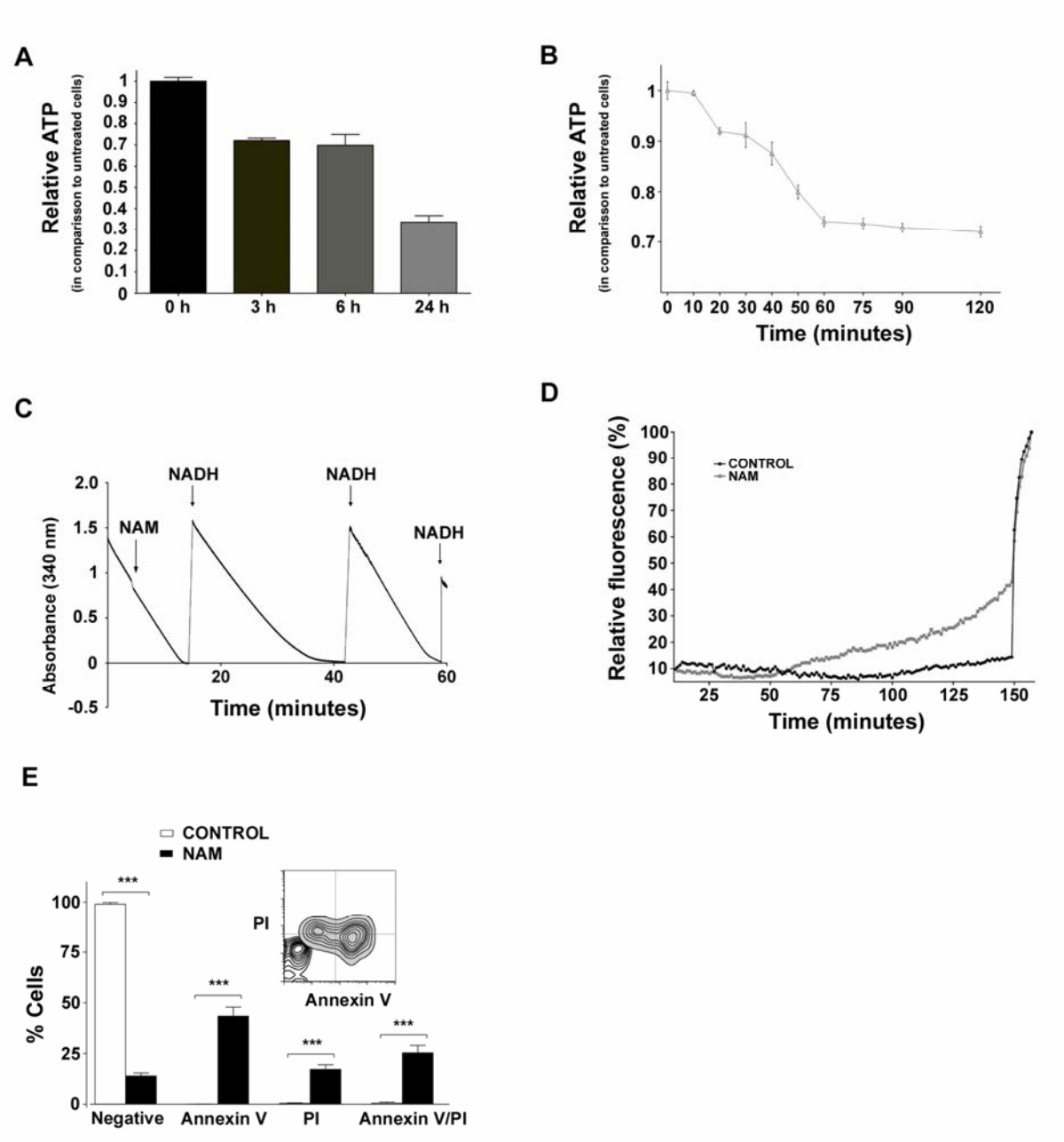

Figure 12. (A) Relative ATP levels after NAM treatment. The bars represent the mean ± SD of three independent experiments. **(B)** Time course of intracellular ATP drops after NAM treatment. ATP levels were calculated relative to 100% of the control. Data are the means ± SD from three independent experiments. **(C)** Relative fluorescence percent of SYTOX Green. The fluorescence of the nuclei acid dye was used to measure parasites with compromised membranes. The values were normalized to the 100% for maximum fluorescence achieved by addition of 0.1% Triton X-100. **(D)** Pyruvate efflux measure. Pyruvate production was quantified by monitoring the kinetics of NADH oxidation (absorbance at 340 nm). **(E)** Analysis of phospatidilserin exposition. FACS analysis of bloodstream forms stained with Annexin V-FITC and PI as describe in materials and methods. Bars represent the mean ± SD of three independent experiments. The percentages were determined using the CellQuest® software. Statistical significance (***, $P < 0.0001$ 99.9% Confidence interval) was determined by a Bonferroni's multiples comparison test between treated versus control (untreated). A representative overlay dot plot, performed with FlowJo software, to compare the difference of populations among NAM-treated and untreated.

As shown in Fig. 12A, ATP declined about 28 % (SD ± 0.01), 31% (SD ± 0.08) and 69% (SD ± 0.05) after 3, 6 and 24 hours of treatment with NAM, respectively. Next, a time course experiment was conducted to determine the kinetics of the ATP fall. Bloodstream trypanosomes were incubated in the presence of NAM and samples were taken at different time points as indicated in Fig. 12B. A progressive decrease in intracellular ATP levels was observed within the first 60 minutes and then remained constant until the end of the experiment (120 minutes). The results show that in *T. brucei* bloodstream forms the intracellular ATP drop is an early event within the programmed cell death triggers by NAM.

Glycolisis is the sole source ATP production in bloodstream trypanosomes. We investigated whether the ATP fall induced by NAM was due to an inhibitory effect on glycolisis. For this purpose, pyruvate production was quantified by monitoring the kinetics of NADH oxidation produced during pyruvate efflux. No changes in pyruvate efflux rate was observed after NAM addition indicating that glycolisis was not inhibited (Fig. 12C).

Next cell death marker analyzed was cellular membrane integrity. Plasma membrane disruption was assay with SYTOX green, a high affinity nucleic acids stain that is impermeant to live cells but penetrates compromised cell surface membranes [185,186]. The plasma membrane of bloodstream forms appeared unharmed during the first 60 minutes of incubation with NAM. After this time point, the SYTOX green fluorescence signal was increasing slowly for 90 minutes, reaching a 40% of the maximal permeabilization obtained by the addition of detergent (Fig. 12D). These results suggest that NAM compromised bloodstream membrane integrity after a relative short period of incubation.

The externalization of phosphatidyl serine was next analyzed. In mammalian cells, during the early stages of apoptosis, phosphatidyl serine becomes exposed on the outside of the cell membrane. *In vivo*, this is a signal to phagocytes to engulf the dying cell before it loses its plasma membrane integrity and releases inflammatory mediators into the surroundings. This early stage of apoptosis can be specifically detected by phosphatidyl serine binding proteins, like annexin V. During the early stage of apoptosis, the cell membrane is intact and the cells exclude propidium iodide. Later, during the apoptotic process *in vitro*, the membrane becomes porous and propidium iodide becomes associated with DNA in the nucleus. The uptake of propidium iodide is an indication of necrosis. Therefore, annexin V/PI double staining was performed (Fig. 12E). *T. brucei* bloodstream forms were incubated for 24 hours with NAM and then

phospatidyl serine exposure was quantified by flow cytometry. After 24 h, about 44% of treated cells were annexin V positive/PI negative (early apoptotic) (Fig. 12E). In addition, 25.35% (SD ± 3.60) of annexin V-positive/PI-positive (late apoptotic) and 17.2% (SD ± 2.26) annexin V-negative/PI-positive (early necrotic) bloodstream forms could be detected after incubation with NAM for 24 h (Fig. 12E).

Altogether, theses results suggest that cell death induced by NAM treatment in bloodstream trypanosomes shares some biochemical characteristics of programmed cell death by apoptosis in mammalian cell.

A.1.6. Effects of NAM on *T. brucei* parasitemia in mice.

The potential *in vivo* activity of NAM was tested in a murine model of chronic trypanosomiasis [187]. Mice were inoculated with pleomorphic AnTat 1.1 strain and NAM was daily administrated starting one day after infection. NAM treatment reduced and delayed the first peak of parasitemia compared with the control group (Fig. 13A). The second peak of parasitemia in NAM treated group coincided with the end of the second peak in control mice. All the infected mice in the control group died before day 40 after infection, while the NAM treated group survived until day 48 (Fig. 13B). NAM administration reduced the number of parasites in blood and in organs (data not shown); however the survival was only delayed eight days. No visible adverse effects were noticed for the administration of high dose of NAM.

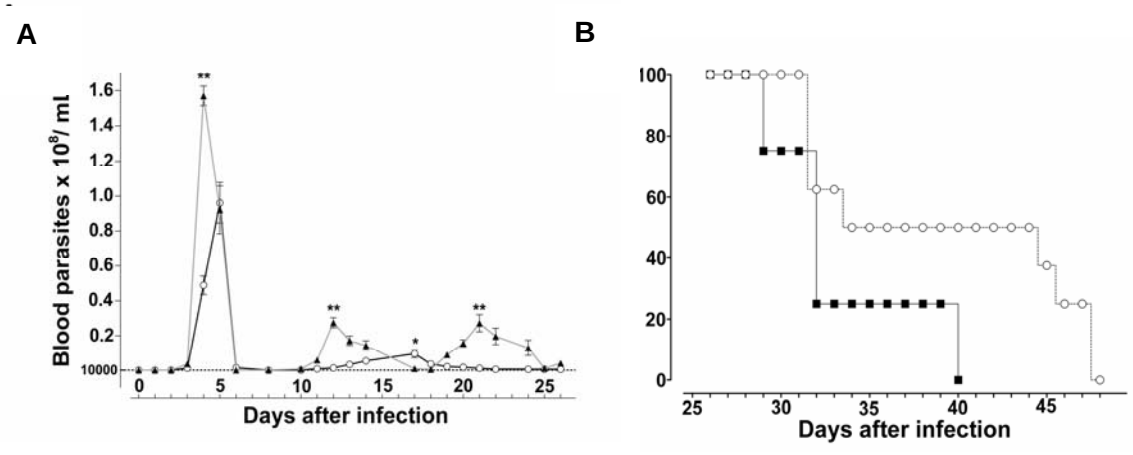

Figure 13. Effects of Nicotinamide in experimental model of chronic trypanosomiasis. Female C57BL/6J mice were infected with the pleomorphic AnTat1.1 strain of *T. brucei*. NAM treated mice (12.2 mg/mouse) were i.p. injected everyday from day 1 after infection. **(A)** Number of parasites in the blood of infected animals was counted daily, n=7-10 mice/group. Bars represent mean ± SD. ** P < 0.01 untreated versus NAM-treated. Open circles, NAM-treated. Filled triangles, untreated. **(B)** Survival was monitored daily n=7–10 mice/group. Open circles, NAM-treated. Filled squares, untreated.

A.2. Discussion.

NAM exhibits antimicrobial activity towards different microorganisms ranging from bacteria to parasite protozoa, fungi and virus. These studies indicate that NAM has the potential to be used against different diseases however the antimicrobial mechanism of action of NAM remains largely unknown.

We have identified cathepsin B-like of *T. brucei* (TbCatB) as a new target of NAM. Both, *in vitro* and *in vivo* studies have previously shown that TbCatB activity is essential for *T. brucei*. Here we report that NAM has an inhibitory effect on bloodstream trypanosomes cell growth and induces morphological changes clearly detectable by light microscopy. Electron transmission studies revealed an increase of electrodense vacuoles in the cytoplasm of treated cells and a gross enlargement of the flagellar pocket (Fig. 9A). Theses morphological abnormalities are similar to those observed in studies using cystein protease inhibitors. Treatment of bloodstream trypanosomes with Z-Phe-Ala-CHN_2 led to an enlargement of the lysosomal/endosomal region [108,109]. A similar phenotype was observed in cathepsin B-like depleted parasites by RNAi [110].

Moreover, like in cathepsin depletion, NAM treatment also induced miss localization of the lysosomal protein p67 suggesting a negative effect on lysosome function (Fig. 10A). Subsequent transferrin uptake experiments demonstrated that NAM inhibits host protein degradation, specifically host transferrin. Furthermore, unlike Z-Phe-Ala-CHN_2 inhibitor, NAM also interferes with endocytosis in bloodstream trypanosomes. Both, receptor mediated and fluid phase endocytosis, were affected by NAM Fig. 9C and 10A.

This observation is in agreement with the gross enlargement of the flagellar pocket detected by electron transmission analysis. However, as shown in Fig. 10C, incubation of bloodstream trypanosome with Z-Phe-Ala-CHN_2 inhibitor did not affected transferrin endocytosis. In contrast, treatment with cystein protease inhibitors and cathepsin depletion also induced the swelling of the flagellar pocket [109,167]. Such enlargement was associated to the accumulation of undegraded protein and the osmotic consequents that this accumulation might exert on intracellular trafficking between the flagellar pocket and the endosomal/lysosomal compartment. On the other hand, several studies have previously shown that the *big-eye* phenotype is always associated to failures in the endocytosis process [80]. Thus, our results suggest that NAM is also targeting unidentified components of the endocytic machinery.

NAM treatment induced a cell cycle arrest at G_2 phase and a block in cytokinesis. Both phenomena have been also described in *TbCatB* RNAi cells and are likely to be due to a downstream effect of inhibition of lysosomal function (protein degradation). Cathepsin B depleted and NAM treated parasites were able to complete several rounds of genomic and kinetoplast replication and mitosis as evidenced by the appearance of multiple kinetoplasts and nuclei but were not able to carry out cytokinesis. It was proposed that TbCatB might be involved in microtubule regulation or alternatively cell cycle arrest and lack of cytokinesis are both an indirect effect of iron depletion because the incapacity of the parasites to degrade transferrin.

In order to further analyze the mechanism of cell death induced by NAM several cell death markers have been analyzed. The drop of ATP level is an early event in cell death induced by NAM (Fig. 12B). However, glycolisis, the unique source of ATP production in bloodstream trypanosomes, was not affected by NAM treatment. No change in the rate of pyruvate production was observed after NAM addition (Fig. 12C). Thus, this might be a consequence of the inhibition of transferrin degradation considering that iron is important for viability of *T. brucei*.

The cellular consequences of iron depletion in *T. brucei* are not fully understood. Four iron dependent enzymes have been identified so far in African trypanosomes, alternative oxidase [188,189], superoxide dismutase [190], aconitase [191] and ribonucleotidereductase [192,193]. Aconitase is a dispensable enzyme since deletion of both alleles of the single copy gene does not alter cell viability in culture trypanosomes [194]. Alternative oxidase is an essential enzyme responsible for the reoxidation of NAM adenine dinucleotide produced during glycolisis. Ribonucleotidereductase is involved in the reduction of ribonucleotides to deoxyribonucleotides required for DNA synthesis. Finally, superoxide dismutase eliminates superoxide radicals which, for instance, are released during generation of the tyrosyl radical in the R2 subunit of ribonucleotidereductase. Therefore, the programmed cell death produced by NAM may be due to the indirect effect exerted by iron deprivation in the activity of these iron dependent enzymes present in bloodstream trypanosomes.

On the other hand, NAM inhibits several enzymes in which NAM are one of the end reaction products. For instances, sirtuins proteins, a family of NAD dependent deacetilase and/or mono ADP ribosyltransferase are inhibited by nM concentration of NAM. In *T. brucei* there are three members of the sirtuin family and all of them are dispensable. The first one characterized is a nuclear protein associated to

chromosomes and involved in DNA repair [195]. The rest, Tbsir2rp2 and Tbsir2rp3 are mitochondrial and their function is not known. NAM also inhibits poly ADP ribosyltransferase, an enzyme involved in DNA repair. A poly ADP ribosyltranferase activity has been reported in *T. brucei* [196]. However, the protein has not been identified so far nor functional characterized. Therefore nothing is known about its inhibition effect on *T. brucei*.

Finally, NAM applied intraperitoneally to *T. brucei*-infected mice at a daily dosage of 12.2 mg/mouse from days 1 to 26 postinfection had only a slight effect on the course of parasitemia compared with infected control mice injected with PBS alone. The failure of NAM to clear the parasites from the blood of the host is probably due to its short half-life *in vivo*. From human blood NAM disappears with a half-life of 5 hours [197]. Future work should focus on the development of NAM derivated compounds with prolonged biological half-lives and selectivity for parasite uptake. Such compounds may provide a new class of antitrypanosomal drugs specifically interfering with the iron metabolism of the parasite.

Although NAM exhibits trypanocidal activity a high concentrations this vitamin is well tolerated and high-dose treatment and it is being used as medication for certain pathologies [198]. NAM is particularly cheap to produce, to distribute and to deliver to human. It can be orally administered and cross the blood brain barrier. Thus, nicotinamide may be a valuable and rational candidate for combination therapy in areas where African trypanosomiasis are endemic as well as to serve as a lead compound for drug development.

<u>Objective B</u>: Generation of nanobody phage display library constructed against recombinant *T. brucei* Oligopeptidase B.

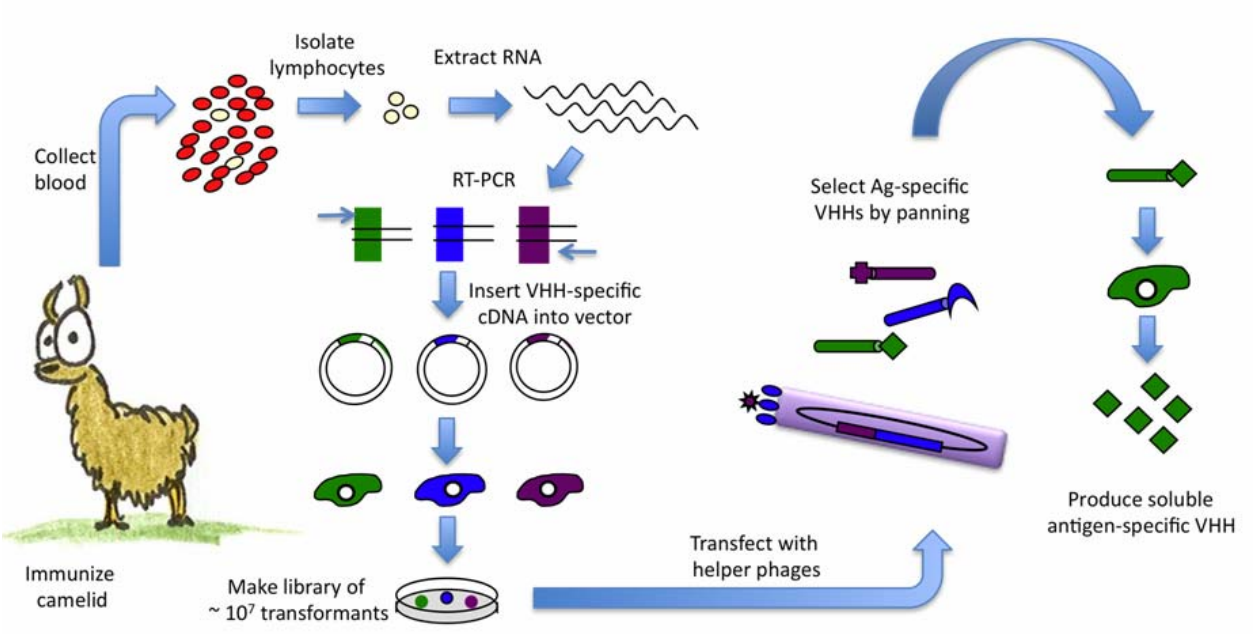

Schematic illustration of generation of Nb library. **Flor La Greca, unpublished.**

B.1. Results.

B.1.1. PCR amplification of alpaca Nbs repertoire.

Nbs repertoire was isolated by performing PCR amplification on cDNA prepared from peripheral blood mononuclear cells RNA isolated from an alpaca immunized with recombinant TbOPB. The primers employed (CALL001/ CALL002) anneal to the leader sequence and to CH2 exon of camelids immunoglobulins, respectively. Two fragments were amplified: one fragment of ~900 bp, encoding part of the CH2 exon, the CH1 exon, the hinge region and the variable region of the heavy chain of the conventional antibodies (VHs); and a second fragment of ~700 bp, encompassing part of the CH2 exon (CH1 exon is absent in HcAbs), the hinge region and the variable region of the heavy-chain antibodies (VHHs or Nbs) (Fig. 14A). After electrophoresis separation, the 700 bp PCR fragment was used as a template in a second PCR to amplify the specific sequence of the Nbs repertoire (VHHs sequences).

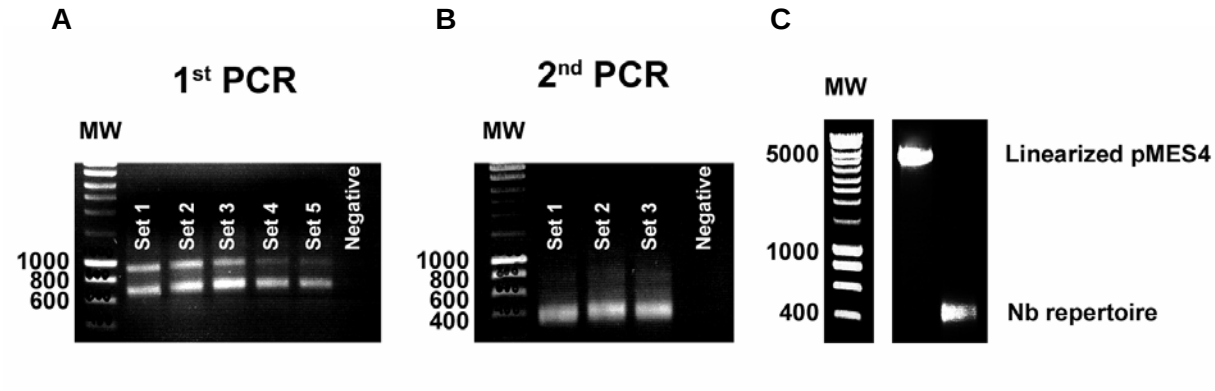

Figure 14. (A) Agarose electrophoresis of first PCR. Five different cDNA input concentrations were assessed (0.5, 1, 2, 3 and 4 µL of cDNA). MW, molecular weight (base pair, bp). **(B)** Agarose electrophoresis of second PCR. Three different sets were performed (3 sets: 1, 2 and 3 µL of purified 1st PCR). MW, molecular weight (bp) **(C)** Agarose electrophoresis of the digested phagemid pMES4 vector and the digested Nbs repertoire.

The reamplification was performed using a nested pair of primers (A6E/ 38) which anneal to framework-1 and framework-4 regions of the variable domains, respectively, leading to the specific amplification of the Nbs sequences repertoire (~ 450 bp fragments) (Fig. 14B).

B.1.2. Construction of nanobody library.

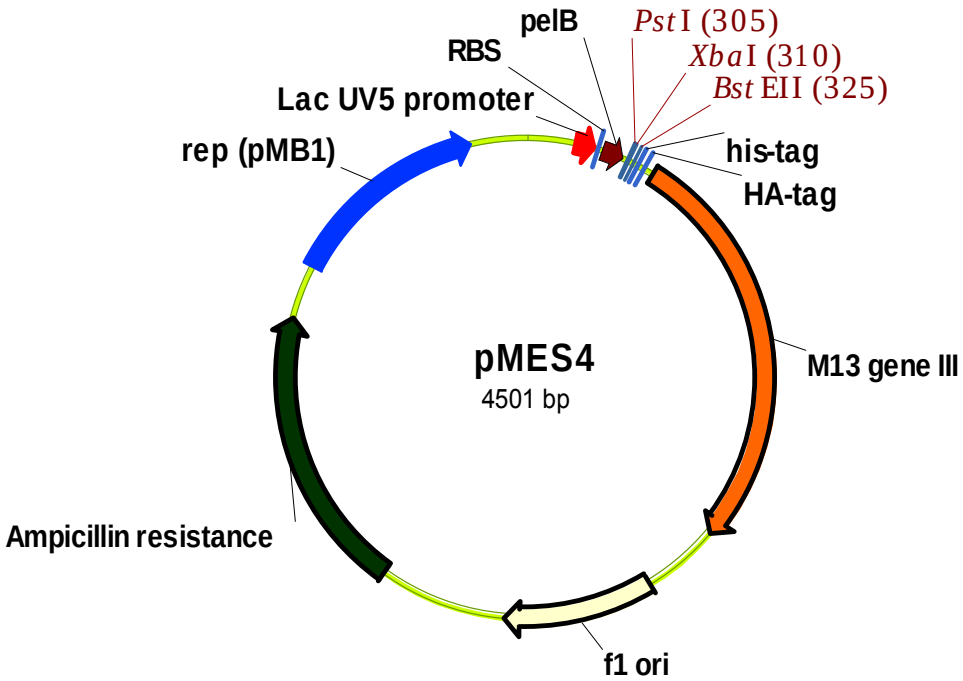

Figure 15. pMES4 map and reference sequence points (*GenBank: GQ907248.1*). Lac UV5 promoter: bases 143-198; RBS (Ribosome binding site): bases 211-215; pelB (signal peptide): bases 225-290; Multiple cloning site (*Pst* I, *Xba* I, *Bst* EII): bases 305-325; His-tag (six histidins in tandem): bases 340-357; HA-tag (hemagglutinin): bases 361-385; M13 gene III: bases 391-1623; f1 ori: bases 1859-2314; ampicillin resistance: bases 2701-3558; rep (pMB1): bases 3721-4335.

The Nbs repertoire was cloned between the PelB leader sequence (5' end), and HA (hemagglutinin) and 6His tags (at the 3' end) present in phage displayed pMES4 vector, to generate Nbs chimeras with PelB leader sequence at the N-terminus and a 6His-tag at the C-terminus (Fig. 15). Cloning in pMES4 vector offers the advantage that PelB leader sequence leads the Nb to the periplasmic space of the *E. coli*, where the sequence is removed by a signal peptidase, facilitating the purification of the Nb. The HA tags is used for detection when the Nb is expressed in the amber suppressor strain of *E. coli* TG1. pMES4 vector contains a stop codon TAG between 6His and HA tags that is not recognize by TG1 cells. Therefore, Nanobodies expressed in this bacterial carry both 6His and HA tags at their carboxi-terminal end. However when a Nb is expressed in a non suppressor *E. coli* strain, the protein end with the 6His tag facilitating protein purification. The Nb library was transformed in fresh electrocompetent *E. coli* TG1 cells (amber-TAG suppressor strain) and a library of 1.7 x 10^8 colonies was obtained. A PCR screening on randomly picked colonies showed that the 74.2 % of the checked colonies contained a plasmid with the expected size of insert. Only libraries with a size ≥ 10^7 transformants and with a percentage of right insert size ≥ 70% are suitable to perform the next step. Moreover, the little differences in the fragment size between positive colonies gave us information about the diversity (heterogeneity) of the library (Fig. 16).

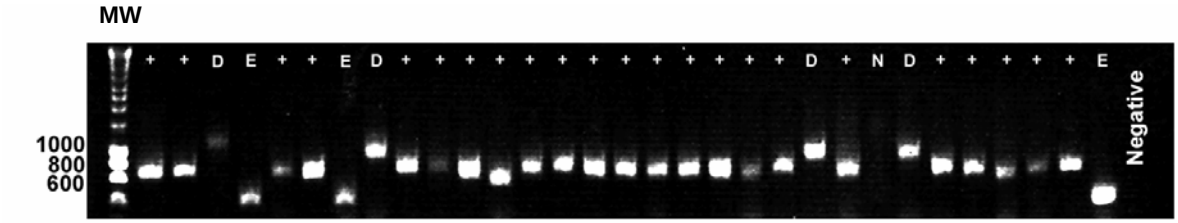

Figure 16. Agarose electrophoresis of colony PCR. White "+" symbol: colonies with correct size ~700 bp (Nb sequence cloned). D: colonies with two copies of Nb sequence (size ~1050 bp). E: colonies with empty plasmid (size ~350 bp). N: non transformed (no band). MW, molecular weight (bp).

B.1.3. Phage selection (biopanning).

To perform the biopanning selection, the *E. coli* TG1 cells harbouring the Nb library were infected with M13K07 phages to produce virus particles with the cloned Nb at their tips due to the fusion to M13 gene III. After overnight amplification, the phages particles isolated from the supernatant were used to perform serial rounds of panning.

The enrichment obtained in each round, calculated by comparing the number of colonies from cells infected with different dilutions of Ag-specific phages versus unspecific phages, was of 88.4-times, 1030.3-times and 2338.5-times after the first, second and third round (Fig. 17A) of panning, respectively. As example the enrichment was calculated comparing the number of colonies counting at the dilution 10^{-5} from the Ag + lane versus the colonies at the dilution 10^{-2} from the Ag - lane. Calculation: 152 colonies in dilution 10^{-5} lane Ag +; 65 colonies at dilution 10^{-2} lane Ag -; enrichment= $(152x10^{5})/(65x10^{2})$=2338.5 times (Fig. 17A).

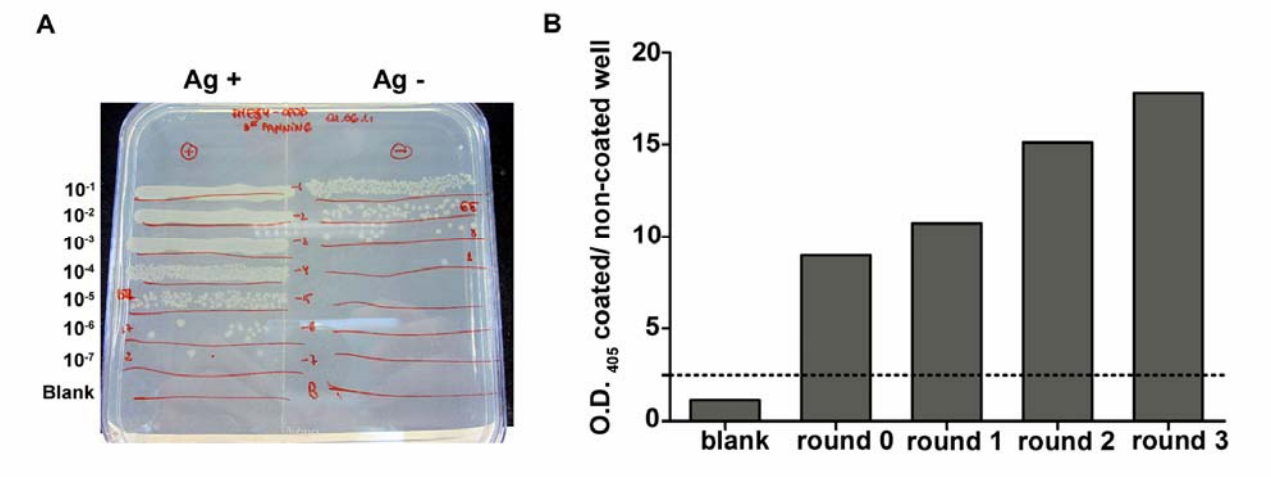

Figure 17. (A) Plate showing the antigen specific Nb enrichment of the third round of panning. Ag+: cells infected with phages eluted from Ag coated well. Ag-: cells infected with phages eluted from uncoated well. Blank: uninfected TG1 cells. **(B)** Phage ELISA. The results from each round of panning were represented with the ratio of the O.D. 405 nm coated well/ O.D. 405 nm un-coated well compared with the same ratio of the blank (10^{10} M13K07 phages without Nbs). Round zero: phages after infection of the library before first panning. Rests of rounds are phages after pannings.

The enrichment of phages was also visualized by ELISA against recombinant TbOPB (Fig. 17B). In the first round is expected to identify high number of different Nbs (high diversity) but with low affinity, however in the third round is expected to identify less number of different Nbs but with high affinity.

B.1.4. Identification of specific nanobodies.

Randomly selected colonies were tested to identify high affinity binders Nbs for recombinant TbOPB. After IPTG induction of the colonies, these amber suppressor cells expressed, in the periplasmic space, a soluble chimera protein made up for the Nb fused to (6His tag)–(HA tag)–(pIII). The detection of antigen specific Nbs in each colony was tested by ELISA over the periplasmic extract (PE) using an anti-hemaglutinin (HA) tag mouse mAb.

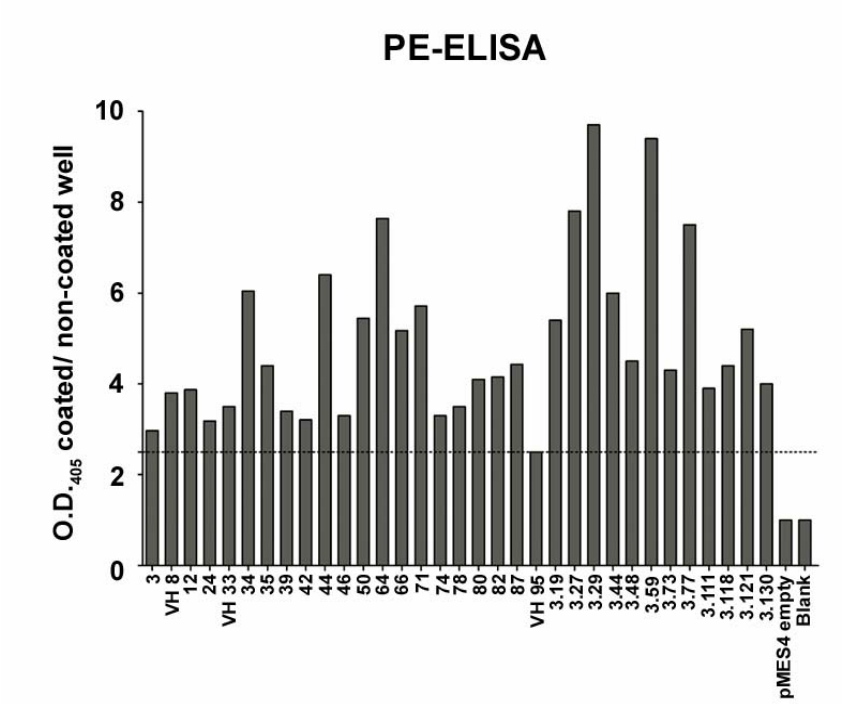

Figure 18. Periplasmic Extract (PE)-ELISA of clones with highest signal. The results were represented with the ratio of the O.D. 405 nm coated well/ O.D. 405 nm un-coated well compared with ratio of the blank (untransformed TG1) and with the ratio of the TG1 cells transformed with empty pMES4

Periplasmic extract (PE)-ELISA performed over 95 different colonies from the first round of panning showed 65 positive clones; this number was increased in the third round up to 127 positive clones were identified over 140 colonies tested. After identification of positive clones in the rounds of panning tested, the 94 clones with the highest signals (good binders) in PE-ELISA where screened by colony PCR to check the presence of expected size of insert. The 100% of the clones were positive by PCR (data not shown) and the sequencing analysis confirmed the heterogeneity of the PCR amplicons. This analysis put these clones sequences into 33 groups; some of them were composed of only one clone, other by a couple of clones and others for high numbers of clones. Checking the positions 42, 49, 50 and 52 (IMGT numbering) of the Framework-2, and the position 118 of the Framework-4, were identified 30 groups as Nbs and 3 groups (VH 8, VH 33 and VH 95) were classified as variable domains (VH) of the conventional antibodies, see supplementary fig. 1 (Amino acids sequences of the selected Nbs). Within of these 30 groups were selected those clones into with the highest signal in the PE-ELISA (Fig. 18).

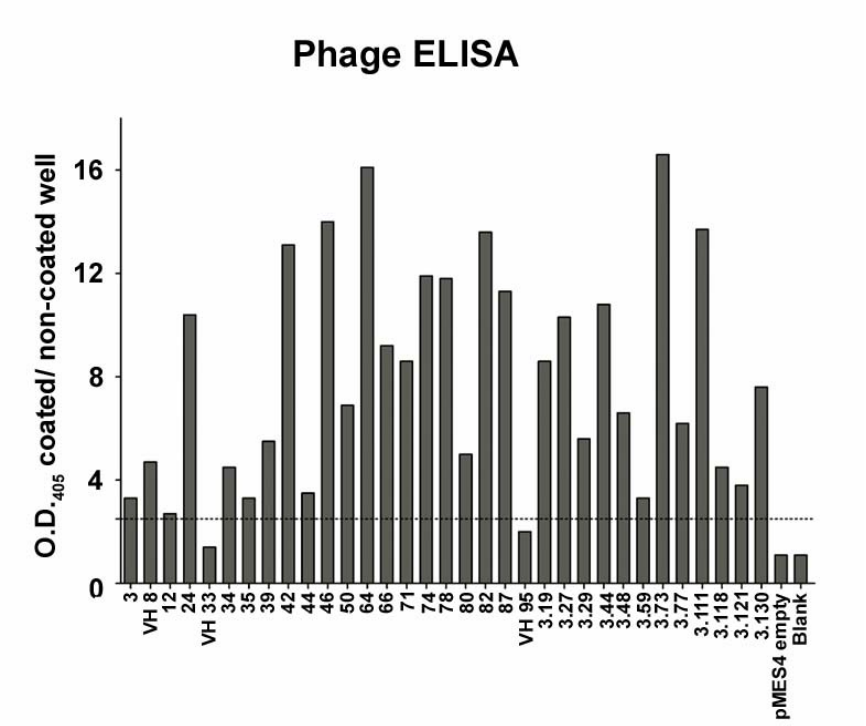

Figure 19. Phage ELISA in microtiter plates over positive clones to PE-ELISA. The results were represented with the ratio of the O.D. 405 nm coated well/ O.D. 405 nm un-coated well compared with the same ratio of the blank (untransformed TG1) and with the same ratio of the TG1 cells transformed with empty pMES4.

These 33 selected clones, including the VH clones, were growth in a microtiter plate and, after helper phage infection, were re-checked by a new phage-ELISA. Only two clones had a weak signal in the new phage ELISA, the clone 33 and 95, both identified above as VH in the sequencing. All the rest of clones were positive in this new phage ELISA, including the clone VH 8 (Fig. 19). However the clones with the highest signal in both ELISAs were Nbs and not VH.

B.2. Discussion.

In the generation of an anti-recombinant TbOPB Nb library we have obtained 30 positive clones good binders Nbs which amino acids sequences consistent with the *camelids* VHHs sequence. These good binders Nbs selected and identified by biopanning have to be characterised in antigen-binding and epitope recognition in their soluble form. The selected clones have to be transformed into non-suppressor strains of *E. coli* WK6 cells to obtain an optimal production of soluble binders. One of the advantages of the phagemid pMES4 vector versus others phagemid vectors is the

presence of His_6-tag sequence. The nanobody sequences, in pMES4, are cloned like a chimera protein where the nanobody is fused to His_6-tag tail, which is used to purify directly the Nb by Immobilized Metal Affinity Chromatography (IMAC).

The inclusion of this Chapter in this thesis aims to explain the recombinant gene technology to obtain Nbs derived from camelids heavy chains antibodies that can be used to target biological active components [153,154]. Nbs have applications as biosensors and in diagnosis and treatment of diseases such as trypanosomiasis, or cancer, due to their small size, stability, solubility and because they are able to recognize their Ag with high affinity and specificity.

Supplementary 1. The sequencing was realized with the primer MP57. The analysis of the sequence was made using two softwares: MEGA4 (Molecular Evolutionary Genetics Analysis software version 4.0.) and Serial Cloner 2.5. The differentiation of the CDR and FR was performing using the IMGT numbering. The positions 42, 49, 50 and 55, and the W in the first position of the FR4 were used to distinguish between Nanobodies and VH.

Objective C: Preparation and evaluation of pentamidine-loaded functionalized PEGlycated-chitosan nanoparticles coated by a nanobody that target the surface of *T. brucei*.

C.1. Results.

C.1.1. Preparation of NbAn33-coated pentamidine-loaded PEGlycated-chitosan nanoparticles (NbAn33-pentamidine-chNPs).

NbAn33-pentamidine-chNPs were generated by a coacervation method (entrapment procedure) which allowed to obtain well-stabilized spherical NPs with a diameter average size of 130 nm (SD ± 30) (Fig. 20A). Zeta (ζ) potential value analysis showed no significant differences between the surface charge properties of pentamidine loaded NPs and empty NPs indicating that pentamidine was trapped into NPs (Fig. 20B, 20C). The maximal pentamidine concentration loaded into NPs, expressed as encapsulation efficiency and drug loading capacity, was 67% (SD ± 4) and 11.2% (SD ± 0.5), respectively. The *in vitro* characterization of pentamidine release showed a bi-phasic profile: 40% of the encapsulated pentamidine was rapidly released within the first 12 h while the remaining 60% was released in a constant rate during the following 4.5 days (Fig. 20D).

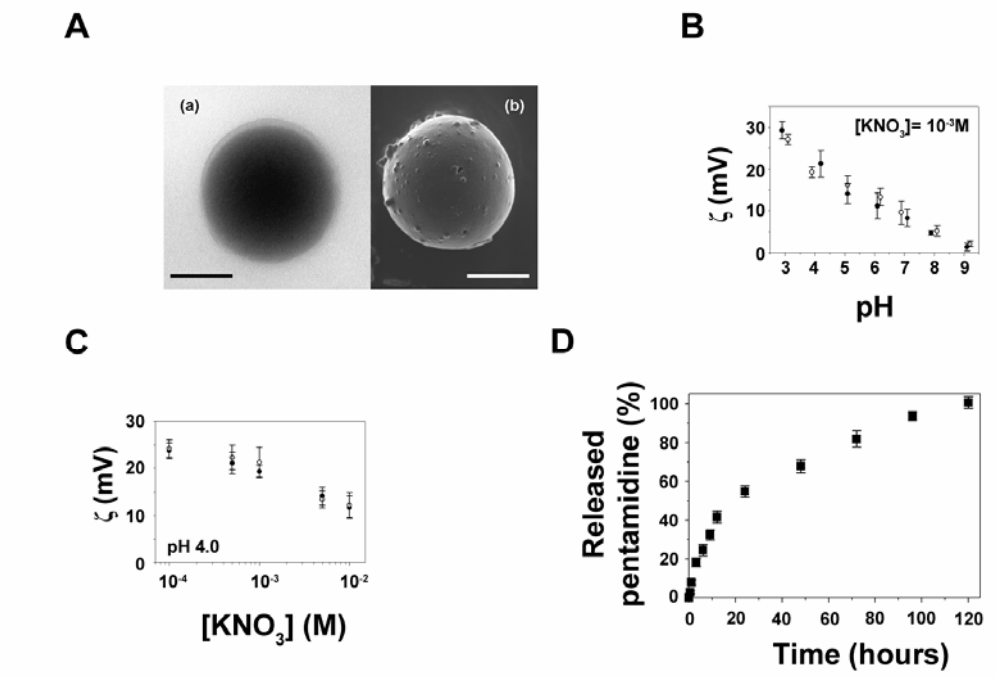

Figure 20. NbAn33-coated pentamidine-loaded PEGlycated-chitosan nanoparticles characterization. **A.** High-resolution transmission electron microscopy (a) and field emission scanning electron microscopy (b). Bar length: 50 nm. **B.** Potential zeta value (ζ mV) of pentamidine loaded NPs (full circles) and non pentamidine loaded NPs (open circles) as function of the pH at ionic strength of 10^{-3}M KNO_3. **C.** Potential zeta value (ζ mV) of pentamidine loaded NPs (full circles) and non pentamidine loaded NPs (open circles) as function of the KNO_3 concentration at natural pH (≈4.0). **D.** Release of pentamidine from NbAn33-pentamidine-chNPs as a function of the incubation time in NaOH-KH_2PO_4 pH 7.4±0.1 buffer as the release medium.

C.1.2. NbAn33 is internalized and accumulated in the endocytic pathway.

T. brucei AnTat1.1 bloodstream-forms was incubated in the presence of Alexa-488 labelled NbAn33. As expected, labelled NbAn33 was immediately detected at the surface of trypanosomes and internalized by endocytosis within 10 min (Fig. 21).

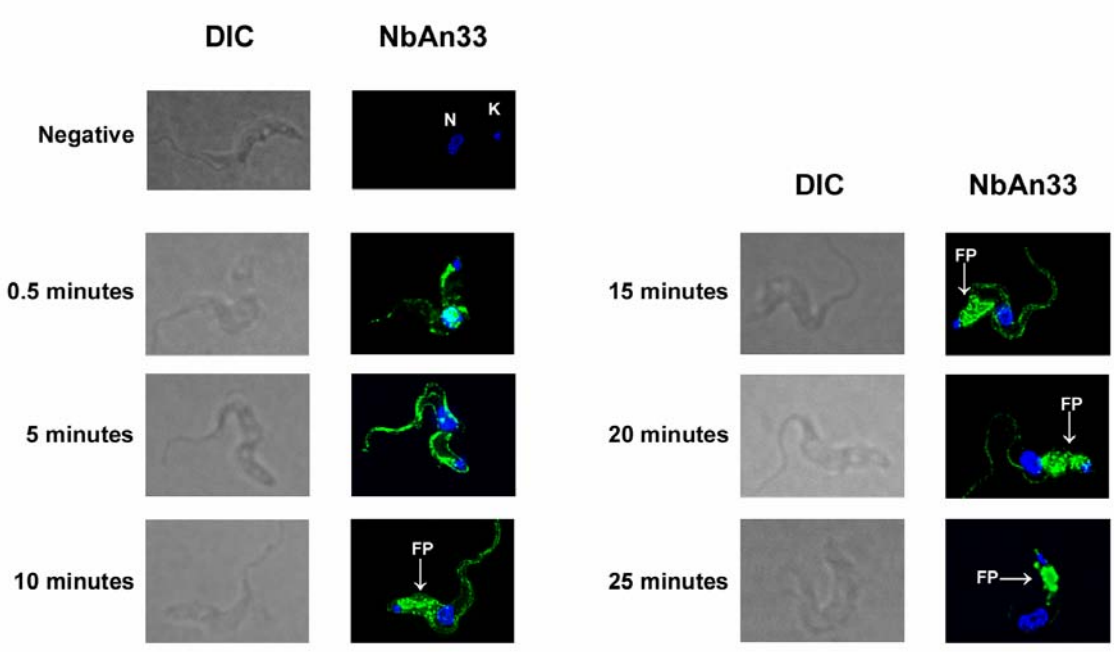

Figure 21. Alexa 488-laballed NbAn33 accumulates in the FP. Live bloodstream-forms of *T. brucei* monomorphic AnTat1.1 strain were incubated in trypanosome dilution buffer (TDB) at 37° C with Alexa-488 labelled NbAn33. Samples were taken at 0.5, 5 and 10 min. Then, Nb excess was removed and the following samples were taken at 15, 20 and 25 minutes after the start of the assay. Alexa-488 labelled NbAn33 is shown in green. Nuclei and Kinetoplast were stained with DAPI, in blue. N, nuclei. K, kinetoplast. FP, flagellar pocket.

C.1.3. NbAn33-pentamidine-chNPs improves pentamidine efficiency in *T. brucei.*

The half-inhibitory concentration (IC50) value of pentamidine on bloodstream *T. brucei* was 9.58 nM (SD ± 0.27) (Fig. 22). The trypanolytic effect of pentamidine was remarkably improved when loaded into NbAn33-chNPs. The IC50 value was 0.69 nM (SD ± 0.02) which meant 13.93-fold reduction relative to free pentamidine (Fig. 22). To evaluate the contribution of NbAn33 to the nanoparticles, the inherent effect of pentamidine-chNPs non-coated by the NbAn33 was tested in parallel. The trypanocidal activity of non-coated NPs was higher than pentamidine alone showing an IC50 of 1.94 nM (SD ± 0.11) (4.93-fold reduction, Fig. 22), but lower than NbAn33-coated

pentamidine-chNPs. Controls (NbAn33 alone, chNPs empty and NbAn33-chNPs empty) did not show any effect in parasites.

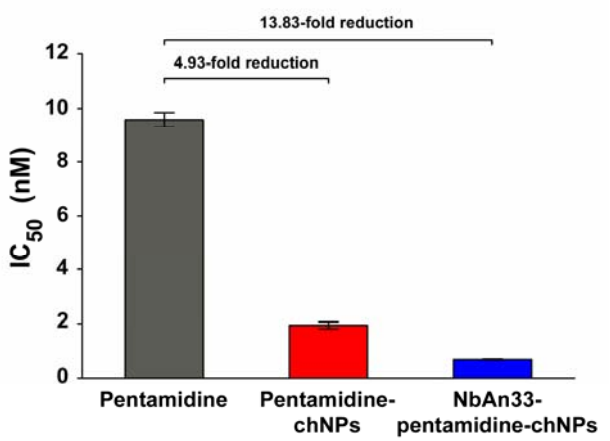

Figure 22. Trypanocidal activity of pentamidine formulations. Gray column: IC50 value for pentamidine. Red column: IC50 value for pentamidine-chNPs. Blue column: IC50 value for NbAn33-pentamidine-chNPs. Errors bars indicate SD from 3-9 independent experiments. are indicated in the graph.

C.1.4. NbAn33-pentamidine-chNPs reduces 100-fold the minimal full curative dose of pentamidine in mouse model of acute trypanosomiasis.

The minimal full curative dose of pentamidine in mouse model of acute infection of *T. brucei* was four doses of 2.5 mg·kg^{-1} administrated daily by i.p. injection in four consecutive days, starting upon detection of parasites in blood (day 3 after infection). When mice were treated with 10 times lower pentamidine dose (4 x 0.25 mg·kg^{-1}) the parasites disappeared from the peripheral blood after the third dose (Fig. 23A). However, the infection relapsed and the mice began to die at day 22 after infection, curing only a 20% of the treated animals (Fig. 23B)

Once established the suboptimal pentamidine curative dose, we treated mice with equal dose of pentamidine loaded into NbAn33-chNPs. In this group, clearance of parasites was complete after the first dose and the treatment was successful, curing 100% of the animals (Fig. 23A-B). Next, a dose 100 times lower than the minimal curative dose of pentamidine was tested. At that low concentration (4 x 0.025 mg·kg^{-1}), free pentamidine did not cure mice from trypanosome infection. While the parasitemia levels were slowed down relative to untreated mice, the parasites never disappeared from the blood, dying 100% of treated mice between the days 7-12 after infection (Fig. 23A-B). Remarkably, treatment with 4 doses of NbAn33-pentamidine-chNPs at 0.025 mg·kg^{-1} was able to abrogate the parasitemia after the second dose cured all treated mice (Fig. 23A-B).

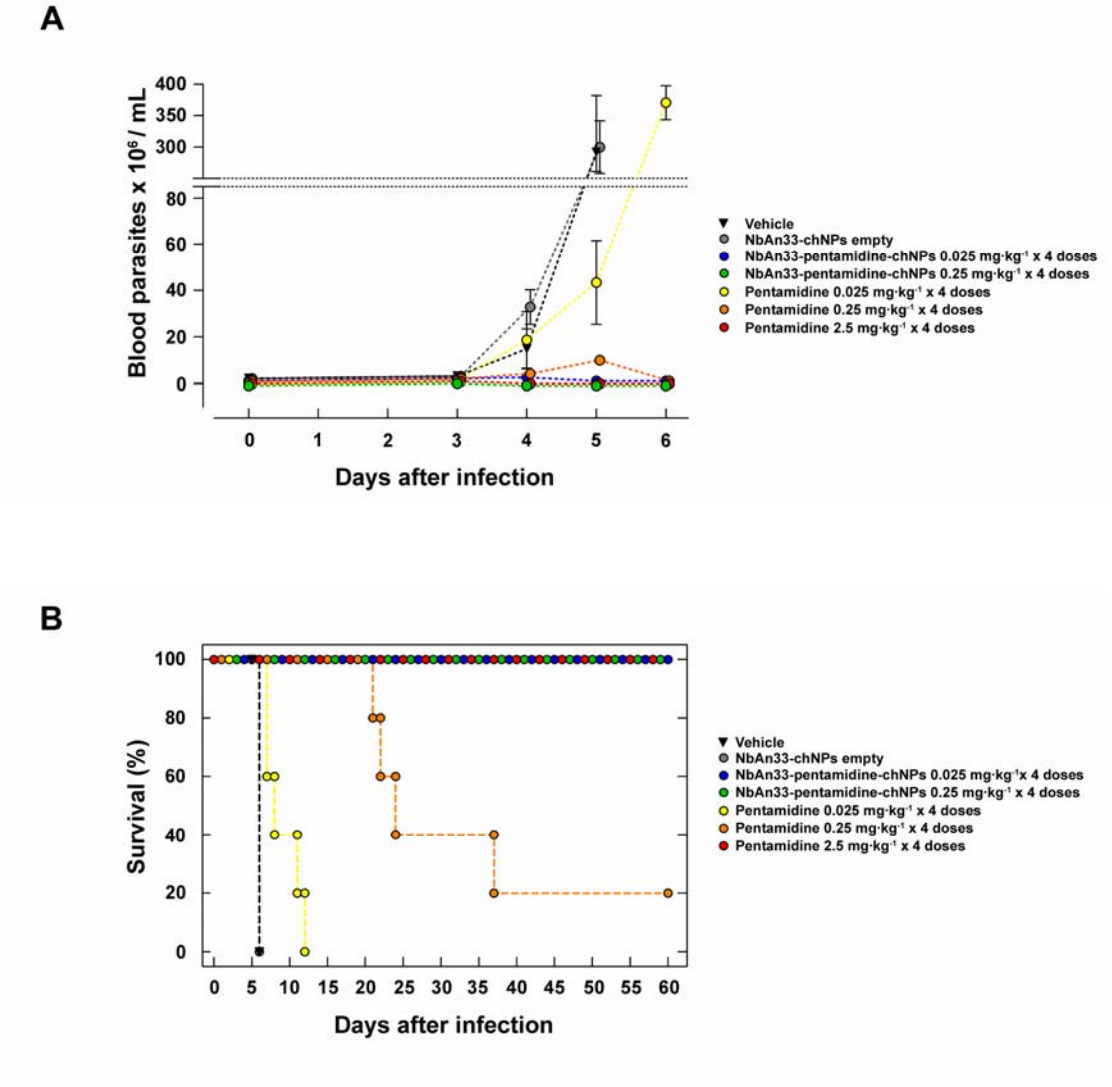

Figure 23. Therapeutic effect of the NbAn33-pentamidine-chNPs in *T. brucei* mouse model. Parasitemia (**A**) and survival (**B**) (Kaplan-Meier plot) of female C57BL/6J mice infected with *T. brucei* AnTat1.1 (inoculum $1X10^4$ parasites). Groups: *NbAn33-pentamidine-chNPs*, nanobody-coated pentamidine-loaded PEGlycated chitosan nanoparticles. *NbAn33-chNPs empty*, empty nanobody-coated PEGlycated-chitosan nanoparticles. *Pentamidine,* free pentamidine. *Vehicle*; physiological serum. Errors bars represent SD.

C.1.5. Generation and characterization of a *T. brucei* pentamidine resistant cell line.

All known resistances to pentamidine are associated to mutations in the surface proteins TbAT1/P2-adenosine transporter or aquaglyceroporin 2 (*AQP2*) channel [22,23,24,25,26,27,28,29,199]. We reasoned that pentamidine loaded into nanoparticles coated by nanobody would be endocytosed by the parasite circumventing drug resistance. To test this hypothesis a *T. brucei* resistant clone was selected after *in vitro* exposure to increasing concentrations of pentamidine. The

resistant clone, designated *Tb*R25, was genetic and functionally characterized to determine whether resistance was due to a mutation in one known pentamidine surface transporter.

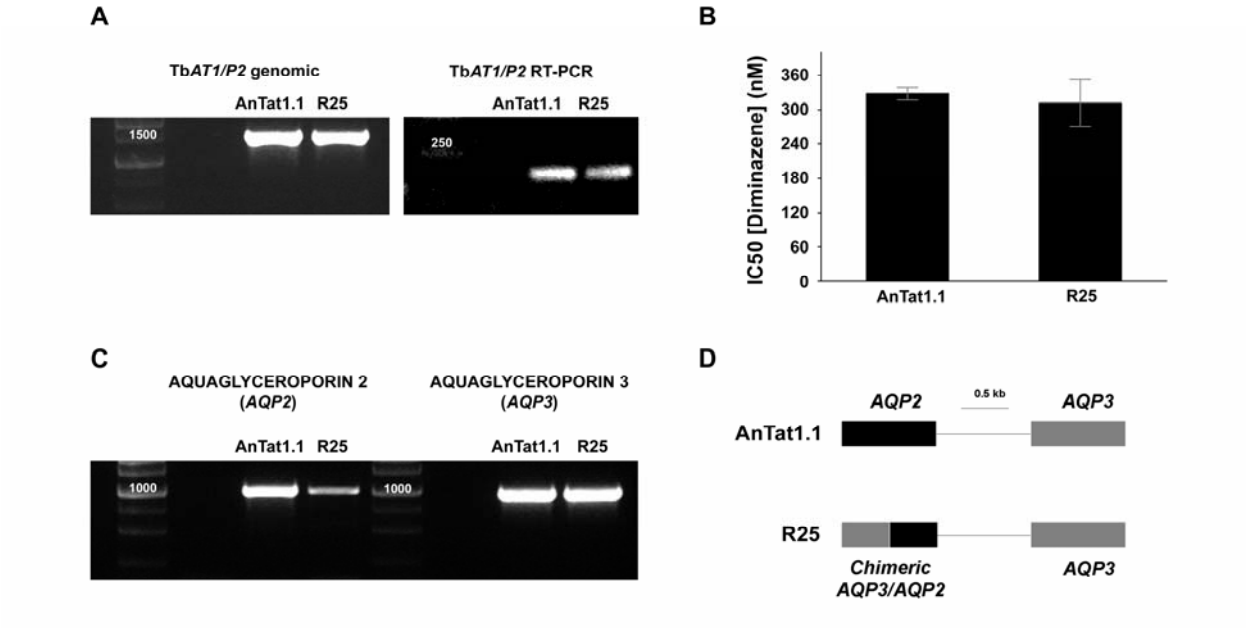

Figure 24. Pentamidine resistant *Tb*R25 cell line characterization. **A.** Tb*AT1/P2* genomic PCR amplification and expression analysis by RT-PCR. **B.** IC50 value for diminazene aceturate. Errors bars indicate SD from 3 independent experiments. **C.** PCR products of *AQP2* and *AQP3* genes. **D.** Schematic illustration of the AQP locus, showing the chimeric gene in R25 strain.

Tb*AT1/P2*-adenosine transporter gene was amplified from wild-type and *Tb*R25 genomic DNA. No differences in length or sequence were observed between both PCR products. Moreover, no significant change in TbAT1/P2 expression profile was noted by RT-PCR analysis between both wild type and resistant cell lines (Fig. 24A). Finally, TbR25 and wild type trypanosomes were equally sensitive to diminazene aceturate (Fig. 24B), another trypanocidal aromatic diamidine whose uptake is partially mediated by TbAT1/P2 adenosine transporter. These results ruled out the implication of the Tb*AT1/P2* in the resistance mechanism of *Tb*R25 cell line to pentamidine (Fig. 24B) [200].

We next searched for mutations in the genomic locus encoding the closely related AQP2 and AQP3 surface channels. Interestingly, semiquantitative genomic PCR analysis of *AQP2/3* genes showed differences in the amount of *AQP2* amplification product between wild type and *Tb*R25 cells (Fig. 24C). Sequencing analysis of *AQP2/3*

PCR products revealed the presence of an *AQP3/AQP2* chimeric gene instead of *AQP2*, The first 453 nucleotides corresponded to *AQP3* and the rest, 462 nucleotides, to *AQP2* (Fig. 24D). In contrast, *AQP3* sequence was intact. These results suggested that the mechanism of acquired resistance to pentamidine in the TbR25 cell line could be due predominantly to the replacement of *AQP2* by the chimera *AQP3/AQP2*.

C.1.6. NbAn33-pentamidine-chNPs overcome pentamidine resistance of *Tb*R25 cell line.

Next, we tested whether NbAn33-pentamidine-chNPs were able to circumvent pentamidine resistance in our trypanosome resistant cell line. Pentamidine IC50 value for bloodstream *Tb*R25 was 114.77 nM (SD ± 5.08) (Fig. 25). Remarkably, NbAn33-pentamidine-chNPs reduced the pentamidine IC50 to wild type sensitivity levels 9.87 nM (SD ± 0.68). The reduction was 11.62-fold, similar to those obtained in wild type *T. brucei* (Fig. 22). Uncoated pentamidine-chNPs also reduced 2.06-fold the IC50 compared to free pentamidine (Fig. 25).

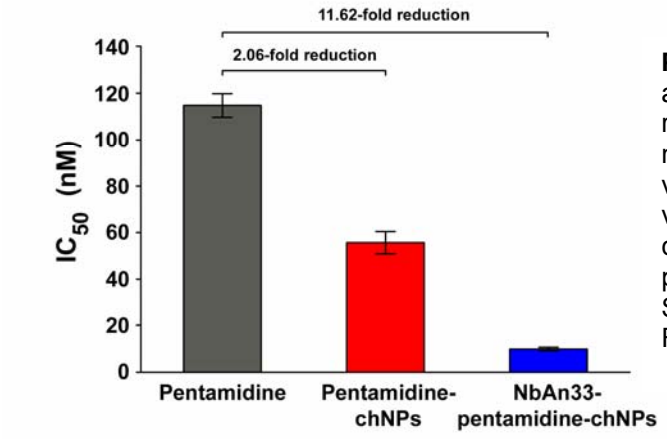

Figure 25. R25 sensitive profile. IC50 was assessed using an adapted version of the resarzurin sodium salt procedure, see material and methods. Gray column: IC50 value for pentamidine. Red column: IC50 value for pentamidine-chNPs. Blue column: IC50 value for NbAn33-pentamidine-chNPs. Errors bars indicate SD from 3-9 independent experiments. Fold reductions are indicated in the graph.

C.2. Discussion.

New approaches in currents chemotherapies are focused in the use of targeted drug delivery systems. In this context, we have validated an immunology-targeted delivery system which improves selectivity and effectiveness of pentamidine, the drug of choice in the early stage of *T. b. gambiense* infection. We have prepared pentamidine-loaded nanoparticles of chitosan polymer coated by a nanobody (NbAn33) that target the surface of *T. brucei*. The optimal characteristics in size, shape, entrapment efficiency and control drug release control make these nanobody-coated

nanoparticles suitable for parenteral administration and for efficient deliver of drugs to African trypanosomes.

The new formulation was significantly more efficient than free pentamidine in killing trypanosomes. *In vitro* studies revealed that the half-inhibitory concentration (IC50) of pentamidine-loaded in nanobody-coated PEGlycated chitosan nanoparticles was ~14 fold lower than pentamidine alone (Fig. 22). Interestingly, also pentamidine-loaded into nanobody-uncoated nanoparticles was more effective against *T. brucei* than free pentamidine. This improvement might be the consequence of electrostatic interactions between the slight positive charges of chitosan nanoparticles with negative charges present on the parasite cell membrane, boosted by the high rate of endocytosis of *T. brucei* bloodstream-forms [54,201,202]. Nevertheless, the antitrypanocidal effect of NbAn33-coated-pentamidine-chNPs was approximately 9-fold higher than nanobody-uncoated pentamidine-chNPs, highlighting the crucial role of NbAn33 in the significant improvement of treatment efficiency.

Remarkably, this new immunologically-targeted delivery system reduced 100-fold the minimal full curative dose of pentamidine in an *in vivo* model of *T. b. brucei* infection (Fig. 23A-B). The administration of pentamidine-loaded into functionalized PEGlycated-chitosan nanoparticles protected the drug from rapid degradation and clearance from the bloodstream. This protecting effect, together with the slow release from the nanoparticles probably exerts a beneficial effect on the pharmacokinetic profile of pentamidine.

The emergence of resistance is the major concern nowadays together with the absence of vaccines. Most of trypanocidal drugs do not diffuse freely across parasite cell membrane, but several transporters are responsible for their uptake. Initially, resistance mechanisms have been associated to mutations which reduce drug import. However, it is not well understood if these mutations could involve overexpression of drug exporters, loss of drug importers or changes in drug transporter-substrate specificity [203]. A recent genomic-scale up screening has linked main current HAT drugs, except nifurtimox, to specific genes encoding surface transporters which are involved in drug uptake [28]. Eflornithine to amino acid transporter family member AAT6, suramin to invariant surface glycoprotein ISG75, melarsoprol to adenosine transporter AT1/P2, pentamidine to P-type H^+-ATPases and pentamidine/melarsoprol cross resistant to aquaglyceroporins, specifically to aquaglyceroporin 2 which controls the susceptibility to both drugs 2 [28,29].

The association between resistance and mutations in surface proteins would explain why *Tb*R25 pentamidine-resistant cell lines were not longer resistant to pentamidine loaded into chitosan nanoparticles and coated by NbAn33. In a resistant strain, drug uptake is blocked by the loss of functionality of specific transporters. However, the NbAn33 introduces the nanoparticles by endocytosis taking advantage of the natural process of VSG recycling and internalization. This alternative uptake route make possible that a pentamidine resistant strain due to the substitution AQP2 by a chimeric AQP3/AQP2 is killed at pentamidine wild-type levels using NbAn33-pentamidine-chNPs.

This new formulation can be used with the current drugs employed in HAT which a recent high-throughput screening has linked to genes encoding cell surface transporters [28]. The development of current antitrypanocidal drugs loaded chitosan nanoparticles coated by a specific nanobody against trypanosomes can reduce the minimal curative dose of these drugs, enhancing the efficiency, minimizing the toxicity and circumventing resistance mechanisms associated to mutation in surface transporters. The possibilities that offer this targeted nanobody-system are enormous due to its versatility, as it can be adapted to encapsulate any substance with a reported trypanocidal action. This opens up a plethora of new possible therapies to treat Trypanosomal and other parasitic infections.

CONCLUSSIONS

1. Nicotinamide, a soluble compound of vitamin B3, possesses trypanocidal activity. Nicotinamide treatment results in *T. brucei* cell growth inhibition and dimorphism of the flagellar pocket, the site for both endocytosis and exocitosis and the subjacent endocytic compartment. Protease assays on cellular extract shows that nicotinamide inhibits lysosomal protease cathepsin B and subsequently blocks endocytosis causing programmed cell death. Moreover, nicotinamide exerts a direct inhibitory effect on recombinant TbCatB. Therefore, the trypanocidal activity of nicotinamide is due to direct inhibition of cathepsin-like B protease. Finally, an *in vivo* study shows that nicotinamide has an alleviating effect on infective mice. The results presented here support the possible use of NAM in HAT therapy.

2. Nanobody-coated pentamidine-loaded chitosan nanoparticles are more efficient than pentamidine alone in killing trypanosomes. *In vitro* studies revealed a notably reduction of the IC50 compared with pentamidine alone. Moreover, an *in vivo* experiment in murine model of the acute phase of African trypanosomiasis determined that the curative dose of pentamidine loaded in Nb-chitosan nanoparticles was 100 fold lower than pentamidine alone, improving strongly the efficiency of the pentamidine.

3. Nanobody-coated pentamidine-loaded chitosan nanoparticles are able to circumvent resistance mechanism associated to cell surface transporters making that a resistant cell line was not resistant to nanobody-coated pentamidine-loaded nanoparticles.

CONCLUSIONES

1. La nicotinamida, un compuesto soluble de vitamina B3, posee actividad tripanocida. El tratamiento con nicotinamida produce en *T. brucei,* la inhibición del crecimiento celular y el dimorfismo de la bolsa flagelar, lugar donde se producen los procesos endocitosis y exocitosis. La medida de la actividad proteasa realizada sobre extractos celulares demuestran que la nicotinamida inhibe a la proteasa lisosomal catepsina B (TbCatB) y posteriormente bloquea la endocitosis causando muerte celular programada. Además, la nicotinamida ejerce un efecto inhibidor directo sobre TbCatB recombinante. Por lo tanto, la actividad tripanocida de nicotinamida es debido a la inhibición directa de la proteasa catepsina B. Por último, un estudio *in vivo* demuestra que la nicotinamida tiene un efecto aliviador de la enfermedad en ratones infecciosos. Los resultados presentados aquí apoyan el posible uso de la nicotinamida en la terapia de HAT.

2. La nueva formulación consistente en nanopartículas de chitosan cargadas de pentamidina y recubiertas de nanobody contra *T. brucei*, mejora notablemente el efecto tripanocida de la pentamidina sola. Los estudios *in vitro* revelaron una reducción importante de IC50 en comparación con pentamidina solo. Sin embargo esta mejora fue incrementada en un experimento *in vivo* en modelo murino de fase aguda de tripanosomiasis africana donde se determinó que la dosis curativa de nanopartículas de chitosan cargadas de pentamidina y recubiertas de nanobody era 100 veces menor que la dosis de pentamidina sola.

3. Este nuevo sistema basado en nanopartículas recubiertas de nanobodies es capaz de superar, en ensayos *in vitro*, los mecanismos de resistencia asociados a transportadores membrana.

REFERENCES

1. Barrett MP, Burchmore RJ, Stich A, Lazzari JO, Frasch AC, et al. (2003) The trypanosomiases. Lancet 362: 1469-1480.
2. Brun R, Blum J (2012) Human african trypanosomiasis. Infect Dis Clin North Am 26: 261-273.
3. Brun R, Blum J, Chappuis F, Burri C (2010) Human African trypanosomiasis. Lancet 375: 148-159.
4. Odiit M, Kansiime F, Enyaru JC (1997) Duration of symptoms and case fatality of sleeping sickness caused by Trypanosoma brucei rhodesiense in Tororo, Uganda. East Afr Med J 74: 792-795.
5. Blum J, Schmid C, Burri C (2006) Clinical aspects of 2541 patients with second stage human African trypanosomiasis. Acta Trop 97: 55-64.
6. Checchi F, Filipe JA, Haydon DT, Chandramohan D, Chappuis F (2008) Estimates of the duration of the early and late stage of gambiense sleeping sickness. BMC Infect Dis 8: 16.
7. (1986) Epidemiology and control of African trypanosomiasis. Report of a WHO Expert Committee. World Health Organ Tech Rep Ser 739: 1-127.
8. Van Nieuwenhove S, Betu-Ku-Mesu VK, Diabakana PM, Declercq J, Bilenge CM (2001) Sleeping sickness resurgence in the DRC: the past decade. Trop Med Int Health 6: 335-341.
9. Moore A, Richer M (2001) Re-emergence of epidemic sleeping sickness in southern Sudan. Trop Med Int Health 6: 342-347.
10. Barrett MP (1999) The fall and rise of sleeping sickness. The Lancet 353: 1113-1114.
11. Barrett MP (2006) The rise and fall of sleeping sickness. Lancet 367: 1377-1378.
12. Simarro PP, Diarra A, Ruiz Postigo JA, Franco JR, Jannin JG (2011) The human African trypanosomiasis control and surveillance programme of the World Health Organization 2000-2009: the way forward. PLoS Negl Trop Dis 5: e1007.
13. Kristjanson PM, Swallow BM, Rowlands GJ, Kruska RL, de Leeuw PN (1999) Measuring the costs of African animal trypanosomosis, the potential benefits of control and returns to research. Agricultural Systems 59: 79-98.
14. Fevre EM, Wissmann BV, Welburn SC, Lutumba P (2008) The burden of human African trypanosomiasis. PLoS Negl Trop Dis 2: e333.
15. Pays E, Vanhamme L, Perez-Morga D (2004) Antigenic variation in Trypanosoma brucei: facts, challenges and mysteries. Curr Opin Microbiol 7: 369-374.
16. Jacobs RT, Nare B, Phillips MA (2011) State of the art in African trypanosome drug discovery. Curr Top Med Chem 11: 1255-1274.
17. Wang CC (1995) Molecular mechanisms and therapeutic approaches to the treatment of African trypanosomiasis. Annu Rev Pharmacol Toxicol 35: 93-127.
18. Barrett MP, Boykin DW, Brun R, Tidwell RR (2007) Human African trypanosomiasis: pharmacological re-engagement with a neglected disease. Br J Pharmacol 152: 1155-1171.
19. De Koning HP (2001) Uptake of pentamidine in Trypanosoma brucei brucei is mediated by three distinct transporters: implications for cross-resistance with arsenicals. Mol Pharmacol 59: 586-592.
20. Delespaux V, de Koning HP (2007) Drugs and drug resistance in African trypanosomiasis. Drug Resist Updat 10: 30-50.
21. Ortiz D, Sanchez MA, Quecke P, Landfear SM (2009) Two novel nucleobase/pentamidine transporters from Trypanosoma brucei. Mol Biochem Parasitol 163: 67-76.
22. Carter NS, Berger BJ, Fairlamb AH (1995) Uptake of diamidine drugs by the P2 nucleoside transporter in melarsen-sensitive and -resistant Trypanosoma brucei brucei. J Biol Chem 270: 28153-28157.
23. Maser P, Sutterlin C, Kralli A, Kaminsky R (1999) A nucleoside transporter from Trypanosoma brucei involved in drug resistance. Science 285: 242-244.

24. Matovu E, Stewart ML, Geiser F, Brun R, Maser P, et al. (2003) Mechanisms of arsenical and diamidine uptake and resistance in Trypanosoma brucei. Eukaryot Cell 2: 1003-1008.
25. Bernhard SC, Nerima B, Maser P, Brun R (2007) Melarsoprol- and pentamidine-resistant Trypanosoma brucei rhodesiense populations and their cross-resistance. Int J Parasitol 37: 1443-1448.
26. Bridges DJ, Gould MK, Nerima B, Maser P, Burchmore RJ, et al. (2007) Loss of the high-affinity pentamidine transporter is responsible for high levels of cross-resistance between arsenical and diamidine drugs in African trypanosomes. Mol Pharmacol 71: 1098-1108.
27. de Koning HP (2008) Ever-increasing complexities of diamidine and arsenical crossresistance in African trypanosomes. Trends Parasitol 24: 345-349.
28. Alsford S, Eckert S, Baker N, Glover L, Sanchez-Flores A, et al. (2012) High-throughput decoding of antitrypanosomal drug efficacy and resistance. Nature 482: 232-236.
29. Baker N, Glover L, Munday JC, Aguinaga Andres D, Barrett MP, et al. (2012) Aquaglyceroporin 2 controls susceptibility to melarsoprol and pentamidine in African trypanosomes. Proc Natl Acad Sci U S A.
30. Uzcategui NL, Szallies A, Pavlovic-Djuranovic S, Palmada M, Figarella K, et al. (2004) Cloning, heterologous expression, and characterization of three aquaglyceroporins from Trypanosoma brucei. J Biol Chem 279: 42669-42676.
31. Wille U, Schade B, Duszenko M (1998) Characterization of glycerol uptake in bloodstream and procyclic forms of Trypanosoma brucei. Eur J Biochem 256: 245-250.
32. Bassarak B, Uzcategui NL, Schonfeld C, Duszenko M (2011) Functional characterization of three aquaglyceroporins from Trypanosoma brucei in osmoregulation and glycerol transport. Cell Physiol Biochem 27: 411-420.
33. Fairlamb AH, Bowman IB (1980) Uptake of the trypanocidal drug suramin by bloodstream forms of Trypanosoma brucei and its effect on respiration and growth rate in vivo. Mol Biochem Parasitol 1: 315-333.
34. Awadzi K, Hero M, Opoku NO, Addy ET, Buttner DW, et al. (1995) The chemotherapy of onchocerciasis XVIII. Aspects of treatment with suramin. Trop Med Parasitol 46: 19-26.
35. Keiser J, Ericsson O, Burri C (2000) Investigations of the metabolites of the trypanocidal drug melarsoprol. Clin Pharmacol Ther 67: 478-488.
36. Keiser J, Burri C (2000) Physico-chemical properties of the trypanocidal drug melarsoprol. Acta Trop 74: 101-104.
37. Carter NS, Fairlamb AH (1993) Arsenical-resistant trypanosomes lack an unusual adenosine transporter. Nature 361: 173-176.
38. Fairlamb AH, Henderson GB, Cerami A (1989) Trypanothione is the primary target for arsenical drugs against African trypanosomes. Proc Natl Acad Sci U S A 86: 2607-2611.
39. Fairlamb AH, Cerami A (1992) Metabolism and functions of trypanothione in the Kinetoplastida. Annu Rev Microbiol 46: 695-729.
40. Bitonti AJ, Bacchi CJ, McCann PP, Sjoerdsma A (1985) Catalytic irreversible inhibition of Trypanosoma brucei brucei ornithine decarboxylase by substrate and product analogs and their effects on murine trypanosomiasis. Biochem Pharmacol 34: 1773-1777.
41. Bacchi CJ, Nathan HC, Hutner SH, McCann PP, Sjoerdsma A (1980) Polyamine metabolism: a potential therapeutic target in trypanosomes. Science 210: 332-334.
42. Vincent IM, Creek D, Watson DG, Kamleh MA, Woods DJ, et al. (2010) A molecular mechanism for eflornithine resistance in African trypanosomes. PLoS Pathog 6: e1001204.
43. Docampo R (1990) Sensitivity of parasites to free radical damage by antiparasitic drugs. Chem Biol Interact 73: 1-27.

44. Wilkinson SR, Taylor MC, Horn D, Kelly JM, Cheeseman I (2008) A mechanism for cross-resistance to nifurtimox and benznidazole in trypanosomes. Proc Natl Acad Sci U S A 105: 5022-5027.
45. Checchi F, Piola P, Ayikoru H, Thomas F, Legros D, et al. (2007) Nifurtimox plus Eflornithine for late-stage sleeping sickness in Uganda: a case series. PLoS Negl Trop Dis 1: e64.
46. Priotto G, Kasparian S, Ngouama D, Ghorashian S, Arnold U, et al. (2007) Nifurtimox-eflornithine combination therapy for second-stage Trypanosoma brucei gambiense sleeping sickness: a randomized clinical trial in Congo. Clin Infect Dis 45: 1435-1442.
47. Priotto G, Kasparian S, Mutombo W, Ngouama D, Ghorashian S, et al. (2009) Nifurtimox-eflornithine combination therapy for second-stage African Trypanosoma brucei gambiense trypanosomiasis: a multicentre, randomised, phase III, non-inferiority trial. Lancet 374: 56-64.
48. Xong HV, Vanhamme L, Chamekh M, Chimfwembe CE, Van Den Abbeele J, et al. (1998) A VSG expression site-associated gene confers resistance to human serum in Trypanosoma rhodesiense. Cell 95: 839-846.
49. El-Sayed NM, Hegde P, Quackenbush J, Melville SE, Donelson JE (2000) The African trypanosome genome. Int J Parasitol 30: 329-345.
50. Kennedy PG (2004) Human African trypanosomiasis of the CNS: current issues and challenges. J Clin Invest 113: 496-504.
51. Matthews KR (2005) The developmental cell biology of Trypanosoma brucei. J Cell Sci 118: 283-290.
52. McKean PG (2003) Coordination of cell cycle and cytokinesis in Trypanosoma brucei. Curr Opin Microbiol 6: 600-607.
53. Garcia-Salcedo JA, Perez-Morga D, Gijon P, Dilbeck V, Pays E, et al. (2004) A differential role for actin during the life cycle of Trypanosoma brucei. EMBO J 23: 780-789.
54. Overath P, Engstler M (2004) Endocytosis, membrane recycling and sorting of GPI-anchored proteins: Trypanosoma brucei as a model system. Mol Microbiol 53: 735-744.
55. Acosta-Serrano A, Cole RN, Mehlert A, Lee MG, Ferguson MA, et al. (1999) The procyclin repertoire of Trypanosoma brucei. Identification and structural characterization of the Glu-Pro-rich polypeptides. J Biol Chem 274: 29763-29771.
56. Salmon D, Geuskens M, Hanocq F, Hanocq-Quertier J, Nolan D, et al. (1994) A novel heterodimeric transferrin receptor encoded by a pair of VSG expression site-associated genes in T. brucei. Cell 78: 75-86.
57. Steverding D, Stierhof YD, Chaudhri M, Ligtenberg M, Schell D, et al. (1994) ESAG 6 and 7 products of Trypanosoma brucei form a transferrin binding protein complex. Eur J Cell Biol 64: 78-87.
58. Steverding D, Stierhof YD, Fuchs H, Tauber R, Overath P (1995) Transferrin-binding protein complex is the receptor for transferrin uptake in Trypanosoma brucei. J Cell Biol 131: 1173-1182.
59. Vanhamme L, Paturiaux-Hanocq F, Poelvoorde P, Nolan DP, Lins L, et al. (2003) Apolipoprotein L-I is the trypanosome lytic factor of human serum. Nature 422: 83-87.
60. Vanhollebeke B, De Muylder G, Nielsen MJ, Pays A, Tebabi P, et al. (2008) A haptoglobin-hemoglobin receptor conveys innate immunity to Trypanosoma brucei in humans. Science 320: 677-681.
61. Green HP, Del Pilar Molina Portela M, St Jean EN, Lugli EB, Raper J (2003) Evidence for a Trypanosoma brucei lipoprotein scavenger receptor. J Biol Chem 278: 422-427.
62. Liu J, Qiao X, Du D, Lee MG (2000) Receptor-mediated endocytosis in the procyclic form of Trypanosoma brucei. J Biol Chem 275: 12032-12040.
63. Field MC, Carrington M (2009) The trypanosome flagellar pocket. Nat Rev Microbiol 7: 775-786.

64. Hammarton TC (2007) Cell cycle regulation in Trypanosoma brucei. Mol Biochem Parasitol 153: 1-8.
65. Cross GA (1979) Immunochemical aspects of antigenic variation on trypanosomes. The third Fleming Lecture. J Gen Microbiol 113: 1-11.
66. Auffret CA, Turner MJ (1981) Variant specific antigens of Trypanosoma brucei exist in solution as glycoprotein dimers. Biochem J 193: 647-650.
67. Russo DC, Grab DJ, Lonsdale-Eccles JD, Shaw MK, Williams DJ (1993) Directional movement of variable surface glycoprotein-antibody complexes in Trypanosoma brucei. Eur J Cell Biol 62: 432-441.
68. O'Beirne C, Lowry CM, Voorheis HP (1998) Both IgM and IgG anti-VSG antibodies initiate a cycle of aggregation-disaggregation of bloodstream forms of Trypanosoma brucei without damage to the parasite. Mol Biochem Parasitol 91: 165-193.
69. Pal A, Hall BS, Jeffries TR, Field MC (2003) Rab5 and Rab11 mediate transferrin and anti-variant surface glycoprotein antibody recycling in Trypanosoma brucei. Biochem J 374: 443-451.
70. Engstler M, Thilo L, Weise F, Grunfelder CG, Schwarz H, et al. (2004) Kinetics of endocytosis and recycling of the GPI-anchored variant surface glycoprotein in Trypanosoma brucei. J Cell Sci 117: 1105-1115.
71. Engstler M, Pfohl T, Herminghaus S, Boshart M, Wiegertjes G, et al. (2007) Hydrodynamic flow-mediated protein sorting on the cell surface of trypanosomes. Cell 131: 505-515.
72. Johnson JG, Cross GA (1979) Selective cleavage of variant surface glycoproteins from Trypanosoma brucei. Biochem J 178: 689-697.
73. Allen G, Gurnett LP (1983) Locations of the six disulphide bonds in a variant surface glycoprotein (VSG 117) from Trypanosoma brucei. Biochem J 209: 481-487.
74. Carrington M, Miller N, Blum M, Roditi I, Wiley D, et al. (1991) Variant specific glycoprotein of Trypanosoma brucei consists of two domains each having an independently conserved pattern of cysteine residues. J Mol Biol 221: 823-835.
75. Blum ML, Down JA, Gurnett AM, Carrington M, Turner MJ, et al. (1993) A structural motif in the variant surface glycoproteins of Trypanosoma brucei. Nature 362: 603-609.
76. Carrington M, Boothroyd J (1996) Implications of conserved structural motifs in disparate trypanosome surface proteins. Mol Biochem Parasitol 81: 119-126.
77. Borst P, Fairlamb AH (1998) Surface receptors and transporters of Trypanosoma brucei. Annu Rev Microbiol 52: 745-778.
78. Mussmann R, Engstler M, Gerrits H, Kieft R, Toaldo CB, et al. (2004) Factors affecting the level and localization of the transferrin receptor in Trypanosoma brucei. J Biol Chem 279: 40690-40698.
79. Pays E, Vanhollebeke B, Vanhamme L, Paturiaux-Hanocq F, Nolan DP, et al. (2006) The trypanolytic factor of human serum. Nat Rev Microbiol 4: 477-486.
80. Allen CL, Goulding D, Field MC (2003) Clathrin-mediated endocytosis is essential in Trypanosoma brucei. EMBO J 22: 4991-5002.
81. Hung CH, Qiao X, Lee PT, Lee MG (2004) Clathrin-dependent targeting of receptors to the flagellar pocket of procyclic-form Trypanosoma brucei. Eukaryot Cell 3: 1004-1014.
82. Pal A, Hall BS, Nesbeth DN, Field HI, Field MC (2002) Differential endocytic functions of Trypanosoma brucei Rab5 isoforms reveal a glycosylphosphatidylinositol-specific endosomal pathway. J Biol Chem 277: 9529-9539.
83. Zerial M, McBride H (2001) Rab proteins as membrane organizers. Nat Rev Mol Cell Biol 2: 107-117.
84. Seabra MC, Wasmeier C (2004) Controlling the location and activation of Rab GTPases. Curr Opin Cell Biol 16: 451-457.
85. Grosshans BL, Ortiz D, Novick P (2006) Rabs and their effectors: achieving specificity in membrane traffic. Proc Natl Acad Sci U S A 103: 11821-11827.

86. Hall BS, Smith E, Langer W, Jacobs LA, Goulding D, et al. (2005) Developmental variation in Rab11-dependent trafficking in Trypanosoma brucei. Eukaryot Cell 4: 971-980.
87. Hall BS, Pal A, Goulding D, Field MC (2004) Rab4 is an essential regulator of lysosomal trafficking in trypanosomes. J Biol Chem 279: 45047-45056.
88. Kelley RJ, Alexander DL, Cowan C, Balber AE, Bangs JD (1999) Molecular cloning of p67, a lysosomal membrane glycoprotein from Trypanosoma brucei. Mol Biochem Parasitol 98: 17-28.
89. Peck RF, Shiflett AM, Schwartz KJ, McCann A, Hajduk SL, et al. (2008) The LAMP-like protein p67 plays an essential role in the lysosome of African trypanosomes. Mol Microbiol 68: 933-946.
90. Vanhamme L, Paturiaux-Hanocq F, Poelvoorde P, Nolan DP, Lins L, et al. (2003) Apolipoprotein L-I is the trypanosome lytic factor of human serum. Nature 422: 83-87.
91. Hajduk SL, Moore DR, Vasudevacharya J, Siqueira H, Torri AF, et al. (1989) Lysis of Trypanosoma brucei by a toxic subspecies of human high density lipoprotein. J Biol Chem 264: 5210-5217.
92. Tomlinson S, Jansen AM, Koudinov A, Ghiso JA, Choi-Miura NH, et al. (1995) High-density-lipoprotein-independent killing of Trypanosoma brucei by human serum. Mol Biochem Parasitol 70: 131-138.
93. Pays E, Lips S, Nolan D, Vanhamme L, Perez-Morga D (2001) The VSG expression sites of Trypanosoma brucei: multipurpose tools for the adaptation of the parasite to mammalian hosts. Mol Biochem Parasitol 114: 1-16.
94. Vanhamme L, Poelvoorde P, Pays A, Tebabi P, Van Xong H, et al. (2000) Differential RNA elongation controls the variant surface glycoprotein gene expression sites of Trypanosoma brucei. Mol Microbiol 36: 328-340.
95. De Greef C, Chimfwembe E, Kihang'a Wabacha J, Bajyana Songa E, Hamers R (1992) Only the serum-resistant bloodstream forms of Trypanosoma brucei rhodesiense express the serum resistance associated (SRA) protein. Ann Soc Belg Med Trop 72 Suppl 1: 13-21.
96. Vermelho AB G-d-SS, d'Avila-Levy CM, et al. (2007) Trypanosomatidae peptidases: a target for drugs development. Curr Enzyme Inhib pp. 19-48.
97. Steiger RF, Opperdoes FR, Bontemps J (1980) Subcellular fractionation of Trypanosoma brucei bloodstream forms with special reference to hydrolases. Eur J Biochem 105: 163-175.
98. Letch CA, Gibson W (1981) Trypanosoma brucei: the peptidases of bloodstream trypanosomes. Exp Parasitol 52: 86-90.
99. El-Sayed NM, Donelson JE (1997) African trypanosomes have differentially expressed genes encoding homologues of the Leishmania GP63 surface protease. J Biol Chem 272: 26742-26748.
100. Gruszynski AE, van Deursen FJ, Albareda MC, Best A, Chaudhary K, et al. (2006) Regulation of surface coat exchange by differentiating African trypanosomes. Mol Biochem Parasitol 147: 211-223.
101. Grandgenett PM, Otsu K, Wilson HR, Wilson ME, Donelson JE (2007) A function for a specific zinc metalloprotease of African trypanosomes. PLoS Pathog 3: 1432-1445.
102. Hua S, To WY, Nguyen TT, Wong ML, Wang CC (1996) Purification and characterization of proteasomes from Trypanosoma brucei. Mol Biochem Parasitol 78: 33-46.
103. Wang CC, Bozdech Z, Liu CL, Shipway A, Backes BJ, et al. (2003) Biochemical analysis of the 20 S proteasome of Trypanosoma brucei. J Biol Chem 278: 15800-15808.
104. Steverding D, Spackman RW, Royle HJ, Glenn RJ (2005) Trypanocidal activities of trileucine methyl vinyl sulfone proteasome inhibitors. Parasitol Res 95: 73-76.
105. Mbawa ZR, Webster P, Lonsdale-Eccles JD (1991) Immunolocalization of a cysteine protease within the lysosomal system of Trypanosoma congolense. Eur J Cell Biol 56: 243-250.

106. Troeberg L, Pike RN, Morty RE, Berry RK, Coetzer TH, et al. (1996) Proteases from Trypanosoma brucei brucei. Purification, characterisation and interactions with host regulatory molecules. Eur J Biochem 238: 728-736.
107. Caffrey CR, Hansell E, Lucas KD, Brinen LS, Alvarez Hernandez A, et al. (2001) Active site mapping, biochemical properties and subcellular localization of rhodesain, the major cysteine protease of Trypanosoma brucei rhodesiense. Mol Biochem Parasitol 118: 61-73.
108. Scory S, Caffrey CR, Stierhof YD, Ruppel A, Steverding D (1999) Trypanosoma brucei: killing of bloodstream forms in vitro and in vivo by the cysteine proteinase inhibitor Z-phe-ala-CHN2. Exp Parasitol 91: 327-333.
109. Scory S, Stierhof YD, Caffrey CR, Steverding D (2007) The cysteine proteinase inhibitor Z-Phe-Ala-CHN2 alters cell morphology and cell division activity of Trypanosoma brucei bloodstream forms in vivo. Kinetoplastid Biol Dis 6: 2.
110. Mackey ZB, O'Brien TC, Greenbaum DC, Blank RB, McKerrow JH (2004) A cathepsin B-like protease is required for host protein degradation in Trypanosoma brucei. J Biol Chem 279: 48426-48433.
111. Abdulla MH, O'Brien T, Mackey ZB, Sajid M, Grab DJ, et al. (2008) RNA interference of Trypanosoma brucei cathepsin B and L affects disease progression in a mouse model. PLoS Negl Trop Dis 2: e298.
112. Morty RE, Lonsdale-Eccles JD, Morehead J, Caler EV, Mentele R, et al. (1999) Oligopeptidase B from Trypanosoma brucei, a new member of an emerging subgroup of serine oligopeptidases. J Biol Chem 274: 26149-26156.
113. Morty RE, Lonsdale-Eccles JD, Mentele R, Auerswald EA, Coetzer TH (2001) Trypanosome-derived oligopeptidase B is released into the plasma of infected rodents, where it persists and retains full catalytic activity. Infect Immun 69: 2757-2761.
114. Morty RE, Troeberg L, Pike RN, Jones R, Nickel P, et al. (1998) A trypanosome oligopeptidase as a target for the trypanocidal agents pentamidine, diminazene and suramin. FEBS Lett 433: 251-256.
115. Morty RE, Troeberg L, Powers JC, Ono S, Lonsdale-Eccles JD, et al. (2000) Characterisation of the antitrypanosomal activity of peptidyl alpha-aminoalkyl phosphonate diphenyl esters. Biochem Pharmacol 60: 1497-1504.
116. Liu G, Foster J, Manlapaz-Ramos P, Olivera BM (1982) Nucleoside salvage pathway for NAD biosynthesis in Salmonella typhimurium. J Bacteriol 152: 1111-1116.
117. Jackson TM, Rawling JM, Roebuck BD, Kirkland JB (1995) Large supplements of nicotinic acid and nicotinamide increase tissue NAD+ and poly(ADP-ribose) levels but do not affect diethylnitrosamine-induced altered hepatic foci in Fischer-344 rats. J Nutr 125: 1455-1461.
118. Sakai Y, Jiang J, Kojima N, Kinoshita T, Miyajima A (2002) Enhanced in vitro maturation of fetal mouse liver cells with oncostatin M, nicotinamide, and dimethyl sulfoxide. Cell Transplant 11: 435-441.
119. Vaca P, Berna G, Martin F, Soria B (2003) Nicotinamide induces both proliferation and differentiation of embryonic stem cells into insulin-producing cells. Transplant Proc 35: 2021-2023.
120. Guruprasad KP, Vasudev V, Anilkumar MN, Chethan SA (2002) Inducible protective processes in animal systems. X. Influence of nicotinamide in methyl methanesulfonate-adapted mouse bone marrow cells. Mutagenesis 17: 1-8.
121. Sun AY, Cheng JS (1998) Neuroprotective effects of poly (ADP-ribose) polymerase inhibitors in transient focal cerebral ischemia of rats. Zhongguo Yao Li Xue Bao 19: 104-108.
122. Mokudai T, Ayoub IA, Sakakibara Y, Lee EJ, Ogilvy CS, et al. (2000) Delayed treatment with nicotinamide (Vitamin B(3)) improves neurological outcome and reduces infarct volume after transient focal cerebral ischemia in Wistar rats. Stroke 31: 1679-1685.
123. Klaidman L, Morales M, Kem S, Yang J, Chang ML, et al. (2003) Nicotinamide offers multiple protective mechanisms in stroke as a precursor for NAD+, as a

PARP inhibitor and by partial restoration of mitochondrial function. Pharmacology 69: 150-157.
124. Kallmann B, Burkart V, Kroncke KD, Kolb-Bachofen V, Kolb H (1992) Toxicity of chemically generated nitric oxide towards pancreatic islet cells can be prevented by nicotinamide. Life Sci 51: 671-678.
125. Murray MF (2003) Nicotinamide: an oral antimicrobial agent with activity against both Mycobacterium tuberculosis and human immunodeficiency virus. Clin Infect Dis 36: 453-460.
126. Murray MF, Srinivasan A (1995) Nicotinamide inhibits HIV-1 in both acute and chronic in vitro infection. Biochem Biophys Res Commun 210: 954-959.
127. Sereno D, Alegre AM, Silvestre R, Vergnes B, Ouaissi A (2005) In vitro antileishmanial activity of nicotinamide. Antimicrob Agents Chemother 49: 808-812.
128. Gazanion E, Vergnes B, Seveno M, Garcia D, Oury B, et al. (2011) In vitro activity of nicotinamide/antileishmanial drug combinations. Parasitol Int 60: 19-24.
129. Soares MB, Silva CV, Bastos TM, Guimaraes ET, Figueira CP, et al. (2012) Anti-Trypanosoma cruzi activity of nicotinamide. Acta Trop 122: 224-229.
130. Prusty D, Mehra P, Srivastava S, Shivange AV, Gupta A, et al. (2008) Nicotinamide inhibits Plasmodium falciparum Sir2 activity in vitro and parasite growth. FEMS Microbiol Lett 282: 266-272.
131. Ha HC, Juluri K, Zhou Y, Leung S, Hermankova M, et al. (2001) Poly(ADP-ribose) polymerase-1 is required for efficient HIV-1 integration. Proc Natl Acad Sci U S A 98: 3364-3368.
132. Tonegawa S (1983) Somatic generation of antibody diversity. Nature 302: 575-581.
133. Padlan EA (1994) Anatomy of the antibody molecule. Mol Immunol 31: 169-217.
134. Hamers-Casterman C, Atarhouch T, Muyldermans S, Robinson G, Hamers C, et al. (1993) Naturally occurring antibodies devoid of light chains. Nature 363: 446-448.
135. Greenberg AS, Avila D, Hughes M, Hughes A, McKinney EC, et al. (1995) A new antigen receptor gene family that undergoes rearrangement and extensive somatic diversification in sharks. Nature 374: 168-173.
136. Roux KH, Greenberg AS, Greene L, Strelets L, Avila D, et al. (1998) Structural analysis of the nurse shark (new) antigen receptor (NAR): molecular convergence of NAR and unusual mammalian immunoglobulins. Proc Natl Acad Sci U S A 95: 11804-11809.
137. Muyldermans S, Atarhouch T, Saldanha J, Barbosa JA, Hamers R (1994) Sequence and structure of VH domain from naturally occurring camel heavy chain immunoglobulins lacking light chains. Protein Eng 7: 1129-1135.
138. Nguyen VK, Muyldermans S, Hamers R (1998) The specific variable domain of camel heavy-chain antibodies is encoded in the germline. J Mol Biol 275: 413-418.
139. Vu KB, Ghahroudi MA, Wyns L, Muyldermans S (1997) Comparison of llama VH sequences from conventional and heavy chain antibodies. Mol Immunol 34: 1121-1131.
140. Nguyen VK, Hamers R, Wyns L, Muyldermans S (1999) Loss of splice consensus signal is responsible for the removal of the entire C(H)1 domain of the functional camel IGG2A heavy-chain antibodies. Mol Immunol 36: 515-524.
141. Conrath KE, Wernery U, Muyldermans S, Nguyen VK (2003) Emergence and evolution of functional heavy-chain antibodies in Camelidae. Dev Comp Immunol 27: 87-103.
142. Chothia C, Novotny J, Bruccoleri R, Karplus M (1985) Domain association in immunoglobulin molecules. The packing of variable domains. J Mol Biol 186: 651-663.
143. De Genst E, Saerens D, Muyldermans S, Conrath K (2006) Antibody repertoire development in camelids. Dev Comp Immunol 30: 187-198.

144. Davies J, Riechmann L (1994) 'Camelising' human antibody fragments: NMR studies on VH domains. FEBS Lett 339: 285-290.
145. Decanniere K, Muyldermans S, Wyns L (2000) Canonical antigen-binding loop structures in immunoglobulins: more structures, more canonical classes? J Mol Biol 300: 83-91.
146. Nguyen VK, Hamers R, Wyns L, Muyldermans S (2000) Camel heavy-chain antibodies: diverse germline V(H)H and specific mechanisms enlarge the antigen-binding repertoire. EMBO J 19: 921-930.
147. Riechmann L, Muyldermans S (1999) Single domain antibodies: comparison of camel VH and camelised human VH domains. J Immunol Methods 231: 25-38.
148. Arbabi Ghahroudi M, Desmyter A, Wyns L, Hamers R, Muyldermans S (1997) Selection and identification of single domain antibody fragments from camel heavy-chain antibodies. FEBS Lett 414: 521-526.
149. Lauwereys M, Arbabi Ghahroudi M, Desmyter A, Kinne J, Holzer W, et al. (1998) Potent enzyme inhibitors derived from dromedary heavy-chain antibodies. EMBO J 17: 3512-3520.
150. Harmsen MM, De Haard HJ (2007) Properties, production, and applications of camelid single-domain antibody fragments. Appl Microbiol Biotechnol 77: 13-22.
151. Vincke C, Loris R, Saerens D, Martinez-Rodriguez S, Muyldermans S, et al. (2009) General strategy to humanize a camelid single-domain antibody and identification of a universal humanized nanobody scaffold. J Biol Chem 284: 3273-3284.
152. Nguyen VK, Desmyter A, Muyldermans S (2001) Functional heavy-chain antibodies in Camelidae. Adv Immunol 79: 261-296.
153. Muyldermans S (2001) Single domain camel antibodies: current status. J Biotechnol 74: 277-302.
154. Stijlemans B, Conrath K, Cortez-Retamozo V, Van Xong H, Wyns L, et al. (2004) Efficient targeting of conserved cryptic epitopes of infectious agents by single domain antibodies. African trypanosomes as paradigm. J Biol Chem 279: 1256-1261.
155. Baral TN, Magez S, Stijlemans B, Conrath K, Vanhollebeke B, et al. (2006) Experimental therapy of African trypanosomiasis with a nanobody-conjugated human trypanolytic factor. Nat Med 12: 580-584.
156. De Vooght L, Caljon G, Stijlemans B, De Baetselier P, Coosemans M, et al. (2012) Expression and extracellular release of a functional anti-trypanosome Nanobody(R) in Sodalis glossinidius, a bacterial symbiont of the tsetse fly. Microb Cell Fact 11: 23.
157. Vinogradov SV, Bronich TK, Kabanov AV (2002) Nanosized cationic hydrogels for drug delivery: preparation, properties and interactions with cells. Adv Drug Deliv Rev 54: 135-147.
158. Arias JL (2008) Novel strategies to improve the anticancer action of 5-fluorouracil by using drug delivery systems. Molecules 13: 2340-2369.
159. Allemann E, Leroux JC, Gurny R, Doelker E (1993) In vitro extended-release properties of drug-loaded poly(DL-lactic acid) nanoparticles produced by a salting-out procedure. Pharm Res 10: 1732-1737.
160. Kroubi M, Daulouede S, Karembe H, Jallouli Y, Howsam M, et al. (2010) Development of a nanoparticulate formulation of diminazene to treat African trypanosomiasis. Nanotechnology 21: 505102.
161. Allahverdiyev AM, Abamor ES, Bagirova M, Ustundag CB, Kaya C, et al. (2011) Antileishmanial effect of silver nanoparticles and their enhanced antiparasitic activity under ultraviolet light. Int J Nanomedicine 6: 2705-2714.
162. Doroud D, Rafati S (2012) Leishmaniasis: focus on the design of nanoparticulate vaccine delivery systems. Expert Rev Vaccines 11: 69-86.
163. Raz B, Iten M, Grether-Buhler Y, Kaminsky R, Brun R (1997) The Alamar Blue assay to determine drug sensitivity of African trypanosomes (T.b. rhodesiense and T.b. gambiense) in vitro. Acta Trop 68: 139-147.

164. Gould MK, Vu XL, Seebeck T, de Koning HP (2008) Propidium iodide-based methods for monitoring drug action in the kinetoplastidae: comparison with the Alamar Blue assay. Anal Biochem 382: 87-93.
165. Nicoletti I, Migliorati G, Pagliacci MC, Grignani F, Riccardi C (1991) A rapid and simple method for measuring thymocyte apoptosis by propidium iodide staining and flow cytometry. J Immunol Methods 139: 271-279.
166. Landeira D, Navarro M (2007) Nuclear repositioning of the VSG promoter during developmental silencing in Trypanosoma brucei. J Cell Biol 176: 133-139.
167. O'Brien TC, Mackey ZB, Fetter RD, Choe Y, O'Donoghue AJ, et al. (2008) A parasite cysteine protease is key to host protein degradation and iron acquisition. J Biol Chem 283: 28934-28943.
168. Mendoza-Palomares C, Biteau N, Giroud C, Coustou V, Coetzer T, et al. (2008) Molecular and biochemical characterization of a cathepsin B-like protease family unique to Trypanosoma congolense. Eukaryot Cell 7: 684-697.
169. (2010) Antimicrobial peptides : methods and protocols; Giuliani A, Rinaldi AC, editors. New York :: Humana Press.
170. Gray CW, Brown RS, Marvin DA (1981) Adsorption complex of filamentous fd virus. J Mol Biol 146: 621-627.
171. Armstrong J, Perham RN, Walker JE (1981) Domain structure of bacteriophage fd adsorption protein. FEBS Lett 135: 167-172.
172. Crissman JW, Smith GP (1984) Gene-III protein of filamentous phages: evidence for a carboxyl-terminal domain with a role in morphogenesis. Virology 132: 445-455.
173. Smith GP (1985) Filamentous fusion phage: novel expression vectors that display cloned antigens on the virion surface. Science 228: 1315-1317.
174. Parmley SF, Smith GP (1988) Antibody-selectable filamentous fd phage vectors: affinity purification of target genes. Gene 73: 305-318.
175. Arias JL, Lopez-Viota M, Gallardo V, Adolfina Ruiz M (2010) Chitosan nanoparticles as a new delivery system for the chemotherapy agent tegafur. Drug Dev Ind Pharm 36: 744-750.
176. Frommel TO, Balber AE (1987) Flow cytofluorimetric analysis of drug accumulation by multidrug-resistant Trypanosoma brucei brucei and T. b. rhodesiense. Mol Biochem Parasitol 26: 183-191.
177. Berger BJ, Carter NS, Fairlamb AH (1993) Polyamine and pentamidine metabolism in African trypanosomes. Acta Trop 54: 215-224.
178. Thuita JK, Karanja SM, Wenzler T, Mdachi RE, Ngotho JM, et al. (2008) Efficacy of the diamidine DB75 and its prodrug DB289, against murine models of human African trypanosomiasis. Acta Trop 108: 6-10.
179. Frearson JA, Brand S, McElroy SP, Cleghorn LA, Smid O, et al. (2010) N-myristoyltransferase inhibitors as new leads to treat sleeping sickness. Nature 464: 728-732.
180. Stewart ML, Burchmore RJ, Clucas C, Hertz-Fowler C, Brooks K, et al. (2010) Multiple genetic mechanisms lead to loss of functional TbAT1 expression in drug-resistant trypanosomes. Eukaryot Cell 9: 336-343.
181. Lim CS, Potts M, Helm RF (2006) Nicotinamide extends the replicative life span of primary human cells. Mech Ageing Dev 127: 511-514.
182. Kang HT, Lee HI, Hwang ES (2006) Nicotinamide extends replicative lifespan of human cells. Aging Cell 5: 423-436.
183. Kooy RF, Hirumi H, Moloo SK, Nantulya VM, Dukes P, et al. (1989) Evidence for diploidy in metacyclic forms of African trypanosomes. Proc Natl Acad Sci U S A 86: 5469-5472.
184. Morgan GA, Laufman HB, Otieno-Omondi FP, Black SJ (1993) Control of G1 to S cell cycle progression of Trypanosoma brucei S427cl1 organisms under axenic conditions. Mol Biochem Parasitol 57: 241-252.
185. Roth BL, Poot M, Yue ST, Millard PJ (1997) Bacterial viability and antibiotic susceptibility testing with SYTOX green nucleic acid stain. Appl Environ Microbiol 63: 2421-2431.

186. Luque-Ortega JR, Saugar JM, Chiva C, Andreu D, Rivas L (2003) Identification of new leishmanicidal peptide lead structures by automated real-time monitoring of changes in intracellular ATP. Biochem J 375: 221-230.
187. Delgado M, Anderson P, Garcia-Salcedo JA, Caro M, Gonzalez-Rey E (2009) Neuropeptides kill African trypanosomes by targeting intracellular compartments and inducing autophagic-like cell death. Cell Death Differ 16: 406-416.
188. Fairlamb AH, Bowman IB (1977) Trypanosoma brucei: suramin and other trypanocidal compounds' effects on sn-glycerol-3-phosphate oxidase. Exp Parasitol 43: 353-361.
189. Clarkson AB, Jr., Bienen EJ, Pollakis G, Grady RW (1989) Respiration of bloodstream forms of the parasite Trypanosoma brucei brucei is dependent on a plant-like alternative oxidase. J Biol Chem 264: 17770-17776.
190. Le Trant N, Meshnick SR, Kitchener K, Eaton JW, Cerami A (1983) Iron-containing superoxide dismutase from Crithidia fasciculata. Purification, characterization, and similarity to Leishmanial and trypanosomal enzymes. J Biol Chem 258: 125-130.
191. Overath P, Czichos J, Haas C (1986) The effect of citrate/cis-aconitate on oxidative metabolism during transformation of Trypanosoma brucei. Eur J Biochem 160: 175-182.
192. Dormeyer M, Schoneck R, Dittmar GA, Krauth-Siegel RL (1997) Cloning, sequencing and expression of ribonucleotide reductase R2 from Trypanosoma brucei. FEBS Lett 414: 449-453.
193. Hofer A, Schmidt PP, Graslund A, Thelander L (1997) Cloning and characterization of the R1 and R2 subunits of ribonucleotide reductase from Trypanosoma brucei. Proc Natl Acad Sci U S A 94: 6959-6964.
194. Fast B, Kremp K, Boshart M, Steverding D (1999) Iron-dependent regulation of transferrin receptor expression in Trypanosoma brucei. Biochem J 342 Pt 3: 691-696.
195. Alsford S, Kawahara T, Isamah C, Horn D (2007) A sirtuin in the African trypanosome is involved in both DNA repair and telomeric gene silencing but is not required for antigenic variation. Mol Microbiol 63: 724-736.
196. Farzaneh F, Shall S, Michels P, Borst P (1985) ADP-ribosyl transferase activity in Trypanosoma brucei. Mol Biochem Parasitol 14: 251-259.
197. Petley A, Macklin B, Renwick AG, Wilkin TJ (1995) The pharmacokinetics of nicotinamide in humans and rodents. Diabetes 44: 152-155.
198. Knip M, Douek IF, Moore WP, Gillmor HA, McLean AE, et al. (2000) Safety of high-dose nicotinamide: a review. Diabetologia 43: 1337-1345.
199. Teka IA, Kazibwe AJ, El-Sabbagh N, Al-Salabi MI, Ward CP, et al. (2011) The diamidine diminazene aceturate is a substrate for the high-affinity pentamidine transporter: implications for the development of high resistance levels in trypanosomes. Mol Pharmacol 80: 110-116.
200. de Koning HP, Anderson LF, Stewart M, Burchmore RJ, Wallace LJ, et al. (2004) The trypanocide diminazene aceturate is accumulated predominantly through the TbAT1 purine transporter: additional insights on diamidine resistance in african trypanosomes. Antimicrob Agents Chemother 48: 1515-1519.
201. Prabaharan M, Mano JF (2005) Chitosan-based particles as controlled drug delivery systems. Drug Deliv 12: 41-57.
202. Bowman K, Leong KW (2006) Chitosan nanoparticles for oral drug and gene delivery. Int J Nanomedicine 1: 117-128.
203. Maser P, Luscher A, Kaminsky R (2003) Drug transport and drug resistance in African trypanosomes. Drug Resist Updat 6: 281-290.